Controlling Reactivity in the Conversion of Biomass-Derived Levoglucosenone to Renewable Chemicals over Metal and Acid Catalysts

By

Siddarth H. Krishna

A dissertation submitted in partial fulfillment of

the requirements for the degree of

Doctor of Philosophy

(Chemical Engineering)

at the

UNIVERSITY OF WISCONSIN-MADISON

2019

Date of final oral examination: June 20th, 2019

This dissertation is approved by the following members of the Final Oral Committee:

George W. Huber, Professor, Chemical and Biological Engineering

James A. Dumesic, Professor, Chemical and Biological Engineering

Brian P. Pfleger, Professor, Chemical and Biological Engineering

Ive Hermans, Professor, Chemistry

Abstract

We have investigated the catalytic conversion of biomass-derived intermediates to a variety of renewable chemicals over metal and acid catalysts, with an emphasis on the platform molecule levoglucosenone. Lignocellulosic biomass and sugars are sustainable sources of carbon which can be converted, through selective C-O cleavage and hydrogenation reactions, to precursors to high-value chemicals such as polymers and non-toxic solvents. Metal catalysts facilitate hydrogenation of C=C and C=O bonds; acid catalysts facilitate C-O cleavage reactions; and bifunctional metal-acid catalysts facilitate these reactions in tandem. As biomass-derived feedstocks are highly functionalized, controlling the selectivity to desired products is a critical component of economically viable conversion processes. Reaction pathways were elucidated using a combination of techniques including analysis of products formed over time, variation of reaction conditions, variation of active site properties, investigation of stereochemistry, and isotopic labeling. Reactions studied include the acid-catalyzed isomerization of levoglucosenone to 5-hydroxymethylfurfural; the metal-catalyzed hydrogenation to Cyrene and levoglucosanol; hydrogenolysis of levoglucosanol to tetrahydrofurandimethanol; hydrogenolysis of levoglucosanol to 1,2,5,6-hexanetetrol; and conversion of methyl glycosides to hexane-tetrols and hexane-triols. We demonstrated how a fundamental understanding of the catalytic chemistry leads to the ability to tune selectivity towards desired products, thereby providing directions for the rational design of processes to produce valuable chemicals from biomass.

Acknowledgements

This PhD not only represents my achievements in graduate school, but the culmination of the efforts and support from my advisers, department, family, and friends. I owe a tremendous debt of gratitude to my advisers, George Huber and James Dumesic. They have given me invaluable guidance and mentorship throughout the past five years, while also giving me room to grow as an independent researcher. I am beyond grateful to have worked with them, and will take their research philosophies and insights with me for the rest of my career. I thank the thesis committee for their time and valuable comments on this thesis. The numerous administrative staff in the CBE department, as well as scientists at user facilities (especially the NMR facilities in Chemistry), deserve credit for their assistance. I also thank Prof. Alexis T. Bell at UC-Berkeley and my mentors during my Chevron internships, for providing me with research experiences as an undergraduate that influenced my decision to come to graduate school.

I was extremely lucky to have parents who are both PhD chemical engineers, for giving me confidence that I could be a scientist and engineer from a young age. Their accomplishments and the numerous sacrifices they made for me, while balancing various burdens (such as my brother and, later, myself), still amaze and inspire me. The support from my brother, grandparents, and cousins has also been invaluable. My fellow lab members also been a critical part of this journey. I received a great deal of help and knowledge from senior students Dan, Kevin, Joe, Pranav, Insoo, and Tom. It has also been a pleasure to work alongside Nat, Maddie, Peter, Keishla, Ted, Anthony, Mark, Alvin, Paolo, Maddie, Lifeng, Elise, Bengi, Leida, Hochan, and others. I have also made a group of lifelong friends here in Madison, with whom I have shared the many ups and downs of graduate school.

The research work presented in this thesis was funded by the Department of Energy's Office of Energy Efficiency and Renewable Energy, award number DE-EE0006878; and the National Science Foundation, grant number DGE-1256259.

Table of Contents

List of Figures

List of Tables

List of Acronyms

1,2,3,6-hexanetetrol 1236-HT
1,2,5,6-hexanetetrol 1256-HT
1,2,6-hexanetriol 126-HT
1,5-pentanediol 15-PDO
1,6-hexanediol 16-HDO
1,2,5-hexanetriol 125-HT
1,4,5-hexanetriol 145-HT
2,3-dideoxymannose 23-Dman
2,3-dideoxyrhamnose 23-Drha
2-methyl-tetrahydrofurfurylalcohol 2MTHFA
3,4-dideoxyfructose 34-Dfru
3,4-dideoxyfucose 34-Dfuc
3,4-dideoxyglucose 34-Dglu
3,4-dideoxymannose 34-Dman
Butylated hydroxytoluene ..... BHT
Density functional theory ..... DFT
Dihydrolevoglucosenone ..... Cyrene
Dimethylsulfoxide ..... DMSO
Electrospray ionization ..... ESI
Formic acid ..... FA
Fourier Transform Infrared ..... FTIR
Furandicarboxylic acid ..... FDCA
Gas chromatography ..... GC
High pressure liquid chromatography ..... HPLC
Hydroxymethylfurfural ..... HMF
Incipient wetness impregnation ..... IWI
Inductively coupled plasma optical emission spectroscopy ..... ICP-OES

Isopropylamine ..... IPA
Levoglucosan ..... LGA
Levoglucosanol ..... Lgol
Levoglucosenone ..... LGO
Levulinic acid..... LA
Mass spectrometry ..... MS
Methyl-2,3-dideoxymannopyranoside ..... MDM
Methyl-2,3-dideoxyrhamnopyranoside..... MDR
Methyl-3,4-dideoxyfucopyranoside..... MDF
Methyl-3,4-dideoxygalactopyranoside ..... MDG
Nuclear magnetic resonance ..... NMR
Polyethersulfone ..... PES
Polytetrafluoroethylene..... PTFE
Refractive index ..... RI
Temperature-programmed desorption ..... TPD
Tetrahydrofuran ..... THF
Tetrahydrofurandimethanol ..... THFDM
Tetrahydrofurfuryl alcohol..... THFA
Tetrahydropyran-2-methanol-5-hydroxyl THP2M5H
Tetrahydropyran-2-methanol-5-ketone..... THP2M5one
Threo/erythro ..... t/e
Turnover frequency..... TOF

Chapter 1. Introduction

1.1 Biomass as a Feedstock for Renewable Chemicals

Biomass is an abundant source of renewable carbon which could form the basis for sustainable fuels and chemicals to replace those derived from fossil fuel resources.[1] During the past decade there have been multiple large projects focused on producing renewable fuels from biomass. These pioneer processes have often struggled to reach commercialization due to operational challenges, scale up challenges, and the low margins and high product volumes required for economic viability. The production of oxygenated chemicals from biomass offers several advantages compared to production of biofuels including: i) chemicals are higher value, allowing for profitability at moderate scale (10-30 kton/yr); ii) oxygenated chemicals require less deoxygenation, and therefore require less hydrogen input and have higher product mass yields compared to completely deoxygenated fuels; and, iii) target chemicals use the inherent functionalities (e.g. alcohols, cyclic ethers, C=C and C=O bonds, chiral centers) present in biomass. Bio-based chemicals could be co-produced with lower value biofuels, thereby improving the economics of bio-refineries.[2] Synergies between bio-refineries and conventional refineries (e.g., utilizing hydrogen surplus for hydrogenation; integrating refinery waste heat) could further improve economic viability.

In recent years, multiple renewable chemicals have been produced from lignocellulosic biomass. These molecules can be divided into two classes: i) chemicals that are identical to petroleum derived chemicals, and ii) new biomass derived chemicals that are not currently in the petrochemical infrastructure. The opportunity with this first route is that there is already a well-

established market for these products. However, the challenge with this route is that it directly competes with the existing petroleum derived infrastructure, which is often at large scale where the chemicals are produced with depreciated assets. In contrast, the molecules synthesized in this thesis are difficult to produce from petroleum feedstocks and could have unique properties, with applications in areas including solvents, polymers, and surfactants. However, the market for these products is not established and it will take time for these products to gain market acceptability. The fully loaded production price of these new biomass derived chemicals could be comparable ($1,000-5,000/ton) to existing petroleum-derived commodity chemicals if they are produced at commercial scale. Rigorous life cycle assessment models have shown that biomass based chemicals can have >60% (even 95%) lower carbon footprint than petroleum derived chemicals.[3] Products made from sustainable chemicals are appealing to end users that are increasingly concerned with issues regarding global warming and sustainability.

Several recent studies have shown that heterocyclic platform molecules, including levoglucosenone (LGO), 5-hydroxymethylfurfural (HMF), and furfural, can be produced from biomass in high yields and at low costs ($1,000-$5,000/ton) if produced at scale (>10 kton/yr).[4] Figure 1.1 shows the reaction chemistry of converting biomass-derived heterocycles to oxygenated products with potential applications highlighted. LGO and/or HMF can be produced (depending on the water content of the solvent system) from dehydration of cellulose, glucose, or other carbohydrates in up to 50-60% yield.[5] LGO and HMF can undergo selective hydrogenation over metal catalysts, as well as selective C-O cleavage and hydrogenation over metal-acid catalysts, to produce a variety of reduced oxygenated products.[6] These products include α,ω-diols such as tetrahydrofurandimethanol (THFDM) and 1,6-hexanediol (16-HDO), polyols such as 1,2,6-hexanetriol (126-HT) and 1,2,5,6-hexanetetrol (1256-HT), and renewable solvents such as

dihydrolevoglucosenone (Cyrene).[7] Alternatively, HMF can be selectively oxidized to the polymer precursor furandicarboxylic acid (FDCA).[8] Furfural is produced from dehydration of hemicellulose or C_5 sugars in up to 95% yield.[4c] Similar to the C_6 route, furfural can undergo successive hydrogenation and/or hydrogenolysis reactions to produce polymer precursors furfuryl alcohol, tetrahydrofurfuryl alcohol (THFA), and 1,5-pentanediol (15-PDO)[9], as well as renewable solvents including 2-methyl-tetrahydrofuran, cyclopentanone, and tetrahydropyran.[10] The renewable solvent γ-valerolactone can be synthesized either from hydration of furfuryl alcohol (C_5 pathway) or ring-opening of HMF (C_6 pathway, with loss of formic acid).[11] Lignin, which constitutes approximately 20 wt% of lignocellulose, is generally burnt for process heat and power in the majority of techno-economic analyses of biomass conversion; lignin conversion into valuable products remains challenging but is an ongoing area of research.[12]

16-HDO is an example of an oxygenated commodity chemical currently produced from petroleum but which is an attractive target for production from biomass because of its high cost and volume. Two companies (Rennovia Inc.[3c] and DuPont[13]) have submitted patent applications on technology to produce 16-HDO from biomass. 16-HDO is used as a feedstock to make polyester polyols and has a market price of $3,000-4,500/ton and volume of nearly 150 kton/yr.[14] The petrochemical route for 16-HDO production from benzene involves five reaction steps as shown in Figure 1.2.[15] Benzene is hydrogenated to cyclohexane over a metal catalyst and then oxidized to a mixture of cyclohexanol and cyclohexanone ("KA Oil") over a homogeneous cobalt catalyst. The conversion must be kept low (5-7%) in this process since cyclohexanone and cyclohexanol undergo undesired over-oxidation reactions. This step has a high separation and recycle requirement for the unreacted cyclohexane. There is also a safety hazard of combustion of the hydrocarbon reagent. The KA oil is then oxidized to adipic acid using concentrated nitric acid (a

corrosive reagent) which also releases N_2O in the process. N_2O is a harmful gas which requires additional treatment to avoid its release. Adipic acid is then hydrogenated in methanol solvent via the intermediate dimethyl adipate.

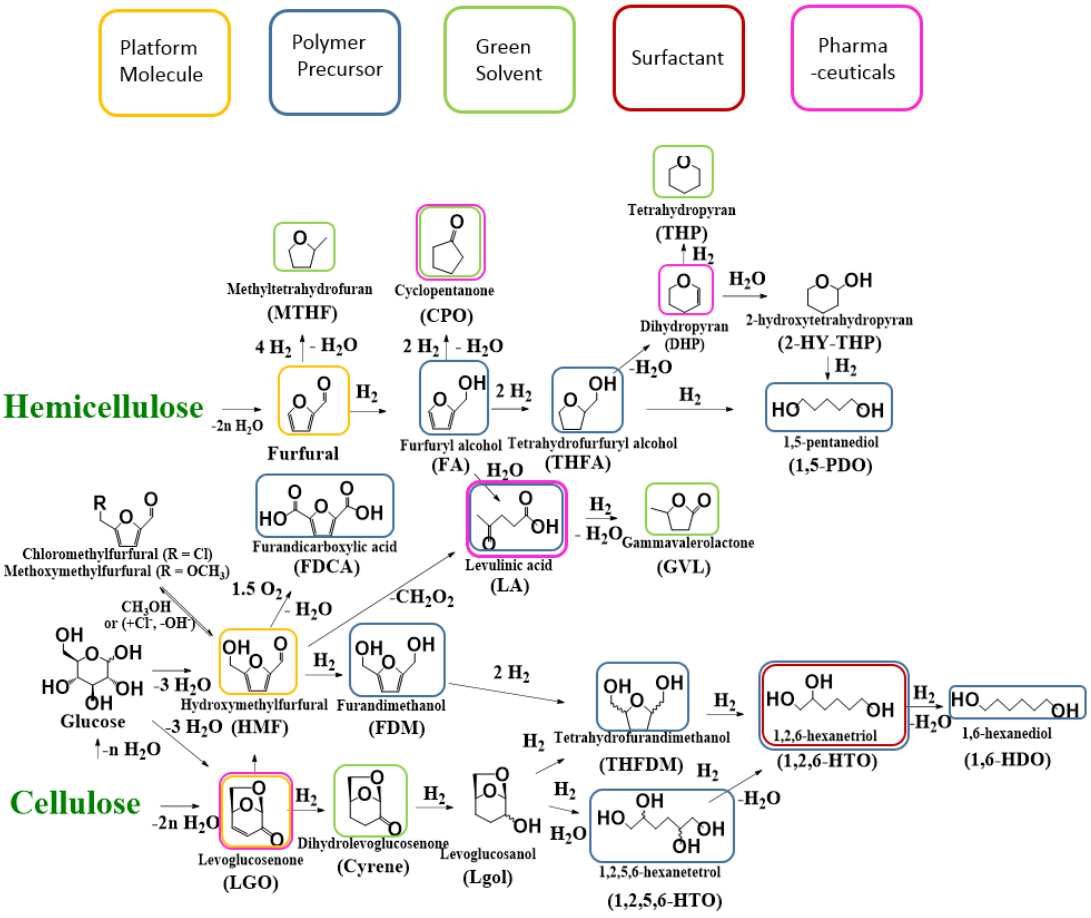

Figure 1.1. *Chemicals from Hemicellulose and Cellulose Fractions of Biomass with Potential Applications Highlighted.*

In contrast, the envisaged biomass-derived route would involve selective hydrodeoxygenation of an oxygenated feedstock (Figure 1.1) rather than reduction and oxidation of a hydrocarbon feedstock, and could potentially be operated at high yield, with fewer reaction steps, avoiding toxic reagents. Surrogate biomass-derived α,ω-diols, such as THFDM and 15-

PDO, could also potentially act as replacements for petroleum-derived 16-HDO (Figure 1.1). Biomass-derived routes also have a lower CO_2 footprint than production from petroleum.[3c] In order to compete with petroleum-derived chemicals, biomass-derived chemicals must offer significant advantages in performance and/or economic viability, in addition to environmental sustainability.

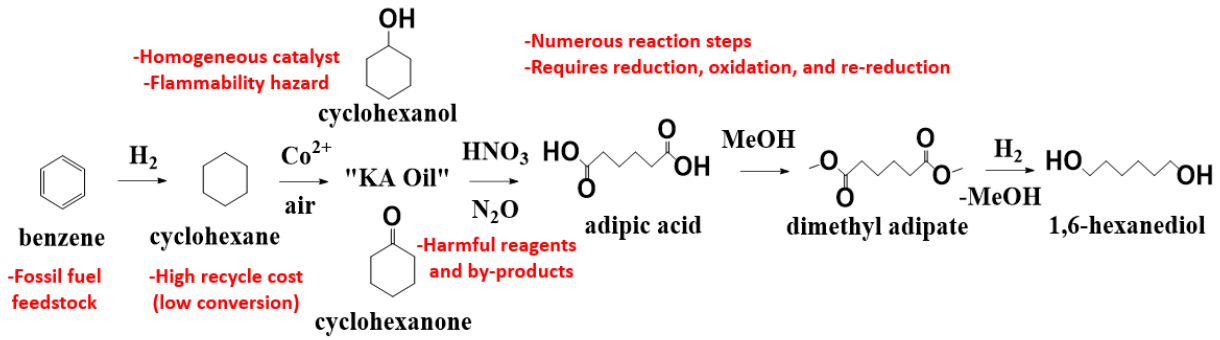

Figure 1.2. *Reaction network for current production of 1,6-hexanediol from petroleum-derived benzene. Undesirable aspects of this process are indicated in red.*

While the reaction chemistries of HMF and furfural conversion have been studied in the literature[16], the chemistry of LGO conversion remains largely unexplored. This is because high-yield routes to produce LGO from cellulose have only recently been reported.[5a] As shown in Figure 1.1, LGO is a precursor to several downstream products (many of which cannot be produced easily from petroleum) which possess desirable functionalities for utilization in the chemical industry as polymer precursors, green solvents, and surfactants. DuPont has reported that LGO can be converted to HMF, Lgol, THFDM, and 16-HDO over metal and acid catalysts.[13, 17] However, the mechanisms for these transformations remain unclear, hindering the rational design of catalytic technologies to control reactivity in these systems. The goal of this thesis is to address these fundamental questions by investigating the catalytic chemistry involved in upgrading biomass-

derived intermediates over metal and acid catalysts, with an emphasis on LGO as a platform molecule.

1.2 Metal and Acid Catalysts for Biomass Conversion

1.2.1. Metal-Catalyzed Hydrogenation

Metal-catalyzed hydrogenation is a critically important reaction in the conversion of both biomass and conventional carbon sources into fuels and chemicals.[18] Nanoparticles of highly reducible metals (e.g. Pt, Pd, Ru, Ni), supported on high surface area thermally stable supports (e.g. SiO_2, Al_2O_3), are useful for the hydrogenation of C=C and C=O bonds. These catalysts dissociate molecular hydrogen and facilitate reaction between an adsorbed, unsaturated compound and hydrogen, typically through a step-wise Horiuti-Polanyi mechanism.[19] Active site densities are typically counted through carbon monoxide (CO) or H_2 chemisorption.[18]

The selectivity of metal catalysts towards hydrogenation of different bonds is a strong function of the structure of both the reactant and catalyst surface.[20] In α,β unsaturated carbonyl compounds, the C=C bond is typically hydrogenated more easily than the C=O bond due its lower thermodynamic stability and lower barrier for reaction.[21] Selectivity can be controlled by changing the reaction conditions (residence time, temperature, pressure), as well as the catalyst properties (metal identity, particle size, support, modifiers).[20, 22] The reactant structure can also greatly influence the selectivity of C=C versus C=O hydrogenation, including through the relative stability of reactive groups (e.g. aldehyde versus ketone C=O bonds; olefin versus aromatic C=C bonds), and through steric hindrance effects, both of which affect the strength and modes of adsorption onto the catalyst surface.[23]

Metal-catalyzed hydrogenation reactions can also display stereoselectivity (producing an excess of one stereoisomer over another), for example when a ketone with two different substituents is hydrogenated to an alcohol and forms a new chiral center. If the starting molecule is not chiral, a conventional metal catalyst cannot form an enantiomeric excess of the product because there is no preference for hydrogenation of the ketone group from the two different directions. However, chiral modifiers can bias the adsorption mode of the reactant and result in an enantiomeric excess.[24] In cases where the reactant is 'prochiral' (already containing chiral centers), the existing chiral centers can bias the direction of hydrogen atom attack via steric effects, resulting in a diastereomeric excess of one product over another.[25]

1.2.2. Brønsted Acid-Catalyzed C-O Cleavage

Brønsted acids are another prototypical class of catalysts for biomass conversion as well as petrochemical upgrading.[26] C-O bond cleavage events are relevant to the depolymerization of biomass polymers (cellulose, hemicellulose and lignin) into monomers, to the removal of oxygen in the form of water (dehydration), and to ring-opening of cyclic ethers.[27] Acid-catalyzed C-O cleavage typically begins with protonation of the oxygen atom, followed by C-O bond rupture, passing through a carbocation transition state.[28] Reactivity is correlated to the stability of the transition state, with more highly substituted carbon atoms posessing more stable carbocations. In cases where there is a neighboring oxygen atom, the transition state can also be stabilized by formation of an oxocarbenium ion, thereby sharing the positive charge between the oxygen and carbon atoms.[27]

In the liquid phase, the energetics of both reactants and acid catalyst are greatly affected by the nature of the solvent. In polar aprotic solvents, the acidic proton is destabilized relative to

water, resulting in changes to the reaction rate depending on the relative changes in the Gibbs free energies of the reactant and protonated transition state.[29] When water is either a reactant (e.g. hydrolysis) or product (e.g. dehydration) of a reaction, its presence can also affect the rates and equilibrium constants for different reactions within a reaction network. In cellulose dehydration over an acid catalyst, the water content in a polar aprotic solvent system (e.g. tetrahydrofuran) dictates the selectivity to LGO versus HMF, where anhydrous conditions favor LGO formation and small amounts of water (1-3 wt%) favor HMF production.[5a] In biomass conversion reactions, desired acid-catalyzed transformations often compete with undesired degradation reactions, either to identifiable downstream monomeric products or to oligomeric humins (formed through coupling reactions).[30] Optimization of yield and selectivity in acid-catalyzed biomass conversion reactions often involves an understanding of competing rates of undesired and desired series and parallel reactions.[31]

Acid sites in heterogeneous catalysts are typically characterized by titration with a basic probe molecule.[26] NH_3-TPD (temperature programmed desorption) is commonly used to count the total number of acid sites (Brønsted plus Lewis sites). FTIR (Fourier transform infrared) spectroscopy of adsorbed pyridine is used to study the proportion of Brønsted and Lewis sites, because the FTIR peak positions are distinguishable for Lewis-site bound pyridine, and Brønsted -site bound, protonated pyridinum ions.[26] Gorte and co-workers have also developed a method to count Brønsted sites using the TPD of amines such as isopropylamine (IPA).[32] Desorbed IPA (bound to the support, Lewis acid sites, or weak Brønsted acid sites) can be distinguished from IPA bound to strong Brønsted sites, which is protonated and decomposes to NH_3 and propylene in a temperature range of 300-400^{o}C. The amount of propylene produced is equal the number of Brønsted sites according to this method.

Proton-form aluminosilicates, including amorphous as well as crystalline zeolite materials, are common acid catalysts used in the petrochemical industry. Examples in industry include catalytic cracking, hydroconversion, isomerization, alkylation, and oligomerization.[33] While neither SiO_2 nor Al_2O_3 possess Brønsted acidity, aluminosilicates (SiAls) possess Brønsted acidity. Al atoms in Al_2O_3 are typically in octahedral coordination, but substitution of Al atoms into a tetrahedral SiO_2 matrix results in a tetrahedral Al atom which is charge compensated by a Brønsted acidic OH group. The catalytic activity of high-silica HZSM5 zeolites was shown to vary linearly with the Al content, suggesting that each Al atom contributes one acid site.[34] On the other hand, the nature of acidity of amorphous SiAls is a matter of ongoing debate due to the highly non-uniform nature of these materials. Hensen and co-workers used a variety of characterization techniques, including FTIR of adsorbed probe molecules and in situ titration during reaction to support their claim that SiAls possess 1-2 orders of magnitude lower concentrations of 'strong Brønsted sites' compared to zeolites.[35]

1.2.3. Bifunctional Metal/Acid -Catalyzed Hydrogenolysis

Bifunctional metal and acid catalysts carry out two reactions (such as C-O cleavage and hydrogenation, or dehydrogenation and isomerization) in tandem. Carrying out these reactions in tandem often has several benefits. The thermodynamics of some C-O cleavage reactions are not highly favorable, while metal-catalyzed hydrogenations are thermodynamically favorable at moderate temperatures and high H_2 pressures.[16, 36] Hydrogenation can thus drive the overall process forward. Furthermore, unsaturated reaction products from acid-catalyzed reactions tend to be unstable due to their tendency to undergo further acid-catalyzed reactions.[37] Hydrogenating these intermediates in situ is a useful strategy to stabilize reaction products.

Both the ratio and proximity of metal and acid sites can have a critical influence on the rate and selectivity of hydrogenolysis reactions.[38] These effects have been studied in the alkane hydro-conversion literature. For example, in decane hydroconversion over Pt/H-Y catalysts, the overall reaction rate initially increases and then plateaus as a function of the metal-acid ratio, as the reaction rate transitions from metal-limited (low Pt loading) to acid-limited (higher Pt loadings)[39] The selectivity towards mono-branched alkanes versus poly-branched alkanes is also a function of the metal loading and metal-acid site proximity, due to competition between series (acid-catalyzed) isomerization reactions and parallel (metal-catalyzed) hydrogenation reactions. Understanding the roles of both types of active sites in facilitating different reactions within a complex reaction network is critical to the rational design bifunctional catalysts.

1.3 Overview of the Dissertation

We have investigated the catalytic conversion of biomass-derived intermediates to a variety of renewable chemicals over metal and acid catalysts. The chemistry of LGO conversion over metal and/or acid catalysts, relevant to Chapters 2-6, is shown in Figure 1.3.

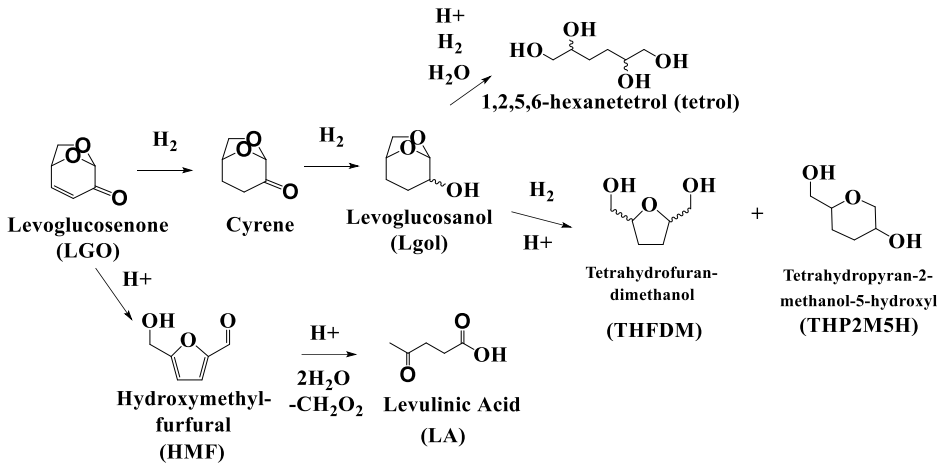

Figure 1.3. *Catalytic Conversion of LGO over metal and/or acid catalysts*

In Chapter 2, we study the acid-catalyzed isomerization of LGO in water to produce HMF and levulinic acid (LA). We develop a reaction kinetics model to describe the experimental data, and propose a reaction mechanism based on initial rate analysis and solvent effects. In Chapter 3, we investigate the metal-catalyzed hydrogenation of LGO to Cyrene and levoglucosanol (Lgol). We show how the selectivity to these two products can be controlled using the reaction temperature. We also study diastereoselectivity in Cyrene hydrogenation to Lgol, showing that an excess of threo- over –erythro is formed, likely due to steric hindrance effects. In Chapter 4, we study the hydrogenolysis of Lgol to THFDM and tetrahydropyran-2-methanol-5-hydroxyl (THP2M5H) over bifunctional metal-acid catalysts in tetrahydrofruran (THF) solvent. We elucidate the reaction network by analyzing key intermediates and series/parallel pathways. A combination of reaction kinetics measurements, isotopic labeling, variation of the metal-acid site properties, and investigation of stereochemistry provide insights into the rate-limiting step and mechanism. In Chapter 5, we examine the hydrolysis and hydrogenation of Lgol to 1256-HT in water. We identify key intermediates formed over acid sites and hydrogenated over metal sites.

We also distinguish between a lower-temperature pathway which preserves the C_2 stereocenter, and a higher-temperature pathway which erases it.

The chemistry of sugar glycoside conversion to hexane-triols and –tetrols, relevant to Chapter 7, is shown in Figure 1.4. In Chapter 7, we show how methyl glycosides can be converted to hexane-triols and –tetrols with high regio- and stereo- selectivity. This is achieved by carrying out selective C-OH cleavage reactions, followed by hydrolysis and hydrogenation which preserves certain stereocenters present in the original sugar feedstock.

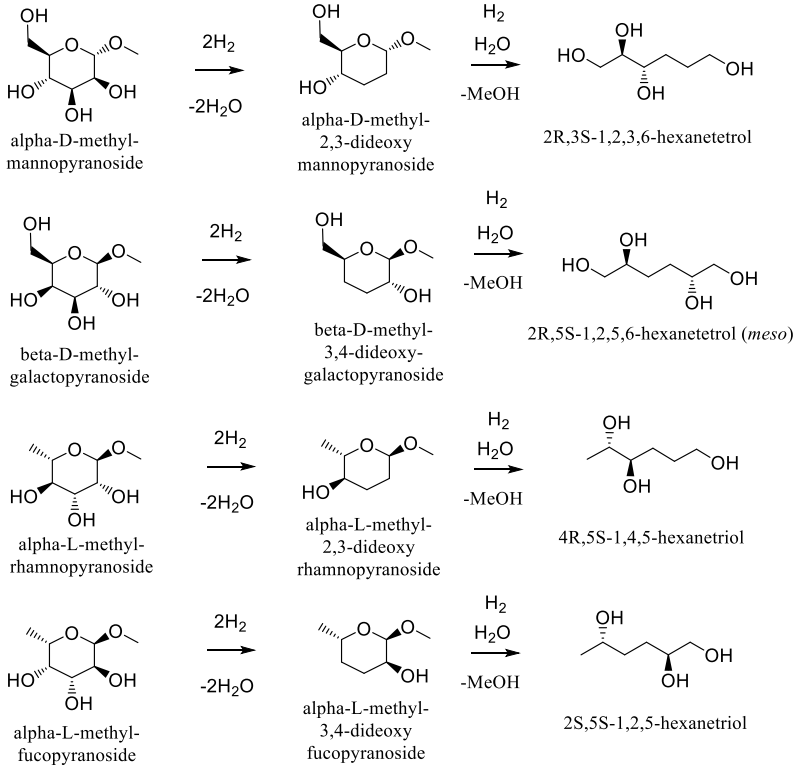

Figure 1.4. Catalytic conversion of methyl glycosides to hexane-triols and -tetrols

1.4 References

1. (a) Corma, A.; Iborra, S.; Velty, A., Chemical Routes for the Transformation of Biomass into Chemicals. *Chemical Reviews* **2007,** *107* (6), 2411-2502; (b) Huber, G. W.; Iborra, S.; Corma, A., Synthesis of Transportation Fuels from Biomass: Chemistry, Catalysts, and Engineering. *Chemical Reviews* **2006,** *106* (9), 4044-4098.

2. (a) Souza, G. M.; Victoria, R. L.; Joly, C. A.; Verdade, L. M., Bioenergy & Sustainability: Bridging the Gaps. Scientific Committee on Problems of the Environment (SCOPE): Sao Paulo, Brazil, 2015; (b) Biddy, M. J.; Davis, R.; Humbird, D.; Tao, L.; Dowe, N.; Guarnieri, M. T.; Linger, J. G.; Karp, E. M.; Salvachúa, D.; Vardon, D. R.; Beckham, G. T., The Techno-Economic Basis for Coproduct Manufacturing To Enable Hydrocarbon Fuel Production from Lignocellulosic Biomass. *ACS Sustainable Chemistry & Engineering* **2016,** *4* (6), 3196-3211; (c) Huang, K.; Won, W.; Barnett, K. J.; Brentzel, Z. J.; Alonso, D. M.; Huber, G. W.; Dumesic, J. A.; Maravelias, C. T., Improving economics of lignocellulosic biofuels: An integrated strategy for coproducing 1,5-pentanediol and ethanol. *Applied Energy* **2018,** *213*, 585-594.

3. (a) Singh, A.; Pant, D.; Korres, N. E.; Nizami, A.-S.; Prasad, S.; Murphy, J. D., Key issues in life cycle assessment of ethanol production from lignocellulosic biomass: Challenges and perspectives. *Bioresource Technology* 2010, *101* (13), 5003-5012; (b) Myriant - Bio-succinic Sustainability. http://www.myriant.com/pdf/myriant-sustainability.pdf (accessed 10/30/18); (c) Lane, J. The Race for Bionylon heats up: Rennovia enters piloting stage of its key bio-based HDO platform. http://www.biofuelsdigest.com/bdigest/2017/03/27/the-race-for-bionylon-heats-up-rennovia-enters-piloting-stage-of-its-key-bio-based-hdo-platform/ (accessed January 26, 2018); (d) Vigon, B. W.; Tolle, D. A.; Evers, D. P.; Freeman, S. L.; Humphreys, K. K.; Wend, C. F.; Landucci, R. In *Life cycle assessment of biomass conversion to feedstock chemicals*, IECEC 96. Proceedings of the 31st Intersociety Energy Conversion Engineering Conference, 11-16 Aug 1996; 1996; pp 2128-2133 vol.3.

4. (a) Cai, C. M.; Nagane, N.; Kumar, R.; Wyman, C. E., Coupling metal halides with a co-solvent to produce furfural and 5-HMF at high yields directly from lignocellulosic biomass as an integrated biofuels strategy. *Green Chemistry* **2014,** *16* (8), 3819-3829; (b) He, J.; Liu, M.; Huang, K.; Maravelias, C. T.; Dumesic, J. A.; Huber, G. W., Production of LGO and HMF from Cellulose in water-polar aprotic solvent mixture. *Green Chemistry, DOI: 10.1039/c7gc0188c* **2017**; (c) Alonso, D. M.; Hakim, S. H.; Zhou, S.; Won, W.; Hosseinaei, O.; Tao, J.; Garcia-Negron, V.; Motagamwala, A. H.; Mellmer, M. A.; Huang, K.; Houtman, C. J.; Labbé, N.; Harper, D. P.; Maravelias, C. T.; Runge, T.; Dumesic, J. A., Increasing the revenue from lignocellulosic biomass: Maximizing feedstock utilization. *Science Advances* **2017,** *3* (5).

5. (a) Cao, F.; Schwartz, T. J.; McClelland, D. J.; Krishna, S. H.; Dumesic, J. A.; Huber, G. W., Dehydration of cellulose to levoglucosenone using polar aprotic solvents. *Energy & Environmental Science* **2015,** *8* (6), 1808-1815; (b) Crisci, A. J.; Tucker, M. H.; Dumesic, J. A.; Scott, S. L., Bifunctional Solid Catalysts for the Selective Conversion of Fructose to 5-Hydroxymethylfurfural. *Topics in Catalysis* **2010,** *53* (15), 1185-1192; (c) He, J.; Liu, M.; Huang, K.; Walker, T. W.; Maravelias, C. T.; Dumesic, J. A.; Huber, G. W., Production of levoglucosenone and 5-hydroxymethylfurfural from cellulose in polar aprotic solvent-water mixtures. *Green Chemistry* **2017,** *19* (15), 3642-3653; (d) Pagán-Torres, Y. J.; Wang, T.; Gallo, J. M. R.; Shanks, B. H.; Dumesic, J. A., Production of 5-Hydroxymethylfurfural from Glucose Using a Combination of Lewis and Brønsted Acid Catalysts in Water in a Biphasic Reactor with an Alkylphenol Solvent. *ACS Catalysis* **2012,** *2* (6), 930-934; (e) Weingarten, R.; Rodriguez-Beuerman, A.; Cao, F.; Luterbacher, J. S.; Alonso, D. M.; Dumesic, J. A.; Huber, G. W., Selective Conversion of Cellulose to Hydroxymethylfurfural in Polar Aprotic Solvents. *ChemCatChem* **2014,** *6* (8), 2229-2234.

6. (a) He, J.; Huang, K.; Barnett, K. J.; Krishna, S. H.; Alonso, D. M.; Brentzel, Z. J.; Burt, S. P.; Walker, T.; Banholzer, W. F.; Maravelias, C. T.; Hermans, I.; Dumesic, J. A.; Huber, G. W., New catalytic strategies for [small alpha],[small omega]-diols production from lignocellulosic biomass. *Faraday Discussions* **2017,** *202* (0), 247-267; (b) Nakagawa, Y.; Tamura, M.; Tomishige, K., Catalytic Reduction of Biomass-Derived Furanic Compounds with Hydrogen. *ACS Catalysis* **2013,** *3 (12)*, 2655-2668; (c) Tomishige, K.; Nakagawa, Y.; Tamura, M., Selective hydrogenolysis and hydrogenation using metal catalysts directly modified with metal oxide species. *Green Chemistry* **2017,** *19* (13), 2876-2924.

7. (a) he, j.; Burt, S. P.; Ball, M. R.; Zhao, D.; Hermans, I.; Dumesic, J. A.; Huber, G. W., Synthesis of 1,6-Hexanediol from cellulose derived tetrahydrofuran dimethanol (THFDM) with Pt-WOx/TiO2 catalysts. *ACS Catalysis* **2018**; (b) Sherwood, J.; De bruyn, M.; Constantinou, A.; Moity, L.; McElroy, C. R.; Farmer, T. J.; Duncan, T.; Raverty, W.; Hunt, A. J.; Clark, J. H., Dihydrolevoglucosenone (Cyrene) as a bio-based alternative for dipolar aprotic solvents. *Chemical Communications* **2014,** *50* (68), 9650-9652.

8. Motagamwala, A. H.; Won, W.; Sener, C.; Alonso, D. M.; Maravelias, C. T.; Dumesic, J. A., Toward biomass-derived renewable plastics: Production of 2,5-furandicarboxylic acid from fructose. *Science Advances* **2018,** *4* (1).

9. (a) Nakagawa, Y.; Tomishige, K., Production of 1,5-pentanediol from biomass via furfural and tetrahydrofurfuryl alcohol. *Catalysis Today* **2012,** *195* (1), 136-143; (b) Brentzel, Z. J.; Barnett, K. J.; Huang, K.; Maravelias, C. T.; Dumesic, J. A.; Huber, G. W., Chemicals from Biomass: Combining Ring-Opening

Tautomerization and Hydrogenation Reactions to Produce 1,5-Pentanediol from Furfural. *ChemSusChem* **2017,** *10* (7), 1351-1355.
10. (a) Hronec, M.; Fulajtarová, K., Selective transformation of furfural to cyclopentanone. *Catalysis Communications* **2012,** *24*, 100-104; (b) Dong, F.; Zhu, Y.; Ding, G.; Cui, J.; Li, X.; Li, Y., One-step Conversion of Furfural into 2-Methyltetrahydrofuran under Mild Conditions. *ChemSusChem* **2015,** *8* (9), 1534-1537.
11. (a) Mellmer, M. A.; Gallo, J. M. R.; Martin Alonso, D.; Dumesic, J. A., Selective Production of Levulinic Acid from Furfuryl Alcohol in THF Solvent Systems over H-ZSM-5. *ACS Catalysis* **2015,** *5* (6), 3354-3359; (b) Braden, D. J.; Henao, C. A.; Heltzel, J.; Maravelias, C. C.; Dumesic, J. A., Production of liquid hydrocarbon fuels by catalytic conversion of biomass-derived levulinic acid. *Green Chemistry* **2011,** *13* (7), 1755-1765.
12. (a) Zakzeski, J.; Bruijnincx, P. C. A.; Jongerius, A. L.; Weckhuysen, B. M., The Catalytic Valorization of Lignin for the Production of Renewable Chemicals. *Chemical Reviews* **2010,** *110* (6), 3552-3599; (b) Brodin, M.; Vallejos, M.; Opedal, M. T.; Area, M. C.; Chinga-Carrasco, G., Lignocellulosics as sustainable resources for production of bioplastics – A review. *Journal of Cleaner Production* **2017,** *162*, 646-664; (c) Sheldon, R. A., Green and sustainable manufacture of chemicals from biomass: state of the art. *Green Chemistry* **2014,** *16* (3), 950-963.
13. Allgeier, A. M.; Namal De Silva, W. I.; Korovessi, E.; Menning, C. A.; Ritter, J. C.; Sengupta, S. K.; Stauffer, C. S. Process for preparing 1,6-hexanediol. US 8865,940 B2, 2014.
14. 1,6-Hexanediol Market by Application (Polyurethanes, Coatings, Acrylates, Adhesives, Unsaturated Polyester Resins, Plasticizers, and Others) and By Geography (NA, Europe, Asia-Pacific, & ROW) - Trends and Forecasts to 2019. http://www.researchandmarkets.com/research/zs4gnb/16hexanediol (accessed January 22).
15. (a) Van de Vyver, S.; Roman-Leshkov, Y., Emerging catalytic processes for the production of adipic acid. *Catalysis Science & Technology* **2013,** *3* (6), 1465-1479; (b) Cavani, F.; Alini, S., Synthesis of Adipic Acid: On the Way to More Sustainable Production. In *Sustainable Industrial Chemistry*, Wiley-VCH Verlag GmbH & Co. KGaA: 2009; pp 367-425.
16. Chheda, J. N.; Huber, G. W.; Dumesic, J. A., Liquid-Phase Catalytic Processing of Biomass-Derived Oxygenated Hydrocarbons to Fuels and Chemicals. *Angewandte Chemie International Edition* **2007,** *46* (38), 7164-7183.
17. Namal De Silva, W. I.; Ritter, J. C.; Stauffer, C. S. Production of hydroxymethylfurfural from levoglucosenone. US8884036B2, 2014.
18. Gates, B. C., Supported Metal Clusters: Synthesis, Structure, and Catalysis. *Chemical Reviews* **1995,** *95* (3), 511-522.
19. Horiuti, I.; Polanyi, M., Exchange reactions of hydrogen on metallic catalysts. *Transactions of the Faraday Society* **1934,** *30* (0), 1164-1172.
20. Durndell, L. J.; Parlett, C. M. A.; Hondow, N. S.; Isaacs, M. A.; Wilson, K.; Lee, A. F., Selectivity control in Pt-catalyzed cinnamaldehyde hydrogenation. *Scientific Reports* **2015,** *5*, 9425.
21. Mäki-Arvela, P.; Hájek, J.; Salmi, T.; Murzin, D. Y., Chemoselective hydrogenation of carbonyl compounds over heterogeneous catalysts. *Applied Catalysis A: General* **2005,** *292*, 1-49.
22. Lashdaf, M.; Krause, A. O. I.; Lindblad, M.; Tiitta, M.; Venäläinen, T., Behaviour of palladium and ruthenium catalysts on alumina and silica prepared by gas and liquid phase deposition in cinnamaldehyde hydrogenation. *Applied Catalysis A: General* **2003,** *241* (1–2), 65-75.
23. (a) Delbecq, F.; Sautet, P., Competitive C • C and C • O Adsorption of α-β-Unsaturated Aldehydes on Pt and Pd Surfaces in Relation with the Selectivity of Hydrogenation Reactions: A Theoretical Approach. *Journal of Catalysis* **1995,** *152* (2), 217-236; (b) Alcalá, R.; Greeley, J.; Mavrikakis, M.; Dumesic, J. A., Density-functional theory studies of acetone and propanal hydrogenation on Pt(111). *The Journal of Chemical Physics* **2002,** *116* (20), 8973-8980.
24. Maeda, N.; Hungerbühler, K.; Baiker, A., Asymmetric Hydrogenation on Chirally Modified Pt: Origin of Hydrogen in the N–H–O Interaction between Cinchonidine and Ketone. *Journal of the American Chemical Society* **2011,** *133* (49), 19567-19569.
25. (a) Augustine, R. L.; Migliorini, D. C.; Foscante, R. E.; Sodano, C. S.; Sisbarro, M. J., Catalytic hydrogenation of .alpha.,.beta.-unsaturated ketones. IV. Effect of the medium on product stereochemistry. *The Journal of Organic Chemistry* **1969,** *34* (4), 1075-1085; (b) Augustine, R. L., Selective heterogeneously catalyzed hydrogenations. *Catalysis Today* **1997,** *37* (4), 419-440.
26. Gates, B.; R. Katzer, J.; Shuit, G. C. A., *Chemistry of catalytic processes / Bruce C. Gates, James R. Katzer, G.C.A. Schuit*. 2019.

27. Chia, M.; Pagán-Torres, Y. J.; Hibbitts, D.; Tan, Q.; Pham, H. N.; Datye, A. K.; Neurock, M.; Davis, R. J.; Dumesic, J. A., Selective Hydrogenolysis of Polyols and Cyclic Ethers over Bifunctional Surface Sites on Rhodium–Rhenium Catalysts. *Journal of the American Chemical Society* **2011,** *133* (32), 12675-12689.
28. L.G. Wade, J., *Organic Chemistry*. 7 ed.; Prentice Hall: Upper Saddle River, NJ, 2010.
29. Mellmer, M. A.; Sener, C.; Gallo, J. M. R.; Luterbacher, J. S.; Alonso, D. M.; Dumesic, J. A., Solvent Effects in Acid-Catalyzed Biomass Conversion Reactions. *Angewandte Chemie International Edition* **2014,** *53* (44), 11872-11875.
30. Walker, T. W.; Motagamwala, A. H.; Dumesic, J. A.; Huber, G. W., Fundamental catalytic challenges to design improved biomass conversion technologies. *Journal of Catalysis* **2019,** *369*, 518-525.
31. Weingarten, R.; Tompsett, G. A.; Conner Jr, W. C.; Huber, G. W., Design of solid acid catalysts for aqueous-phase dehydration of carbohydrates: The role of Lewis and Brønsted acid sites. *Journal of Catalysis* **2011,** *279* (1), 174-182.
32. (a) Tittensor, J. G.; Gorte, R. J.; Chapman, D. M., Isopropylamine adsorption for the characterization of acid sites in silica-alumina catalysts. *Journal of Catalysis* **1992,** *138* (2), 714-720; (b) Gorte, R. J., What do we know about the acidity of solid acids? *Catal Lett* **1999,** *62* (1), 1-13.
33. Martens, J. A.; Jacobs, P. A., Chapter 14 Introduction to acid catalysis with zeolites in hydrocarbon reactions. In *Studies in Surface Science and Catalysis*, van Bekkum, H.; Flanigen, E. M.; Jacobs, P. A.; Jansen, J. C., Eds. Elsevier: 2001; Vol. 137, pp 633-671.
34. Olson, D. H.; Haag, W. O.; Lago, R. M., Chemical and physical properties of the ZSM-5 substitutional series. *Journal of Catalysis* **1980,** *61* (2), 390-396.
35. (a) Poduval, D. G.; van Veen, J. A. R.; Rigutto, M. S.; Hensen, E. J. M., Brønsted acid sites of zeolitic strength in amorphous silica-alumina. *Chemical Communications* **2010,** *46* (20), 3466-3468; (b) Hensen, E. J. M.; Poduval, D. G.; Degirmenci, V.; Ligthart, D. A. J. M.; Chen, W.; Maugé, F.; Rigutto, M. S.; Veen, J. A. R. v., Acidity Characterization of Amorphous Silica–Alumina. *The Journal of Physical Chemistry C* **2012,** *116* (40), 21416-21429.
36. Lohr, T. L.; Li, Z.; Marks, T. J., Thermodynamic Strategies for C–O Bond Formation and Cleavage via Tandem Catalysis. *Accounts of Chemical Research* **2016,** *49* (5), 824-834.
37. Anderson, E. M.; Stone, M. L.; Katahira, R.; Reed, M.; Beckham, G. T.; Román-Leshkov, Y., Flowthrough Reductive Catalytic Fractionation of Biomass. *Joule* **2017,** *1* (3), 613-622.
38. (a) Samad, J. E.; Blanchard, J.; Sayag, C.; Louis, C.; Regalbuto, J. R., The controlled synthesis of metal-acid bifunctional catalysts: The effect of metal:acid ratio and metal-acid proximity in Pt silica-alumina catalysts for n-heptane isomerization. *Journal of Catalysis* **2016,** *342*, 203-212; (b) G. Acebo, E.; Leroux, C.; Chizallet, C.; Schuurman, Y.; Bouchy, C., Metal/acid bifunctional catalysis and intimacy criterion for ethylcyclohexane hydroconversion: when proximity does not matter. *ACS Catalysis* **2018**; (c) Batalha, N.; Pinard, L.; Pouilloux, Y.; Guisnet, M., Bifunctional Hydrogenating/Acid Catalysis: Quantification of the Intimacy Criterion. *Catal Lett* **2013,** *143* (6), 587-591.
39. Alvarez, F.; Ribeiro, F. R.; Perot, G.; Thomazeau, C.; Guisnet, M., Hydroisomerization and Hydrocracking of Alkanes: 7. Influence of the Balance between Acid and Hydrogenating Functions on the Transformation ofn-Decane on PtHY Catalysts. *Journal of Catalysis* **1996,** *162* (2), 179-189.

Chapter 2. Levoglucosenone Isomerization over Acid Catalysts

2.1 Introduction

While LGO production has previously been reported in low to moderate yields from the pyrolysis of cellulose[1], our group has shown that LGO can be produced from cellulose in 50% yield using polar aprotic solvents at mild conditions[2] (210^{o}C, 20 mM H_2SO_4). Cellulose is first depolymerized to form levoglucosan (LGA), which is then dehydrated to form LGO. Small quantities of water (e.g., 3 wt%) shift the selectivity to HMF rather than LGO. This selectivity shift toward HMF could be due to the rehydration of LGA to glucose followed by glucose conversion to HMF, or via direct isomerization of LGO to HMF in the presence of water and an acid catalyst[1a, 3]. However, the kinetics of LGO isomerization (Figure 2.1) remain unknown. An understanding of the factors which promote LGO isomerization could aid in developing strategies to minimize LGO degradation, thereby improving the yield of LGO from cellulose. Increasing the yield of LGO would, in turn, improve the economic viability of producing of high-value chemicals from lignocellulosic biomass. Optimizing the isomerization of LGO could allow for the production of HMF or LA in high yield, which can in turn be converted to fuels[4] and chemicals [5].

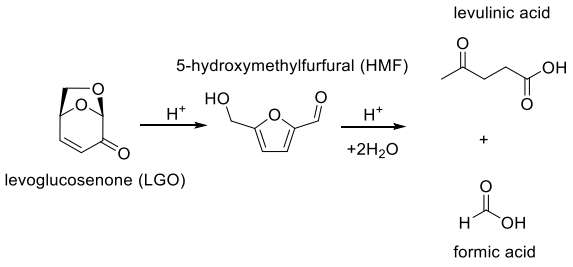

Figure 2.1. *LGO isomerization to HMF, and hydration of HMF to form LA and FA*

The chemistry of LGO isomerization is also relevant to the ring rearrangement of sugars in general. LGO isomerization to HMF involves a transformation from a 6-membered ring to a 5-membered ring, analogous to the isomerization of glucose to fructose. LGO isomerization has been shown to proceed over a Brønsted acid catalyst [1a, 3], while glucose isomerization to fructose requires a Lewis acid catalyst [6]. An investigation of LGO isomerization would provide a basis for comparison to the glucose isomerization mechanism.

Herein, we investigate the isomerization of LGO to HMF in an aqueous solvent system with a sulfuric acid catalyst. We elucidate the reaction network and develop a reaction kinetics model to describe this system across a range of experimental conditions. We propose a mechanism for LGO isomerization analogous to glucose isomerization which is consistent with the experimental results. Our findings provide directions for designing catalytic systems to control the LGO isomerization reaction depending on which products are desired.

2.2. Experimental Methods

Levoglucosenone (98%, Apollo Scientific), 5-hydroxymethylfurfural (99%, Sigma Aldrich), H_2SO_4 (96%, Sigma Aldrich), levulinic acid (99%, Sigma Aldrich), formic acid (98%, Sigma Aldrich), tetrahydrofuran (99.9%, Acros Organics), and HPLC (high pressure liquid

chromatography) grade water (Fisher Scientific) were used as received.

For reactions, 2 mL of solution containing the appropriate solute and sulfuric acid concentrations was added to 10 mL thick-walled glass reactors. The reactors were placed in an oil bath at the desired temperature and stirred at 500 rpm. Reactors were removed from the oil bath and quenched in an ice water bath at the appropriate time. Reaction products were filtered using a 0.2 □m polyethersulfone (PES) syringe filter prior to analysis.

Products were quantified using a Shimadzu HPLC with a BioRad Aminex 87H column with 5 mM H_2SO_4 mobile phase. The column was operated at a flow rate of 0.6 mL/min and a temperature of 30^{o}C. A refractive index (RI) detector was used to quantify levulinic acid, formic acid, and the hydrated form of levoglucosenone. A photodiode array (UV) detector was used to quantify LGO and HMF. Because LGO and HMF elute at nearly the same retention time, LGO and HMF were quantified using two different UV wavelengths. HMF was quantified at 290 nm while LGO was quantified at 370 nm. The contribution of HMF to the LGO peak at 370 nm, and the contribution of LGO to the HMF peak at 290 nm, were taken into account by using the sensitivity of HMF at 370 nm and the sensitivity of LGO at 290 nm, respectively. This quantification method was validated using mixtures of LGO and HMF at known concentrations. Concentrations of all products were calculated based on calibration curves using standards.

When LGO was diluted in water, a single major product of hydration was observed by HPLC. ^{1}H and ^{13}C NMR (nuclear magnetic resonance) were used to identify this compound as the doubly hydrated form of LGO. The LGO-dihydrate (DH) was prepared in 90% yield by diluting LGO in water and allowing the hydration to occur at room temperature for >100 h. NMR spectra were collected using a Bruker Avance 500 MHz spectrometer at room temperature. 10% D_2O was

added to the solution to facilitate locking to the deuterium resonance. The ^{1}H spectrum of the doubly hydrated form of LGO (Figure 8.1 in the Appendix) is in agreement with ^{1}H chemical shift values for this compound in the literature[1a]. The existence of a single identifiable hydration product allowed for an HPLC-RI calibration curve to be developed by tracking the disappearance of LGO as the hydration progressed at room temperature.

Reaction kinetics modeling was carried out using MATLAB (Version 2015b). The set of coupled ODEs describing the concentrations of each species over time were solved using the "ode23t" differential equation solver. The error between the experimental data and the model was minimized using the non-linear optimization function "nlinfit".

2.3. Results and Discussion

Figure 2.2 shows the results of LGO isomerization in water over a sulfuric acid catalyst. DH and HMF are the primary products of LGO conversion. The ratio of the concentrations of DH to LGO approaches a constant value of 1.13 (with a standard deviation of +/- 0.05), suggesting that these species may be in equilibrium. The concentrations of both LGO and DH continue to decrease over time, suggesting that either species can be converted to HMF, which is then hydrated to form LA and formic acid (FA), as reported in the literature [3b, 7]. The carbon balance decreases over the course of the reaction and the product solutions at later reaction times are brownish in color, indicating the formation of unaccounted degradation products (humins).

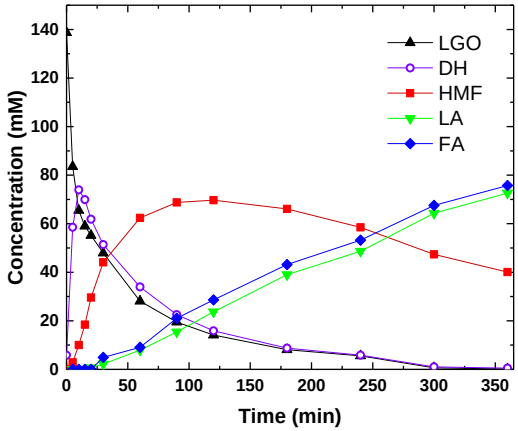

Figure 2.2. *Acid-catalyzed transformation of LGO to HMF in water, and hydration of HMF to form LA and FA. Reaction conditions: 150 mM LGO in 50 mM H_2SO_4 (aq); 125°C. Solid lines are visual aids.*

2.3.1. Equilibrium between LGO and DH

The thermal hydration of LGO to DH, in the absence of an acid catalyst, was studied in water at 125°C (Figure 2.3). At these conditions, the concentrations of the two species remain at a ratio of 1.05 (with a standard deviation of +/- 0.04), similar to the ratio of DH to LGO during the acid-catalyzed reaction as shown in Figure 2.3. The >95% molar carbon balance maintained over the course of 4 hours indicates that LGO and DH exist in equilibrium at the reaction conditions of interest.

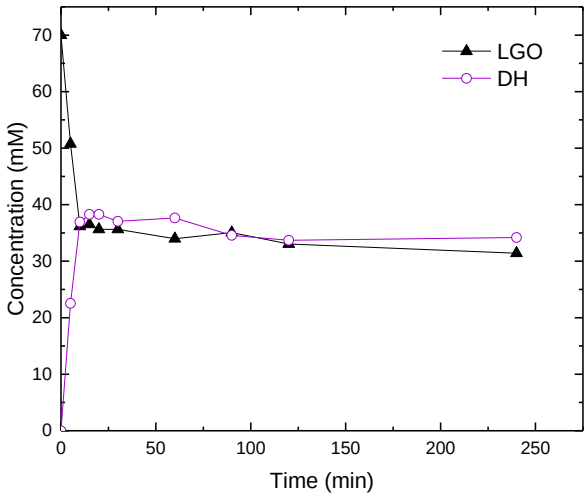

Figure 2.3. *Thermal hydration of LGO in pure water. Reaction conditions: 70 mM LGO, 125°C. Solid lines are visual aids.*

At room temperature, LGO is converted to DH in approximately 90% yield by diluting LGO in water to 75 mM and waiting for 100 h. Using this approach, a sample of DH in water was prepared and used as a feedstock for the acid-catalyzed reaction. As shown in Figure 2.4, DH is converted to LGO rapidly during the reaction. The trends in the concentrations of HMF and LA are similar to those observed in Figure 2.2. Finally, Figure 2.5 shows the ratio of the concentrations of DH to LGO versus time for each of the experiments detailed in Figures 2.2-2.4. Taking these three experiments together, the ratio of the two species is seen to approach a similar value of 1.18 (with a standard deviation of +/- 0.15), which is maintained over the course of the reaction. These results provide further evidence that LGO and DH are in equilibrium at the reaction conditions.

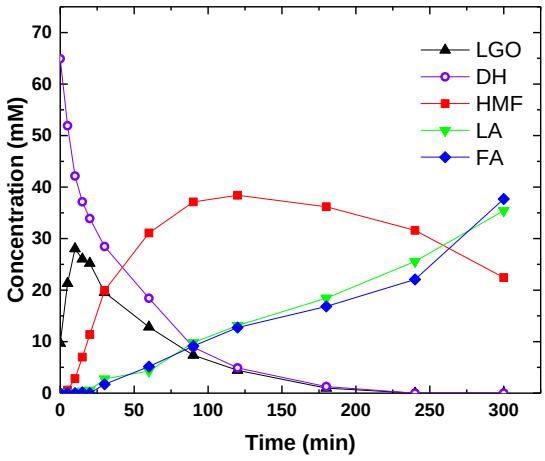

Figure 2.4. *LGO isomerization in water using an LGO-dihydrate rich feed. Reaction conditions: 65 mM DH plus 10 mM LGO; 50 mM H_2SO_4 (aq); 125°C. Solid lines are visual aids.*

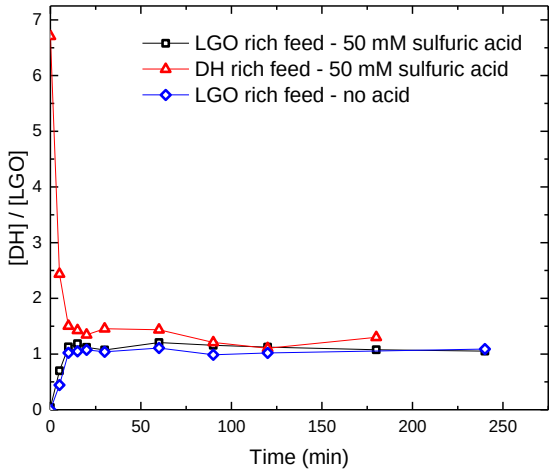

Figure 2.5. *The ratio of DH to LGO vs time for various reaction conditions at 125°C, both with and without acid. Solid lines are visual aids.*

Because LGO and DH are in equilibrium at our experimental conditions, it is possible to express the rate of HMF production in terms of a lumped kinetic parameter multiplied by the

combined concentration of LGO and DH (Section 8.1.1 in the Appendix). Accordingly, and because one reactant (water) is in great excess, the rate of HMF formation can be modeled as being first order in the combined concentration of LGO and DH, as shown in the supplementary information. This approach avoids the use of the measured equilibrium ratio of DH to LGO in the reaction kinetics model described below, and therefore the model is not affected by any noise in the measurement of this value.

2.3.2. Thermal degradation reactions.

As shown in Figure 2.3, the pool of LGO and DH is thermally stable at the reaction conditions of interest. The thermal stabilities of HMF, LA, and FA were also studied by heating these species in water. At 125^{o}C, LA and FA did not degrade over the course of 4 hours. Upon heating in water, HMF degraded at a rate that is described by a first-order model, as can be seen in Figure 2.6. Girisuta, et al. studied the thermal stability of HMF in water[7b]. In that study, HMF was heated at 98^{o}C for 2 hours in 1 molar solutions of FA or LA. Negligible HMF degradation was observed under those conditions, in agreement with our findings. At the higher temperatures and longer reaction times accessed in our experiments, however, thermal degradation of HMF occurred. Therefore, thermal HMF degradation was accounted for in our kinetic model by calculating the pre-exponential factor and activation energy for this reaction.

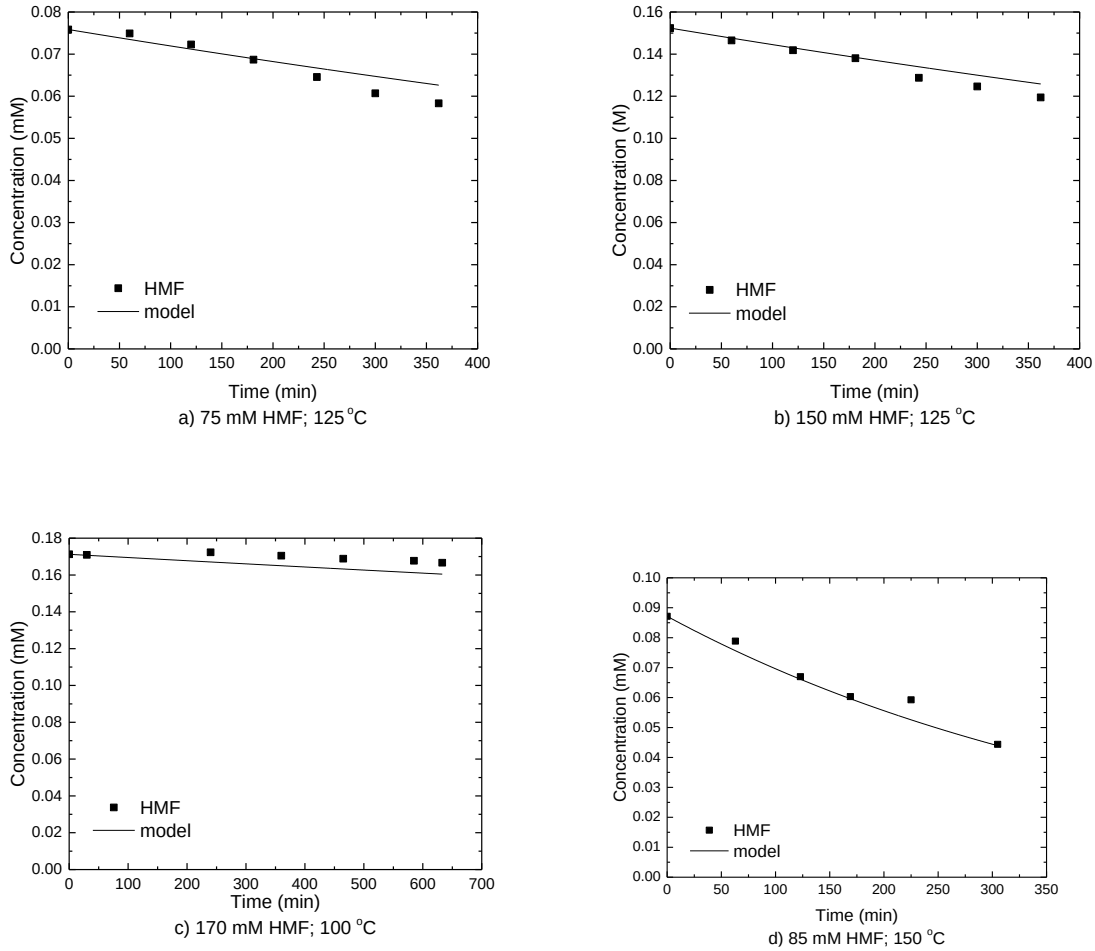

Figure 2.6. *Thermal degradation of HMF in water at various initial concentrations and temperatures. Solid lines are model-predicted values.*

2.3.3. Development of a reaction kinetics model.

Experiments in 100 mM H_2SO_4 (aq) revealed that LA and FA do not degrade appreciably at 125°C. However, LGO and HMF undergo acid-catalyzed transformations at the same conditions (Figure 2.1); therefore, it was not possible to independently measure the rates at which these species are converted. Quantification of these degradation routes was achieved by conducting a series of experiments at a temperature of 125°C, wherein the initial concentrations of HMF, LGO

and H_2SO_4 were independently varied. The results of these experiments are summarized in Figure 2.8, which shows the experimental data along with the model-predicted values. The reaction kinetics model was constructed from the six experiments shown in Figure 2.8, as well as the independently measured parameters for thermal HMF degradation shown in Figure 2.6. In all six experiments, the rate of carbon loss from identifiable products was seen to vary as a function of HMF concentration only, which precludes the possibility that degradation reactions involving LGO are occurring under these conditions. Furthermore, the rate of thermal HMF degradation alone was not sufficient to explain the loss of carbon at the reaction conditions, indicating that a separate, acid-catalyzed degradation reaction of HMF was occurring at these conditions.

Based on the above findings, we propose a reaction network for the acid-catalyzed isomerization of LGO to HMF, and the subsequent reactions of HMF (Figure 2.7). LGO was modeled as existing in equilibrium with DH. The rate of HMF production (r_1) was modeled as being proportional to the combined concentrations of LGO and DH, as discussed previously. HMF undergoes hydration to LA and FA (r_2), as well as thermal (r_4) and acid-catalyzed (r_3) reactions to unaccountable degradation products. The sulfuric acid catalyst was modeled as having a single fully dissociated proton[8].

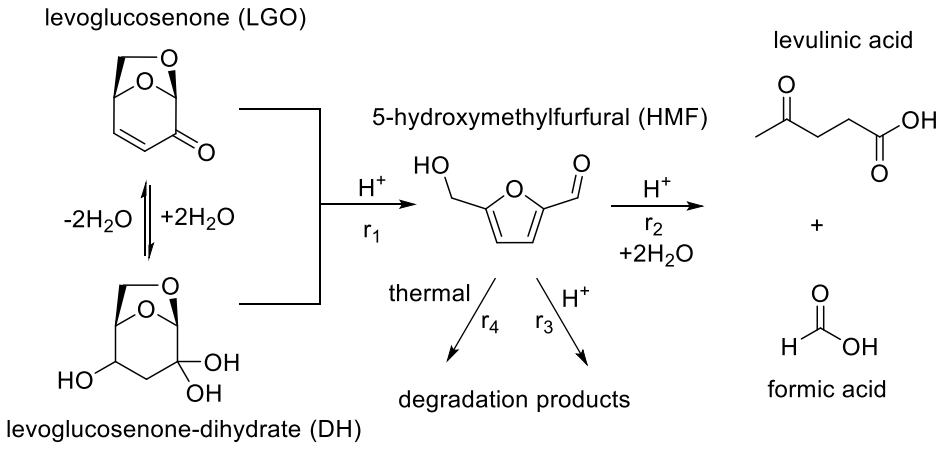

Figure 2.7. *Proposed reaction network for the acid-catalyzed isomerization of LGO to HMF, and subsequent reactions of HMF in water.*

Assuming that first-order kinetics are valid for all reactions in the network, the rates for each step in Figure 2.7 are described by Equations 1-4:

$$r_1 = k_1[\mathrm{LGO} + \mathrm{DH}][H^+] \quad (1)$$

$$r_2 = k_2[\mathrm{HMF}][H^+] \quad (2)$$

$$r_3 = k_3[\mathrm{HMF}][H^+] \quad (3)$$

$$r_4 = k_4[\mathrm{HMF}] \quad (4)$$

The differential equations used in the kinetic model can be found in the Appendix (Section 8.1.2).

As shown in Figure 2.8, the reaction kinetics model describes the data across different reactant concentrations without the need to invoke fractional or higher order rate expressions. Table 2.1 shows the rate constants extracted by the model along with their associated 95% confidence intervals. Note that while the numerical value of k_4^{ref} (5.3E-4 min^{-1}) is an order of magnitude smaller than k_3^{ref} (0.019 L mol^{-1} min^{-1}), the units of these rate constants are different, such that the predicted rates of Steps 3 and 4 are comparable. Accordingly, the thermal degradation of HMF is non-negligible.

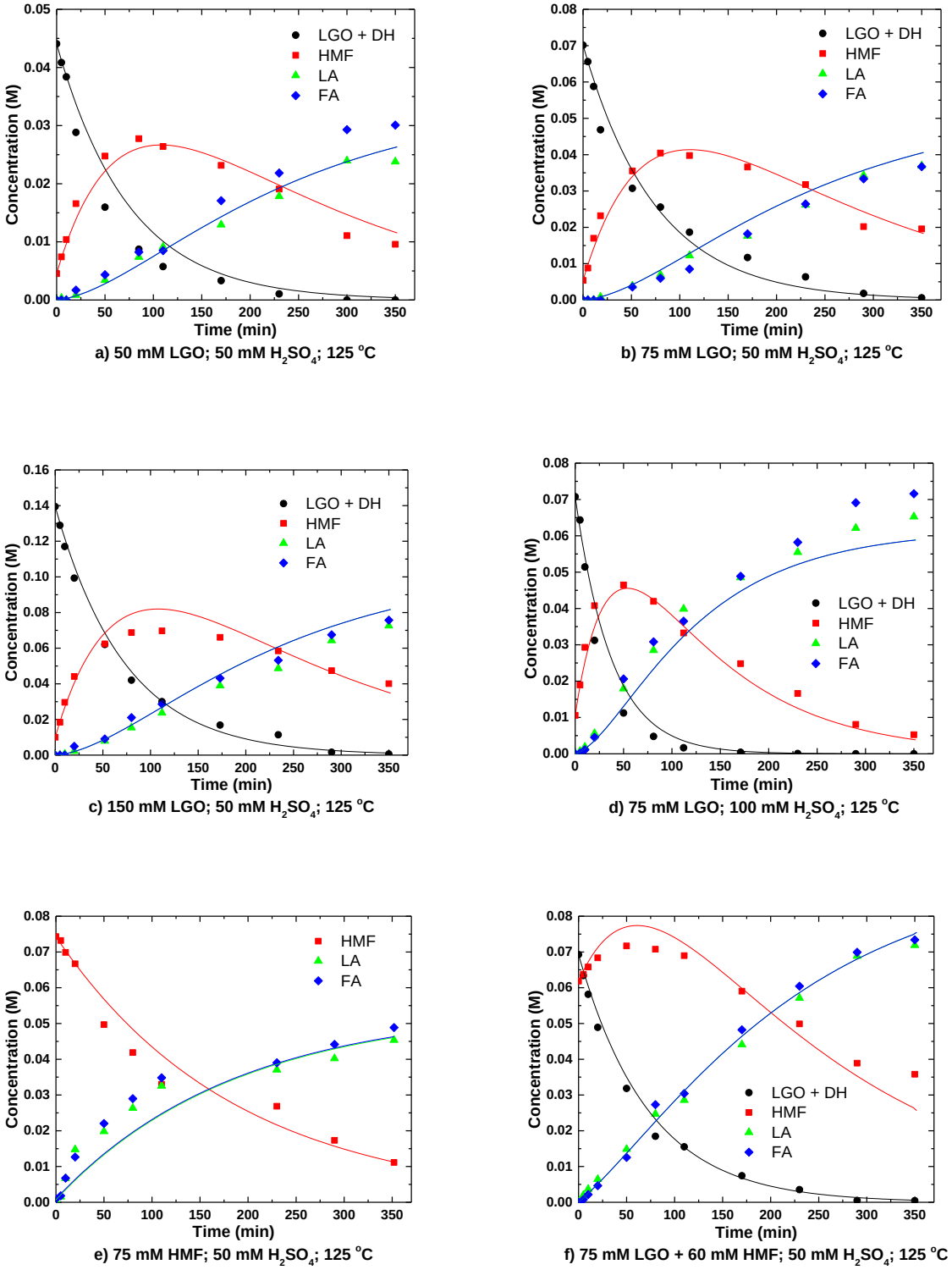

Figure 2.8. *Experimental and model-predicted concentration profiles for the transformation of*

(LGO + DH) to HMF, and subsequent reactions of HMF in water. Solid lines are model-predicted values.

Comparisons of the model-predicted versus experimental carbon balance for reactions of HMF and LGO in water are shown in Figures 7a and 7b, respectively. As seen in Figure 2.9, when LGO is used as a feed, the model under-predicts the carbon loss at early reaction times and accurately predicts the carbon loss at later reaction times. In the case where HMF is used as a feed, however, the model achieves good agreement with experiment across the entire span of the reaction. This behavior indicates that while irreversible degradation reactions are occurring, some fraction of the unidentified species at intermediate reaction times are ultimately converted to products. These unidentified species could potentially be other hydrated derivatives of LGO, or intermediates between LGO and HMF. As seen in Figure 2.9b, the error introduced by this discrepancy is at most about 15%.

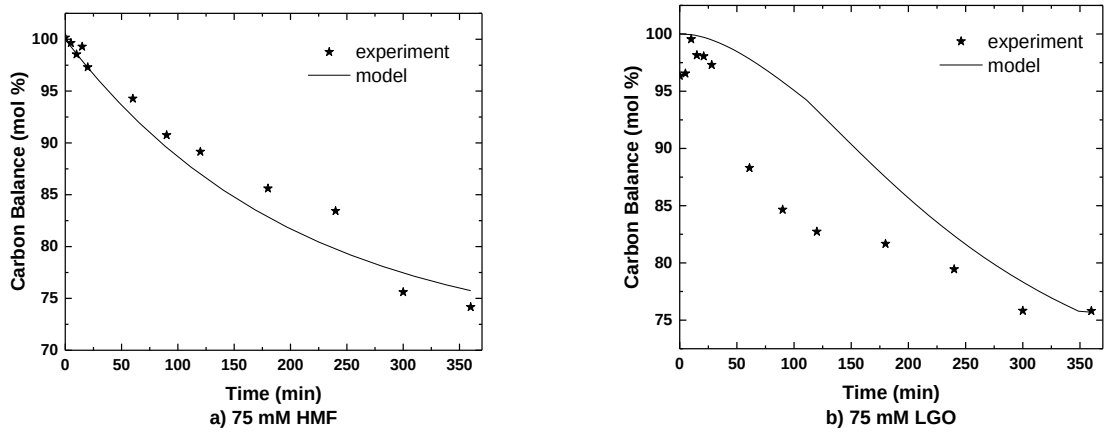

Figure 2.9. *Model-predicted and experimentally determined carbon balance versus time for reaction with (a) HMF and (b) LGO feedstocks. Reaction conditions: 50 mM H_2SO_4 (aq); 125^oC. Solid lines are model-predicted values.*

The temperature dependence of the reaction rates was measured by recasting the rate constants in Equations 1-4 in terms of the Arrhenius relationships below:

$$k_1 = k_1^{ref} \exp\left\{-\frac{E_{a1}}{R}\left(\frac{1}{T}-\frac{1}{T_R}\right)\right\} \qquad (5)$$

$$k_2 = k_2^{ref} \exp\left\{-\frac{E_{a2}}{R}\left(\frac{1}{T}-\frac{1}{T_R}\right)\right\} \qquad (6)$$

$$k_3 = k_3^{ref} \exp\left\{-\frac{E_{a3}}{R}\left(\frac{1}{T}-\frac{1}{T_R}\right)\right\} \qquad (7)$$

$$k_4 = k_4^{ref} \exp\left\{-\frac{E_{a4}}{R}\left(\frac{1}{T}-\frac{1}{T_R}\right)\right\} \qquad (8)$$

where k_i^{ref} is the rate constant for the i^{th} reaction measured at the reference temperature (T_R) of 398 K (125°C), E_{ai} is the activation energy for the i^{th} reaction, T is the reaction temperature in Kelvin, and R is the gas constant. Equations 5-8 were then defined in a separate model, which measured the activation energies by optimizing their values to fit experimental data across four variable temperature experiments between 100-150°C. The results are shown in Figure 2.10, which shows agreement between model and experiment. Table 2.1 summarizes the reaction kinetics parameters measured in this study and their uncertainties.

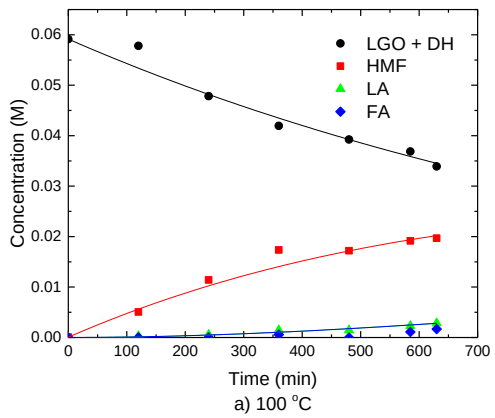

a) 100 °C

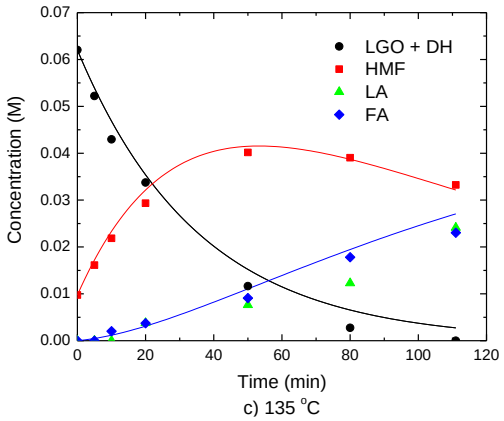

c) 135 °C

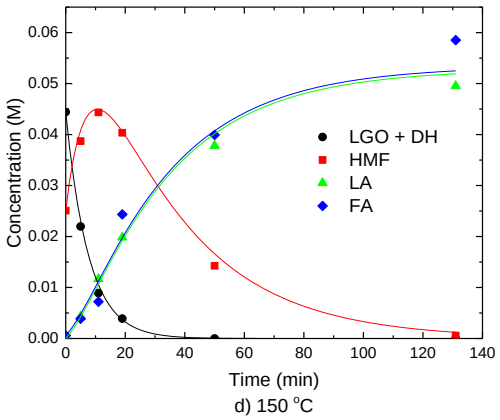

Figure 2.10. *Experimental and model-predicted concentration profiles for variable-temperature experiments. Solid lines are model-predicted values. Reaction conditions: 75 mM LGO, 50 mM H_2SO_4 (aq).*

Table 2.1. *Model-predicted reaction kinetics parameters for the acid-catalyzed isomerization of LGO in water.*

Reaction Step	**Rate constant at T = 125 °C**	**Activation Energy (kJ mol^{-1})**
r_1	0.274 ± 0.012 L mol^{-1} min^{-1}	130.1 ± 4.0
r_2	0.077 ± 0.002 L mol^{-1} min^{-1}	107.7 ± 4.8
r_3	0.019 ± 0.002 L mol^{-1} min^{-1}	102.2 ± 18.0
r_4	4.3E-4 ± 7E-5 min^{-1}	81.0 ± 10.0

Conditions: 100-150°C, 50-100 mM H_2SO_4, 50-150 mM LGO.

As seen in Table 2.1, the activation energy of LGO isomerization (E_{a1}) to HMF is the highest value of all reactions, indicating that the HMF selectivity is maximized at high temperatures and short reaction times. Using the model-predicted reaction kinetics parameters, it is possible to simulate the effects of temperature and reaction time on the maximum obtainable

yield of HMF. The result (Figure 2.11) indicates that a maximum HMF yield of ~76% could be achieved from LGO at a temperature of 220°C in water. However, achieving this yield would require a reaction time of approximately 6 seconds. At a reaction time of 5 minutes, the yield of HMF at 165°C and 50 mM H_2SO_4 is approximately 66%.

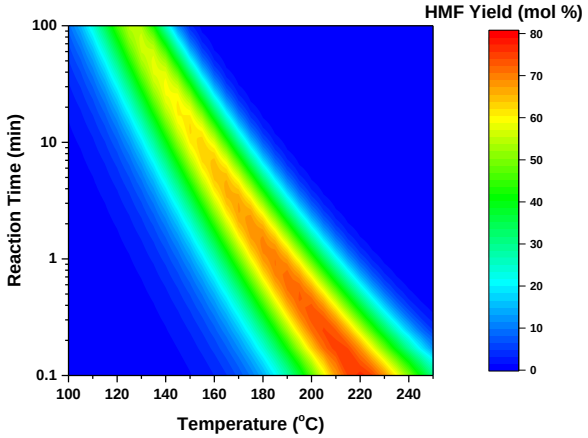

Figure 2.11. *Model-predicted yields of HMF from LGO in water versus temperature and reaction time. Acid strength is held fixed at 50 mM H_2SO_4.*

While the kinetics of LGO isomerization to HMF have not been previously studied in the literature, our results for HMF conversion to LA and FA can be compared to literature reports summarized by Weingarten, et al[7a]. The activation energy for HMF hydration to LA and FA is 95-110 kJ/mol based on the majority of literature reports[7a, b, 9], in agreement with our measurement of 107.7 +/- 4.8 kJ/mol. Weingarten, et al. and Shen, et al. found that the activation energy for HMF degradation to humins over an acid catalyst is approximately 145 kJ/mol[7a, 10], while Girisuta, et al. reported a value of 111 kJ/mol[7b]. Jing, et al. reported an activation energy of 109 kJ/mol for the thermal degradation of HMF in water[11]. In this study, we measured an activation energy of 102.2 +/- 18.0 kJ/mol for catalytic degradation of HMF and an activation energy of 81.0 +/- 10.0 kJ/mol

for thermal degradation of HMF. Our model-predicted activation energy for HMF degradation is on the lower end of the range compared to the literature, most likely because two routes of HMF degradation are incorporated. Both Weingarten, et al. and Girisuta, et al. found that the reaction orders for HMF conversion to LA and FA, as well as HMF degradation, are near unity[7a, b], in agreement with our findings. We note that for the downstream reactions of HMF, while our model is consistent with the reaction kinetics data and is in agreement with results in the literature, it is possible that other models could also fit the HMF conversion data.

2.3.4. Effect of water content on LGO isomerization

The role of water in the isomerization of LGO was investigated by studying the reaction in mixed solvent systems of water and tetrahydrofuran. As shown in Figure 2.12, the yield of HMF plus LA decreases monotonically as the solvent system is changed from water to THF. In pure THF solvent, almost no HMF or LA is observed, and LGO is converted to unidentified products. These results indicate that water plays an important role in the LGO isomerization mechanism. These findings are consistent with our previous work on cellulose dehydration to LGO, in which we suggested that THF inhibits the conversion of LGO to HMF, and that LGO isomerization to HMF could contribute to the selectivity shift from LGO to HMF when water is added to the THF solvent system[2].

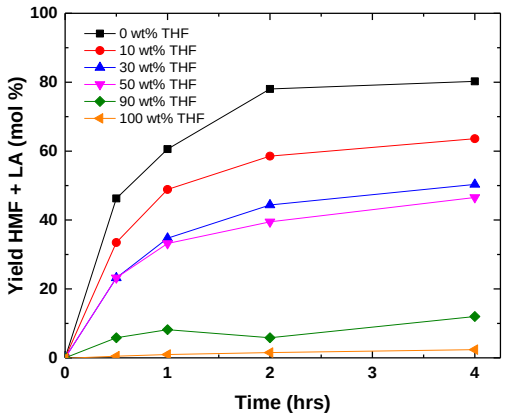

Figure 2.12. *Yield of HMF plus LA versus time in different THF/water solvent systems. Reaction conditions: 55 mM LGO; 50 mM H_2SO_4; 125°C. Solid lines are visual aids.*

2.3.5. Determining the precursor for HMF production.

The observation that water facilitates the LGO isomerization reaction could be interpreted as evidence that DH is the precursor for HMF production. However, we will show that LGO, not DH, is the primary precursor to HMF. Due to the short timescales (<10 min) over which the equilibrium between LGO and DH develops in water at 125°C, it is necessary to identify reaction conditions at which LGO and DH are far from equilibrium during early reaction times. As shown in Figure 2.13, carrying out the reaction in a mixture of 50 wt% of THF in water and lowering the temperature to 100°C shifts the equilibrium between DH and LGO towards LGO, and lengthens the time over which this equilibrium is achieved. Figure 2.14 displays the reaction profile under the same reaction conditions, except starting with a feed which is mostly DH. The carbon balance is near 100% at all times during these experiments, and LA and FA are not observed. Therefore, HMF conversion can be ignored under these conditions. These experiments allow for an analysis of the initial rates of HMF production, LGO consumption, and DH consumption, when LGO and

DH are not near equilibrium.

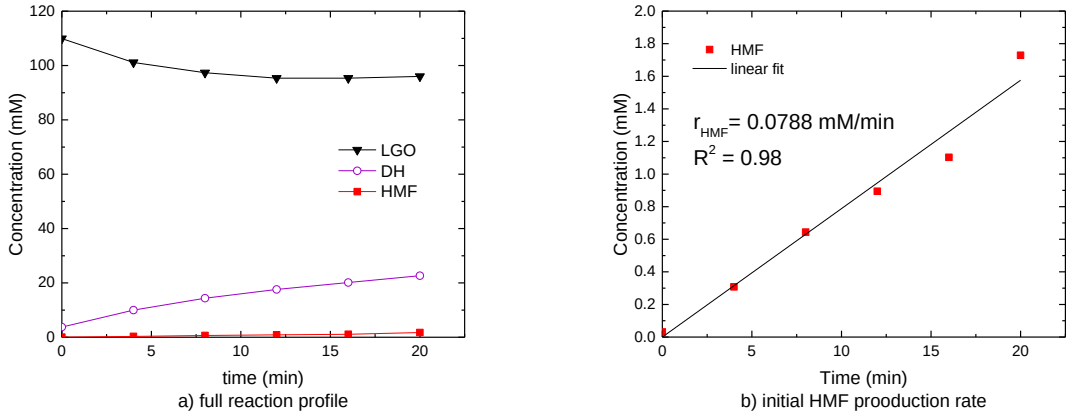

Figure 2.13. *Conversion of an LGO-rich feed to HMF in 50 wt% THF and 50 wt% water. Panels a-b show a single experiment with different scales to aid in visualizing the concentrations of LGO, DH, and HMF over time. Reaction conditions: 109 mM LGO, 4 mM DH; 50 mM H_2SO_4; 100°C. Solid lines are visual aids (a) or linear fits (b).*

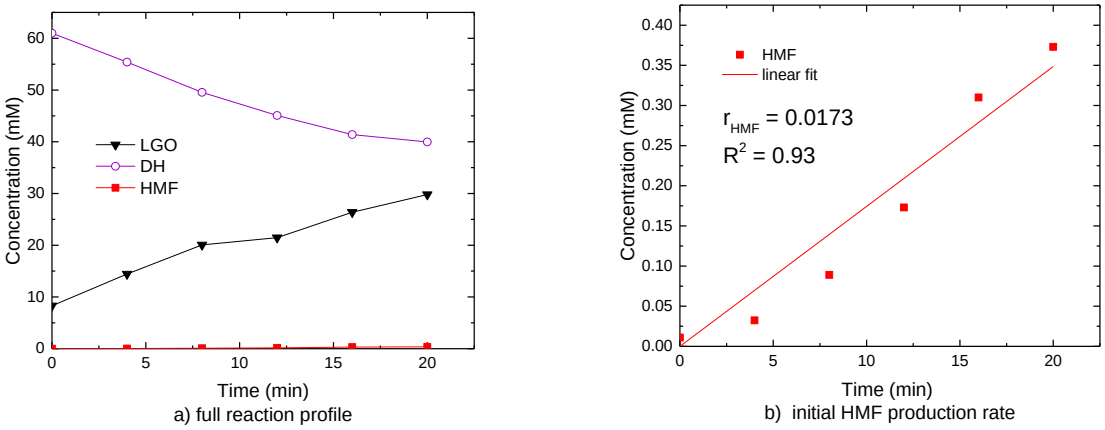

Figure 2.14. *Conversion of a DH-rich feed to HMF in 50 wt% THF and 50 wt% water. Panels a-b show a single experiment with different scales to aid in visualizing the concentrations of LGO,*

DH, and HMF over time. Reaction conditions: 61 mM DH, 8 mM LGO; 50 mM H_2SO_4; 100°C. Solid lines are visual aids (a) or linear fits (b).

Assuming that HMF production is first order in either LGO or DH, the initial rate of HMF production divided by the concentration of that species should be equal to the same value (i.e., the rate constant) in both experiments. When LGO was assumed to be the primary precursor to HMF (Figure 2.13), the values of these rate constants were within 10% for the two experiments (Table 2.2). In contrast, the values of the computed rate constants were different by an order of magnitude when DH was assumed to be the primary precursor (Figure 2.14). Therefore, we conclude that LGO is isomerized directly to HMF.

Table 2.2. *First-order rate constants for HMF production from the initial rate analyses*

	LGO-Rich Feed (Figure 2.13)	**DH-Rich Feed (Figure 2.14)**
$\mathbf{r_{HMF}/[LGO]_{average}}$	8.0E-4 L mol^{-1} min^{-1}	8.7E-4 L mol^{-1} min^{-1}
$\mathbf{r_{HMF}}$ **/ [DH]$_{average}$**	5.3E-3 L mol^{-1} min^{-1}	3.6E-4 L mol^{-1} min^{-1}

2.3.6. Proposed reaction mechanism.

Having shown that hydration of LGO to DH is not necessary for HMF production, we now revisit the finding that LGO isomerization is facilitated by water (Figure 2.12). This observation is consistent with an intermediate proposed by Shafizadeh, et al. involving hydration of the anhydro-bridge prior to ring rearrangement to form HMF[1a]. In agreement with this hypothesis, Kawamoto, et al. found that LGO conversion to furfural in a sulfolane solvent over a sulfuric acid catalyst was promoted by the presence of water[1b]. The authors proposed a mechanism passing through the same hydrated intermediate as that posited by Shafizadeh.

Because the resulting hydrated intermediate resembles glucose, we interpret the subsequent ring rearrangement chemistry by analogy to glucose isomerization. Both the isomerization of glucose to fructose and the isomerization of LGO to HMF involve transformations from a 6-membered ring to a 5-membered ring. However, LGO isomerization proceeds over a Brønsted acid catalyst, while glucose isomerization requires a Lewis acid catalyst. In the case of glucose isomerization, the cyclic pyranose form of glucose exists in equilibrium with an acyclic aldehyde form in solution[6c]. The Lewis acid facilitates a C_1-C_2 hydride shift, converting the aldose into a ketose, which can then ring-close to form the cyclic furanose form of fructose[6a]. The fact that LGO isomerization does not require a Lewis acid suggests that no hydride shift is required for this mechanism to proceed.

We have proposed a mechanism for LGO isomerization consistent with these observations, shown in Figure 2.15. First, the anhydro-bridge of LGO is broken to form the hydrated intermediate, as proposed by Shafizadeh and Kawamoto. Next, this hydrated intermediate is ring-opened to an acyclic species containing both ketone and aldehyde functionalities. This species can then be ring-closed at the C_2 position to form the 5-membered ring of HMF. Because this species already contains a carbonyl group at the C_2 position, no hydride shift is required and therefore no Lewis acid is required.

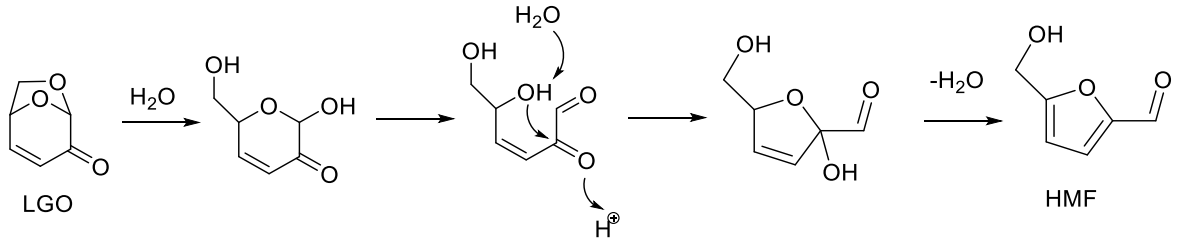

Figure 2.15. *Proposed mechanism for LGO isomerization to HMF*.

The acyclic intermediate shown in Figure 2.15 resembles 3-deoxyglucosone, which was shown by Bols and co-workers to be converted to HMF in >90% yield over a sulfuric acid catalyst[12]. Because 3-deoxyglucosone contains ketone and aldehyde functionalities in the same relative positions as the acyclic intermediate proposed in Figure 2.15, it is possible that this intermediate would react in a similar fashion as 3-deoxyglucosone.

The mechanism in Figure 2.15 is similar to a mechanism for glucose conversion to HMF, with LGO as a side-product, proposed by Bell and co-workers[13]. The mechanism by Bell and co-workers involves glucose conversion to the same acyclic intermediate as the one shown Figure 2.15, followed by parallel pathways for the production of HMF or LGO from this intermediate. This mechanism can be made consistent with Figure 2.15 if the reaction from the acyclic intermediate to LGO is reversible, allowing for ring-opening of LGO to form this intermediate followed by ring closure to form HMF. Note that the study by Bell and co-workers used a solid acid catalyst and ionic liquid solvent, while our study was conducted over a sulfuric acid catalyst in an aqueous solvent.

2.4. Conclusion

We have elucidated a reaction network for acid-catalyzed LGO isomerization in aqueous solvent systems and developed a reaction kinetics model which describes the experimental data. LGO is isomerized to HMF in the presence of a Brønsted acid catalyst, and HMF is further converted to LA and FA. LGO exists in equilibrium with a dihydrated species at reaction conditions. The main sources of carbon loss are thermal and catalytic degradation of HMF. Within the range of experimental conditions studied, the yield of HMF from LGO can be maximized at higher temperatures and shorter reaction times. The yields of HMF and LA decrease monotonically

as the THF/water solvent ratio increases, suggesting that water plays a role in the LGO isomerization reaction. Using a mixed THF/water solvent system and lower temperature to slow the equilibration of LGO and DH, analysis of the initial rate of HMF production showed that HMF is produced primarily from LGO and is not produced from DH. These results are consistent with a mechanism for LGO isomerization which proceeds via hydration of the anhydro–bridge, followed by ring rearrangement analogous to the isomerization of glucose to fructose. Our understanding of the factors which affect LGO isomerization to HMF could aid in designing catalytic processes to produce LGO from cellulose more efficiently, improving the economic viability of renewable chemicals production from lignocellulosic biomass.

2.5. References

1. (a) Shafizadeh, F.; Furneaux, R. H.; Stevenson, T. T., Some reactions of levoglucosenone. *Carbohydrate Research* **1979,** *71* (1), 169-191; (b) Kawamoto, H.; Saito, S.; Hatanaka, W.; Saka, S., Catalytic pyrolysis of cellulose in sulfolane with some acidic catalysts. *J Wood Sci* **2007,** *53* (2), 127-133.
2. Cao, F.; Schwartz, T. J.; McClelland, D. J.; Krishna, S. H.; Dumesic, J. A.; Huber, G. W., Dehydration of cellulose to levoglucosenone using polar aprotic solvents. *Energy & Environmental Science* **2015,** *8* (6), 1808-1815.
3. (a) Namal De Silva, W. I.; Ritter, J. C.; Stauffer, C. S. Production of hydroxymethylfurfural from levoglucosenone. US8884036B2, 2014; (b) Qi, L.; Mui, Y. F.; Lo, S. W.; Lui, M. Y.; Akien, G. R.; Horváth, I. T., Catalytic Conversion of Fructose, Glucose, and Sucrose to 5-(Hydroxymethyl)furfural and Levulinic and Formic Acids in γ-Valerolactone As a Green Solvent. *ACS Catalysis* **2014,** *4* (5), 1470-1477.
4. (a) Román-Leshkov, Y.; Barrett, C. J.; Liu, Z. Y.; Dumesic, J. A., Production of dimethylfuran for liquid fuels from biomass-derived carbohydrates. Nature Publishing Group: 2007; Vol. 447, pp 982-985; (b) Braden, D. J.; Henao, C. A.; Heltzel, J.; Maravelias, C. C.; Dumesic, J. A., Production of liquid hydrocarbon fuels by catalytic conversion of biomass-derived levulinic acid. *Green Chemistry* **2011,** *13* (7), 1755-1765.
5. (a) Buntara, T.; Noel, S.; Phua, P. H.; Melián-Cabrera, I.; de Vries, J. G.; Heeres, H. J., Caprolactam from Renewable Resources: Catalytic Conversion of 5-Hydroxymethylfurfural into Caprolactone. *Angewandte Chemie International Edition* **2011,** *50* (31), 7083-7087; (b) Xiao, B.; Zheng, M.; Li, X.; Pang, J.; Sun, R.; Wang, H.; Pang, X.; Wang, A.; Wang, X.; Zhang, T., Synthesis of 1,6-hexanediol from HMF over double-layered catalysts of Pd/SiO2 + Ir-ReOx/SiO2 in a fixed-bed reactor. *Green Chemistry* **2016,** *18* (7), 2175-2184.
6. (a) Román-Leshkov, Y.; Moliner, M.; Labinger, J. A.; Davis, M. E., Mechanism of Glucose Isomerization Using a Solid Lewis Acid Catalyst in Water. *Angewandte Chemie International Edition* **2010,** *49* (47), 8954-8957; (b) Bermejo-Deval, R.; Assary, R. S.; Nikolla, E.; Moliner, M.; Román-Leshkov, Y.; Hwang, S.-J.; Palsdottir, A.; Silverman, D.; Lobo, R. F.; Curtiss, L. A.; Davis, M. E., Metalloenzyme-like catalyzed isomerizations of sugars by Lewis acid zeolites. *Proceedings of the National Academy of Sciences* **2012,** *109* (25), 9727-9732; (c) Delidovich, I.; Palkovits, R., Catalytic Isomerization of Biomass-Derived Aldoses: A Review. *ChemSusChem* **2016,** *9* (6), 547-561.
7. (a) Weingarten, R.; Cho, J.; Xing, R.; Conner, W. C.; Huber, G. W., Kinetics and Reaction Engineering of Levulinic Acid Production from Aqueous Glucose Solutions. *ChemSusChem* **2012,** *5* (7), 1280-1290; (b) Girisuta, B.; Janssen, L. P. B. M.; Heeres, H. J., A kinetic study on the decomposition of 5-hydroxymethylfurfural into levulinic acid. *Green Chemistry* **2006,** *8* (8), 701-709; (c) Choudhary, V.; Mushrif, S. H.; Ho, C.; Anderko, A.; Nikolakis, V.; Marinkovic, N. S.; Frenkel, A. I.; Sandler, S. I.; Vlachos, D. G., Insights into the Interplay of Lewis and Brønsted

Acid Catalysts in Glucose and Fructose Conversion to 5-(Hydroxymethyl)furfural and Levulinic Acid in Aqueous Media. *Journal of the American Chemical Society* **2013,** *135* (10), 3997-4006.
8. Knopf, D. A.; Luo, B. P.; Krieger, U. K.; Koop, T., Thermodynamic Dissociation Constant of the Bisulfate Ion from Raman and Ion Interaction Modeling Studies of Aqueous Sulfuric Acid at Low Temperatures. *The Journal of Physical Chemistry A* **2003,** *107* (21), 4322-4332.
9. Girisuta, B.; Janssen, L. P. B. M.; Heeres, H. J., Kinetic Study on the Acid-Catalyzed Hydrolysis of Cellulose to Levulinic Acid. *Industrial & Engineering Chemistry Research* **2007,** *46* (6), 1696-1708.
10. Shen, J.; Wyman, C. E., Hydrochloric acid-catalyzed levulinic acid formation from cellulose: data and kinetic model to maximize yields. *AIChE Journal* **2012,** *58* (1), 236-246.
11. Jing, Q.; LÜ, X., Kinetics of Non-catalyzed Decomposition of Glucose in High-temperature Liquid Water. *Chinese Journal of Chemical Engineering* **2008,** *16* (6), 890-894.
12. Jadhav, H.; Pedersen, C. M.; Sølling, T.; Bols, M., 3-Deoxy-glucosone is an Intermediate in the Formation of Furfurals from D-Glucose. *ChemSusChem* **2011,** *4* (8), 1049-1051.
13. Chidambaram, M.; Bell, A. T., A two-step approach for the catalytic conversion of glucose to 2,5-dimethylfuran in ionic liquids. *Green Chemistry* **2010,** *12* (7), 1253-1262.

Chapter 3. Levoglucosenone Hydrogenation over Metal Catalysts

3.1. Introduction

As shown in Figure 1.1, LGO can be hydrogenated into a wide variety of chemicals. At low temperatures (25-60^{o}C) over a Pd/C catalyst, LGO is hydrogenated into Cyrene, a non-toxic solvent with similar properties to environmentally harmful solvents such as N-methylpyrrolidone.[1] DuPont has reported that LGO can be hydrogenated to levoglucosanol over a Pt/C catalyst.[2] Lgol contains three chiral centers and is a potential platform molecule for chiral products relevant to the fine chemicals and pharmaceuticals industry.[3] As will be shown in Chapter 4, Lgol is a precursor to downstream polymer precursors THFDM, 1256-HT, and 16-HDO.

Herein, we study the hydrogenation of LGO over supported palladium catalysts. We elucidate the reaction network and demonstrate catalysts and conditions suitable to produce Cyrene or Lgol. We also investigate the diastereoselectivity of Cyrene hydrogenation to Lgol. Our results provide insight into the mechanism of LGO hydrogenation, and provide directions for designing catalytic systems to optimize the production of renewable chemicals from lignocellulosic biomass.

3.2. Experimental Methods

LGO (98%, Apollo Scientific), Cyrene (99%, Apollo Scientific), THF stabilized with butylated hydroxytoluene (BHT) (99.9%, Acros Organics), and $Pd(NO_3)$ solution (10% in 10% HNO_3, Sigma Aldrich), were used as received. 5% Pd/C and low-soda γ-Al_2O_3 were purchased from Strem Chemicals. 1% Pd/C and Davisil SiO_2, were purchased from Sigma Aldrich.

Palladium catalysts supported on Al_2O_3 were synthesized by incipient wetness impregnation (IWI) of a 10% $Pd(NO)_3$ precursor onto the appropriate support. After impregnation,

catalysts were dried overnight in an oven at 110°C. The catalysts were then calcined in flowing air at 400°C followed by reduction in flowing H_2 at 260°C and passivation in 1% O_2/He at room temperature.

CO chemisorption was carried out in a Micromeritics ASAP2020C instrument. 100 mg of the catalyst was loaded into a glass reactor. Catalysts were degassed followed by *in situ* reduction in flowing H_2 at 400°C and sample evacuation. The CO chemisorption measurement was conducted at 35°C, and repeated after subsequent evacuation to acquire the reversible CO uptake. The irreversible CO uptake was calculated by subtracting the total uptake in the first measurement from the reversible uptake in the second measurement.

Reactions were carried out in 45 or 75 mL Parr Hastelloy high-pressure batch reactors. A magnetic stir bar and appropriate amount of catalyst and feedstock were added to the reactor. The reactor was purged four times with 500 psi H_2, followed by pressurizing to 500 psi H_2. The heat-up time was 10-15 minutes. The reaction mixture was stirred at 750 rpm. After the appropriate time, the reactor was quenched in ice water, depressurized, and opened. The reaction products were filtered using a 0.2 □m PTFE (polytetrafluoroethylene) syringe filter prior to analysis. For LGO hydrogenation at low temperature (40°C), catalysts were pre-reduced at 100°C in flowing H_2 and loaded into Parr reactors in a glovebox to avoid exposure to air. For reactions at higher temperature (>40°C), passivated catalysts were loaded directly into the reactor without pre-reduction. Dip-tube experiments were carried out with 60 mL reaction mixture in a 75 mL Parr batch reactor equipped with a 1/8-inch dip-tube. During sampling, 0.6 mL was purged followed by 0.6 mL collected for analysis. Purging was done to remove dip-tube liquid collected at earlier reaction times. A stainless steel filter (500-mesh) was used to prevent solids from entering the dip-tube. After each sample, the reactor was re-pressurized with H_2.

The Pd/Al_2O_3 catalysts used for LGO and Cyrene conversion were each recycled (without reactivation) to study catalyst stability. For LGO hydrogenation, the catalyst used in the experiment shown in Figure 3.1 was recycled in situ by removing half (30 mL) of the product solution contained in the reactor, then pumping in 30 mL of a doubly concentrated LGO/THF feedstock using an HPLC pump. The reaction was then carried out a second time. This strategy avoided exposure of the catalyst to air. We note that with this recycling method, the product is present at half of its initial concentration at the start of the reaction over the recycled catalyst. It is possible that product adsorption on the catalyst surface could affect the reaction rate.

Products were quantified using a Shimadzu Gas Chromatograph (GC) equipped with a Flame Ionization Detector (FID) with liquid injection. A Restek RTX-VMS capillary column (Length: 30 m, ID: 0.25 mm, film thickness: 1.4 μm) was used. The injection port and FID were maintained at 240°C. The injection volume was 1 μL and a split ratio of 50 was used. The column temperature ramp was as follows: hold 1 min at 40°C, ramp 10°C/min to 180°C, ramp 3°C/min to 240°C, hold 5 min at 240°C.

Quantitative ^{13}C NMR spectra were collected on a Bruker Avance 500 MHz spectrometer at room temperature, using an inverse-gated decoupling pulse sequence with a 30^o pulse. The ^{13}C NMR spectra were absolute-referenced to the associated ^1H NMR spectra. Unless otherwise indicated, 256 scans were used, with an acquisition time of 1 sec and a relaxation delay of 15 sec. Samples were prepared for analysis by evaporating the THF solvent from 5-10 mL of sample, then adding 1-3 mL of d_6-DMSO (dimethylsulfoxide). ^{13}C NMR spectra are provided in the Appendix, Section 8.2.1 .

3.3. Results and Discussion

3.3.1. Hydrogenation of LGO to Cyrene

LGO hydrogenation to Cyrene was carried out over a 0.4 wt% Pd/Al_2O_3 catalyst. THF was selected as the reaction solvent because this solvent was effective in our previous work for cellulose dehydration to LGO.[4] As shown in Figure 3.1, at low temperature (40°C), LGO was hydrogenated to Cyrene in 100% selectivity. These results agree with the findings of Clark et al., who observed quantitative conversion of LGO to Cyrene over a Pd/C catalyst at room temperature.[1a] Levoglucos*e*nol, the unsaturated alcohol resulting from selective hydrogenation of the C=O bond of LGO, was not observed at any time. Similarly, Ronzon et al. found that complete C=C bond hydrogenation occurred prior to C=O hydrogenation in the hydrogenation of 2-cyclohexenone (a molecule with the same 2-enone functionality as is present in LGO) over Rh/SiO_2 catalysts.[5] In general, hydrogenation of C=C bonds is thermodynamically favored compared to hydrogenation of C=O bonds.[6] Based on the data in Figure 3.1, the initial turnover frequency (TOF) for LGO hydrogenation at these conditions was 345 mol Cyrene per mol surface Pd per min. Catalyst recycling data suggest that this catalyst undergoes deactivation under these conditions (Figure 3.2).

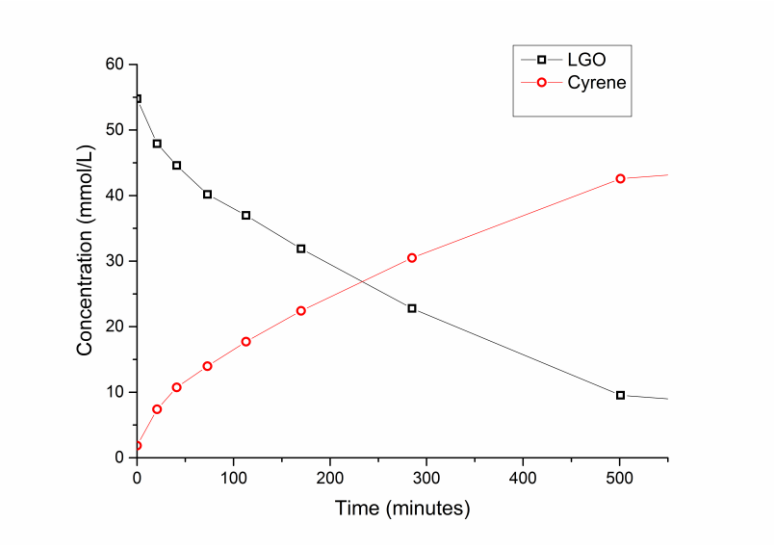

Figure 3.1. *Hydrogenation of LGO over 1.75 mg 0.4 wt% Pd/Al2O3 (17.5 mg diluted 10x in SiO_2) in a batch reactor with dip-tube sampling. Conditions: 40°C, 500 psi H_2, 60 mL 55 mM LGO feed in THF. Solid lines between points are visual aids.*

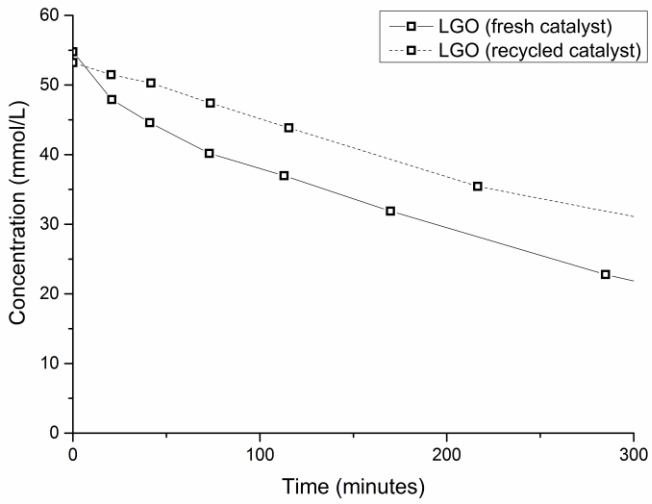

Figure 3.2. *Catalyst recycling test for the hydrogenation of LGO over 1.75 mg 0.4 wt% Pd/Al_2O_3 (17.5 mg diluted 10x in SiO_2) in a batch reactor with dip-tube sampling. Conditions: 40°C, 500 psi H_2, 60 mL 55 mM LGO feed in THF. Lines between points are visual aids.*

3.3.2. Hydrogenation of Cyrene to Lgol

Cyrene hydrogenation to Lgol was investigated at higher temperature (100°C) and at higher catalyst amounts compared to LGO hydrogenation. As shown in Figure 3.3, under these conditions Cyrene was hydrogenated to Lgol in 100% selectivity. Based on the data in Figure 3.3, the initial turnover frequency for Cyrene hydrogenation at these conditions was 8.5 mol Lgol per mol surface Pd per min. Catalyst recycling data suggest that this catalyst undergoes more significant deactivation under these conditions compared to the case of LGO hydrogenation (Figure 3.4). An excess of the threo-Lgol isomer was produced over the erythro-Lgol isomer (threo/erythro [t/e] = 4.6), and the stereoisomer ratio was not a function of conversion. Augustine argued that in the stereoselective hydrogenation of prochiral ketones, hydrogen atom addition from the less hindered direction should be kinetically favored.[7] We hypothesize that the observed excess of threo-Lgol results from preferential hydrogen atom addition to the ketone group of Cyrene from the opposite side as the anhydro-bridge.[8] Similarly, Zanardi et al. found that the C=O bond of LGO was selectively reduced to the threo-alcohol when sodium borohydride was used as the reductant.[3] Based on our results, we have proposed the reaction network for LGO hydrogenation to Lgol shown in Figure 3.5.

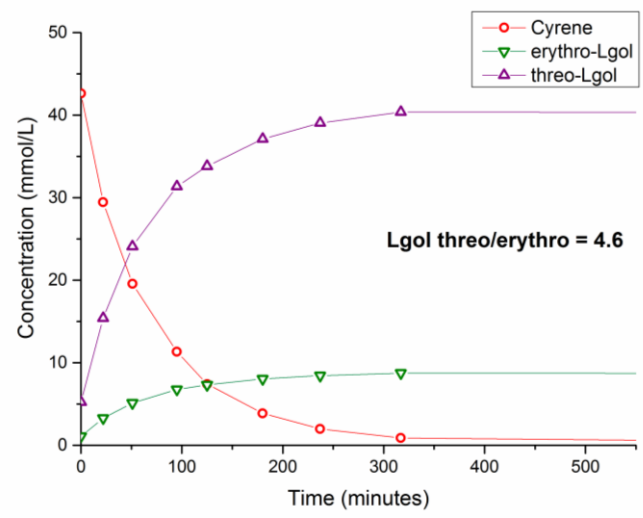

Figure 3.3. *Hydrogenation of Cyrene over 150 mg 0.4 wt% Pd/Al_2O_3 in a batch reactor with dip-tube sampling. Conditions: 100°C, 500 psi H_2, 60 mL 55 mM Cyrene in THF feed. Solid lines between points are visual aids.*

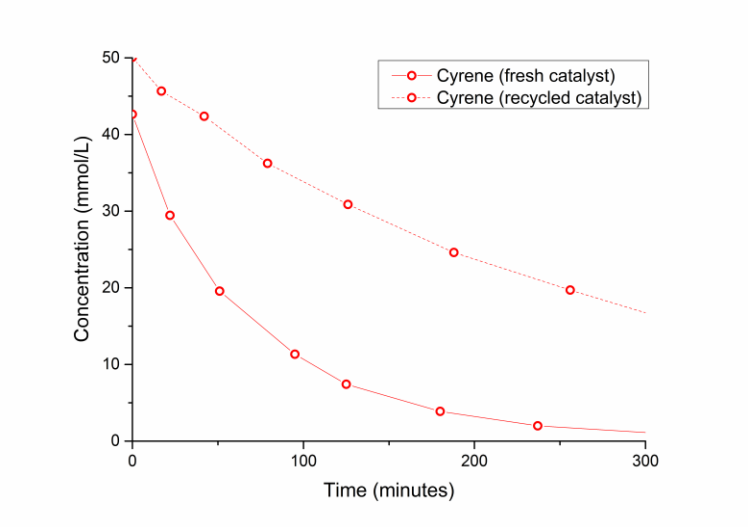

Figure 3.4. *Catalyst recycling test for the hydrogenation of Cyrene over 150 mg 0.4 wt% Pd/Al_2O_3 in a batch reactor with dip-tube sampling. Conditions: 100°C, 500 psi H_2, 60 mL 55 mM Cyrene in THF feed. Lines between points are visual aids.*

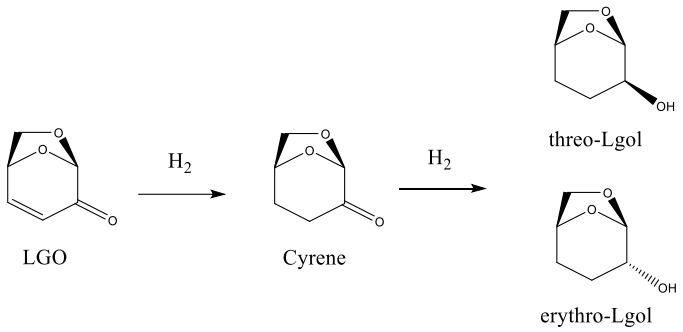

Figure 3.5. *Proposed reaction network for LGO hydrogenation.*

The ratio of threo-Lgol to erythro-Lgol in Cyrene hydrogenation for different supported palladium catalysts is shown in Table 3.1. While the conversion values were different for the different experiments in Table 3.1, Figure 3.3 indicates that the stereoselectivity does not depend on conversion. Cyrene hydrogenation over a 1 wt% Pd/C catalyst resulted in t/e = 2.3, while hydrogenation over a 0.4 wt% Pd/Al_2O_3 catalyst resulted in t/e = 4.6. Since the stereoisomer ratio varies with the catalyst used, it is governed by kinetics rather than thermodynamics. The stereoisomer ratio is a function of the catalyst support, as indicated by the stereoisomer ratio over 1% and 5% Pd/C catalysts (1.7-2.3) versus 0.4% and 5% Pd/Al_2O_3 catalysts (4.6-4.7) and the 1% Pd/SiAl catalyst (3.5). Comparing 0.4 wt% Pd/Al_2O_3 (~2 nm particles, as shown in Table 8.1 in the Appendix) with 5 wt% Pd/Al_2O_3 (~10 nm particles), the stereoisomer ratios were similar, suggesting that the stereoisomer ratio is not affected by changes in the particle size. Additionally, as shown in Table 3.1, the stereoisomer ratios over the 0.4 wt% Pd/Al_2O_3 were comparable at temperatures of 100°C and 150°C. This result suggests that the apparent activation energies for threo-Lgol and erythro-Lgol formation are similar. While the stereoisomer ratio was observed to change with the choice of support, the underlying reason for this dependence is not known at present.

Table 3.1. *Cyrene Hydrogenation –Stereoisomer Ratio*

Catalyst	**Temperature [°C]**	**Conversion [%]**	**Lgol Isomer Ratio (t/e)**
1% Pd/C	100	71	2.3
5% Pd/C	100	100	1.7
0.4% Pd/Al_2O_3	100	0-100*	4.6
0.4% Pd/Al_2O_3	150	100	4.4
5% Pd/Al_2O_3	100	100	4.7
1% Pd/SiAl	100	95	3.5

*Conditions: 500 psi H_2, 10 mL 55 mM Cyrene in THF feed, 50 mg cat, 3h reaction time. *Taken from Figure 3.3.*

3.4. Conclusions

We have shown that the C=C bond of LGO can be selectively hydrogenated to Cyrene at low temperature (40°C), with the C=O bond further hydrogenated to two stereoisomers of Lgol at higher temperatures (100°C). An excess of the threo-Lgol isomer is favored over supported Pd catalysts across multiple particle sizes and temperatures, and the stereoisomer ratio is kinetically controlled. The excess of threo-Lgol over erythro-Lgol is likely due to a steric hindrance effect induced by the prochiral anhydro- bridge group.

3.5. References

1. (a) Sherwood, J.; De bruyn, M.; Constantinou, A.; Moity, L.; McElroy, C. R.; Farmer, T. J.; Duncan, T.; Raverty, W.; Hunt, A. J.; Clark, J. H., Dihydrolevoglucosenone (Cyrene) as a bio-based alternative for dipolar aprotic solvents. *Chemical Communications* **2014,** *50* (68), 9650-9652; (b) De bruyn, M.; Fan, J.; Budarin, V. L.; Macquarrie, D. J.; Gomez, L. D.; Simister, R.; Farmer, T. J.; Raverty, W. D.; McQueen-Mason, S. J.; Clark, J. H., A new perspective in bio-refining: levoglucosenone and cleaner lignin from waste biorefinery hydrolysis lignin by selective conversion of residual saccharides. *Energy & Environmental Science* **2016,** *9* (8), 2571-2574; (c) Zhang, J.; White,

G.; Ryan, M.; Hunt, A. J.; Katz, M. J., Dihydrolevoglucosenone (Cyrene) as a green alternative to N,N-dimethylformamide(DMF) in MOF synthesis. *ACS Sustainable Chemistry & Engineering* **2016**.

2. Allgeier, A. M.; Namal De Silva, W. I.; Korovessi, E.; Menning, C. A.; Ritter, J. C.; Sengupta, S. K.; Stauffer, C. S. Process for preparing 1,6-hexanediol. US 8865,940 B2, 2014.

3. Zanardi, M. M.; Suárez, A. G., Synthesis of a simple chiral auxiliary derived from levoglucosenone and its application in a Diels–Alder reaction. *Tetrahedron Letters* **2009,** *50* (9), 999-1002.

4. Cao, F.; Schwartz, T. J.; McClelland, D. J.; Krishna, S. H.; Dumesic, J. A.; Huber, G. W., Dehydration of cellulose to levoglucosenone using polar aprotic solvents. *Energy & Environmental Science* **2015,** *8* (6), 1808-1815.

5. Ronzón, E.; Del Angel, G., Effect of rhodium precursor and thermal treatment on the hydrogenation of 2-cyclohexenone on Rh/SiO2 Catalysts. *Journal of Molecular Catalysis A: Chemical* **1999,** *148* (1–2), 105-115.

6. Mäki-Arvela, P.; Hájek, J.; Salmi, T.; Murzin, D. Y., Chemoselective hydrogenation of carbonyl compounds over heterogeneous catalysts. *Applied Catalysis A: General* **2005,** *292*, 1-49.

7. Augustine, R. L., Selective heterogeneously catalyzed hydrogenations. *Catalysis Today* **1997,** *37* (4), 419-440.

8. Shafizadeh, F.; Furneaux, R. H.; Stevenson, T. T., Some reactions of levoglucosenone. *Carbohydrate Research* **1979,** *71* (1), 169-191.

Chapter 4. Levoglucosanol Hydrogenolysis to Tetrahydrofurandimethanol over Metal-Acid Catalysts

4.1. Introduction

In this chapter, we investigate the hydrogenolysis of Lgol (produced from LGO, as discussed in Chapter 3) to THFDM over bifunctional Pt/SiAl and Pd/SiAl catalysts. DuPont has reported that Lgol can be converted to THFDM in 84% yield over a Pt/C catalyst, but the mechanism for this transformation is unclear.[1] THFDM can be further upgraded to 16-HDO in >80% yield using a bifunctional catalyst that contains metal and acid sites.[2] THFDM is an α,ω-diol with the potential to be a polymer precursor similar to existing α,ω-diols in the market.[3] 16-HDO is a commodity chemical used in polyurethanes, coatings, and adhesives.[2c, 4] While the biomass-derived intermediate HMF can also be hydrogenated into THFDM and 16-HDO,[2c, 5] LGO upgrading could provide a new route to these chemicals, and we will also show that different THFDM cis/trans ratios can be produced from LGO than from HMF.

The conversion of Lgol to THFDM is a mechanistically complex reaction involving cleavage of two C-O bonds, the formation of a new C-O bond in the 5-membered ring, and hydrogenation. In this study, the reaction network for Lgol conversion to THFDM is determined based on analysis of the selectivity versus conversion and the reactivity of key intermediates, to identify series and parallel reaction pathways. ^{13}C-radio labeling and analysis of the relationship between reactant and product stereochemistry are used to probe the ring rearrangement mechanism. The catalyst stability and reaction kinetics (activation energy, and reaction orders with respect to Lgol and H_2) are measured in a continuous flow reactor. The effect of metal loading and

metal-acid site proximity on reactivity are studied to understand the role of metal and acid sites in kinetically relevant steps and in avoiding degradation reactions. First principles simulations are used to compute the energetics of the proposed reaction intermediates to complement the experimental results.

4.2. Experimental Methods

Lgol was prepared via quantitative hydrogenation of Cyrene (99%, Apollo Scientific or Circa Group), as described in Chapter 3. Cyrene in THF solvent was hydrogenated over a 5% Ru/C catalyst (Strem Chemicals) at 60°C at a pressure of 750 psi H_2 until complete conversion was achieved. THFDM (98%, Alfa Chemicals), THF stabilized with BHT (99.9%, Sigma Aldrich), $^{13}C_1$-labeled glucose (99% isotopic purity), and $Pt(NH_3)_4(NO_3)_2$ solution (99%, Strem Chemicals), were used as received. Grade 135 amorphous SiAl and Davisil grade SiO_2 were purchased from Sigma Aldrich.

Metal catalysts supported on SiAl were synthesized by incipient wetness impregnation followed by calcination in air at 400 °C (the Ru/SiAl catalyst was not calcined, to avoid formation of volatile RuO_4), reduction in H_2 at 260 °C, and passivation in 1% O_2/Ar at room temperature. Catalyst precursors used: Pt: platinum tetraamine nitrate. Pd: palladium nitrate. Rh: rhodium chloride hydrate. Ru: ruthenium nitrosyl nitrate. The Zeolite Y catalyst support (Zeolyst, Si/Al = 30) was calcined in air at 600°C prior to use. After incipient wetness impregnation of platinum tetraamine nitrate, the catalyst was calcined for 2h at 300°C in air, followed by reduction at 450°C in H_2 and passivation in 1% O_2/Ar. For experiments using the bare SiAl support, the support was calcined at 400°C in flowing air prior to use.

CO chemisorption was conducted on a Micromeritics ASAP2020C instrument. 100-500 mg catalyst was loaded into a glass reactor. Catalysts were degassed, then reduced in situ at 400°C in flowing H_2 followed by sample evacuation. The chemisorption measurement was carried out at 35°C, and repeated after subsequent evacuation to acquire the reversible CO uptake. The irreversible CO uptake was calculated by subtracting the total uptake in the first measurement from the reversible uptake in the second measurement.

NH_3 and IPA-TPD were carried out in a Micromeritics Autochem2920 instrument. 100-500 mg of catalyst was loaded into a glass reactor. Samples were dried at 400°C in flowing He prior to analysis. For samples containing Pt, the drying step was replaced with a reduction at 260°C in flowing H_2. For the NH_3-TPD measurement, the catalyst was saturated with flowing NH_3 at 150°C. The sample was then heated to 700°C at a ramp rate of 10°C/min in flowing He. For the IPA-TPD measurement, the catalyst was saturated with ten 100 μL doses of liquid IPA via injection through a septum, with the sample held at 50°C. Then, the sample was heated to 700°C at a ramp rate of 10°C/min in flowing He. A quadrupole mass spectrometer (MKS Instruments) was used to monitor desorption of NH_3 at m/z = 17, (NH_3-TPD) or the formation of propylene at m/z = 41 in the temperature range of 300-450 °C (IPA-TPD). The NH_3 concentration based on m/z = 17 was corrected for the presence of water using the signal at m/z= 18 and the known relative intensity of these peaks for water.[6] Calibrations of NH_3 and propylene were used to convert the mass spectrometer signals to NH_3 or propylene mole fraction.

N_2 physisorption to measure the BET surface area was conducted using an ASAP2020 instrument (Micromeritics) with the temperature held at -196°C. Prior to the adsorption measurement, samples were degassed at 150 °C and evacuated for 6h.

In order to measure the metal loading of Pt/SiAl catalysts, 50 mg of each catalyst was dissolved in 10 g aqua regia solution (a 3:1 mixture of concentrated HCl with concentrated HNO_3) by refluxing the solution at 120°C for 12h. The resulting solution was then analyzed using an inductively coupled plasma optical emission spectrometer (ICP-OES) (Vista-MPX) to determine the Pt content, with calibration standards developed using a Pt ICP standard (Sigma Aldrich).

Reaction products were quantified using a Shimadzu Gas Chromatograph equipped with FID with liquid injection. A Restek RTX-VMS capillary column (length: 30 m, inner diameter: 0.25 mm, film thickness: 1.4 μm) was used. The injection port and FID were maintained at 240°C. The injection volume was 1 μL and a split ratio of 50 was used. The column temperature ramp was as follows: hold 1 min at 40°C, ramp 10°C/min to 180°C, ramp 3°C/min to 240°C, hold 5 min at 240°C.

Quantitative ^{13}C NR spectra were collected on a Bruker Avance 500 MHz spectrometer at room temperature, using an inverse-gated decoupling pulse sequence with a 30° pulse. The ^{13}C NMR spectra were absolute-referenced to the associated ^{1}H NMR spectra. 256 Scans were used, with an acquisition time of 1 sec and a relaxation delay of 15 sec. This relaxation delay was shown to be sufficient for product quantitation in our previous study. Reaction products cis-THFDM, trans-THFDM, tetrahydropyran-2-methanol-5-ketone (THP2M5one), and the two stereoisomers of THP2M5H were identified using ^{13}C NMR (NMR spectra shown in Section 8.3.1 in the Appendix). Samples were prepared for analysis by evaporating the THF solvent from 4.5g of the product sample, then adding 1g of d_6-DMSO.

Because Lgol, THP2M5one, and THP2M5H are not commercially available, the identities of these compounds were confirmed by ^{13}C NMR. Lgol was assumed to have a molar GC-FID sensitivity equal to that of Cyrene. THP2M5one and THP2M5H were synthesized as described in

Section 8.3.2 in the Appendix. THP2M5H and THP2M5one were assumed to have molar GC-FID sensitivities equal to that of THFDM. Because cis-THFDM is overlapped by THP2M5one and trans-THFDM is overlapped by one of the stereoisomers of THP2M5H in the GC, these GC peaks were deconvoluted using ^{13}C NMR. ^{13}C NMR was used to directly measure the ratio of cis-THFDM to trans-THFDM and the ratio of THP2M5one to cis-THFDM. The concentration of the overlapped isomer of THP2M5H was then calculated by subtracting the known concentration of trans-THFDM from the total concentration of these two species in the GC. An example of the product peak deconvolution methods is described in Section 8.3.3 in the Appendix.

Batch reactions were carried out in 75 mL Parr Hastelloy high-pressure batch reactors equipped with a 1/8-inch dip-tube. A magnetic stir bar and appropriate amount of catalyst and feedstock were added to the reactor. The reactor was purged four times with 500 psi H_2, followed by pressurizing to 500 psi H_2. The heat-up time was 10-15 minutes. The reaction mixture was stirred at 750 rpm. The reaction products were filtered using a 0.2 μm PTFE syringe filter prior to analysis. During sampling, 0.6 mL was purged followed by 0.6 mL collected for analysis. Purging was done to remove dip-tube liquid collected at earlier reaction times. A stainless steel filter (500-mesh) was used to prevent solids from entering the dip-tube. After each sample, the reactor was re-pressurized with H_2.

Continuous flow reactions were carried out in a 12 cm ¼ inch Swagelok tube in an up-flow configuration. The catalyst powder was packed between beds of quartz wool to hold the catalyst in place. Temperature control of the reactor was achieved by using aluminum heating blocks with a ¼ inch cylindrical hole to place around the reactor; heating tape was wrapped around the heating block and connected to a temperature controller. The thermocouple was placed at the center of the reactor via a cut-out slot in the aluminum heating block. The system was then insulated using

fiberglass insulation. Gas flows were maintained using a mass flow controller (Brooks). The system pressure was controlled using a back pressure regulator. Liquid was delivered via an HPLC pump (LabAlliance). Liquid-phase products were collected downstream of the reactor in a 100 mL separator immersed in ice water. Products were filtered using a 0.2 μm PTFE syringe filter prior to analysis. A low H_2 gas flow rate (6 mL/min) was used to minimize evaporation of the THF solvent. Catalysts were reduced *in situ* at 260 °C in flowing hydrogen for 1h prior to reaction. To test catalyst regeneration, the catalyst was calcined at 400°C (2°C/min ramp, 1 h hold) followed by reduction at 260°C (2°C/min ramp, 4h hold) after the initial run. Additional details concerning the reaction kinetics measurements, selectivity measurement, and calculation of experimental error are provided in the Appendix, Section 8.3.6.

Trace amounts of water have an effect on the product selectivity (details are provided in Section 8.3.7 in the Appendix). We observed moderate (13%) changes in the product selectivity when using different bottles of THF. This difference was eliminated when 500 ppmv (0.05 vol%) water was added to the Lgol/THF feedstock.

4.3. Results and Discussion

4.3.1 Catalyst Characterization

The CO chemisorption results (Table 4.1) show that the Pt dispersions are approximately 40% for both the 1.1% and 5.3% Pt/SiAl catalysts as well as the 1% Pt/SiO_2 catalyst. This suggests that these catalysts have similar average particle sizes. The 0.06% Pt and 0.25% Pt catalysts have somewhat lower dispersions of 20-25%, however we note that these measurements are subject to greater error due to the lower CO uptake in these cases.

NH_3-TPD was carried out on the SiAl support, the 1.1% Pt/SiAl catalyst used for the reaction kinetics measurements, and the 5.3% Pt/SiAl catalyst. The NH_3-TPD results indicate that the total acidity of the SiAl support decreases moderately upon addition of 1.1% Pt (15% decrease in total acidity per g_{SiAl}) or 5.3% Pt (25% decrease, per g_{SiAl}) (Table 4.1). IPA-TPD was additionally conducted on the SiAl support to measure Brønsted acid sites based on the propylene desorption peak at ~350 °C. The resulting value was 490 μmol/g, indicating that the SiAl support consists predominantly of Brønsted acid sites but that Lewis sites are also present (approximately 180 μmol/g based on the difference between the site densities calculated by NH_3 and IPA-TPD). The plots for NH_3 and IPA-TPD are provided in the Appendix (Section 8.3.4).

The BET surface area decreases modestly with Pt addition from 400 m^2/g on the bare SiAl support to 350 m^2/g for the 5.3% Pt catalyst.

Table 4.1. *Characterization of Metal and Acid Catalysts*

Catalyst	**Metal Site Density [μmol/g]***	**Metal Dispersion (%)**	**Acid Site Density (NH_3-TPD) [μmol/g]**	**BET Surface Area (m^2/g)**
SiAl	-	-	670**	400
0.06% Pt/SiAl	0.6	21	-	-
0.25% Pt/SiAl	3	24	-	-
1.1% Pt/SiAl	24	43	530	390
1% Pt/SiO_2	21	41	-	-
5.3% Pt/SiAl	111	41	480	350
1.1% Pt/SiAl, regenerated post-reaction	26***	45	340	-
1% Pd/SiAl	34.5	37	-	-

Assuming a stoichiometry of 1 Pt/CO, 1.5 Pd/CO. **The Brønsted site density of the SiAl was additionally measured using IPA-TPD, yielding a value of 490 μmol/g. * Measured by pulse CO chemisorption on a Micromeritics Autochem 2920 instrument.*

4.3.2. Batch reactor catalyst screening

The proposed reaction network for Lgol hydrogenolysis in THF solvent over bifunctional metal-acid catalysts is shown in Figure 4.1. The major hydrogenolysis product is cis- and trans-THFDM, with THP2M5H as a side-product of hydrogenolysis and 2-methyl-tetrahydrofurfuryl alcohol (2MTHFA) as a side-product of dehydration and hydrogenation. In the formation of THP2M5H, Lgol is first isomerized to THP2M5one followed by hydrogenation to THP2M5H. The evidence for this reaction network will be discussed in the following sections.

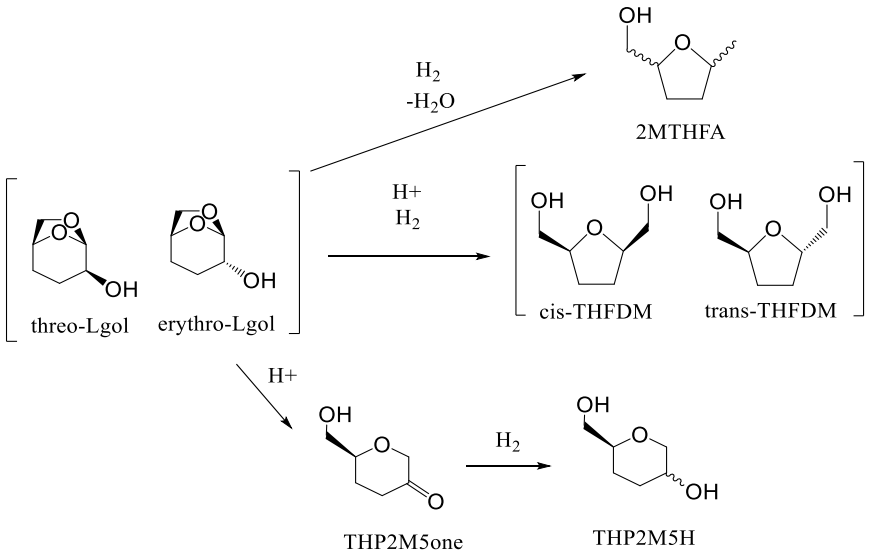

Figure 4.1: *Proposed reaction network for Lgol hydrogenolysis in THF solvent*

Table 4.2 shows batch reactor screening results for a variety of metal-acid catalysts. Note that Pd/Al_2O_3, Pt/Al_2O_3, and Pt/SiO_2 are inactive at these reaction conditions, indicating that Brønsted acid sites are necessary for Lgol hydrogenolysis. Different metals (Pt, Pd, Rh, Ru) supported on

SiAl all show some selectivity to THFDM, as well as side-products THP2M5H and THP2M5Hone. 1% Pt/Y was much more active than the SiAl-supported catalysts, so a lower temperature of 100°C was used to achieve <100% conversion. Pt/Y shows low selectivity to THFDM (27%), with several side-products as well as THF degradation products produced. Based on the screening results, the Pd/SiAl and Pt/SiAl catalysts were selected as the most promising catalysts for further study as they displayed the highest selectivity to THFDM and THP2M5H.

Table 4.2. *Batch reactor catalyst screening for Lgol hydrogenolysis*

		Selectivity [%]					
Catalyst	**Conver-sion (%)**	**THFDM (*cis/trans*)**	**THP2M 5one**	**THP2M5 H**	**2MTHFA**	**THP2M**	**Total identified products**
1.1% Pt/SiAl	76	48 (*1.0*)	6	30	2	0	86
1% Pd/SiAl	90	58 (*2.8*)	3	20	17	0	98
1% Ru/SiAl*	89	54 (*3.2*)	0	14	0	0	68
1% Rh/SiAl	78	35 (1.3)	8	8	1	0	53
1% Pt/Y (T = 100°C)	84	27 (*1.8*)	2	29	25	15	99**

*Conditions: 100 mg cat, T = 150°C, PH_2 = 500 psi, 10 mL ~65 mM Lgol/THF. THP2M refers to tetrahydropyran-2-methanol. *250 mg cat and 6h reaction time were used. ** THF degradation products were observed.*

4.3.3. Selectivity versus conversion over 1% Pd/SiAl

The reaction network for Lgol hydrogenolysis was investigated by carrying out sampling from a batch reactor over time. As calculated from Figure 4.2, the selectivity of Lgol conversion to THFDM was ~55% and was not a strong function of conversion. Because the selectivities to the side-products 2MTHFA and THP2M5H were also not strong functions of conversion, these products are produced in parallel with THFDM rather than in series (Figure 4.1). A separate

experiment with THFDM as feedstock (10 mL 60 mM THFDM feed, cis/trans = 4.8) at the same reaction conditions (150°C, 500 psi H_2, 50 mg 1% Pd/SiAl, 3h reaction time) displayed near-zero conversion with small amounts of 2MTHFA produced (4% yield), providing further evidence that the dominant pathway for 2MTHFA formation is in parallel with THFDM rather than in series. The concentration of THP2M5one is nearly zero throughout the reaction. The carbon balance decreased to ~85% during the reaction, indicating that minor degradation reactions are occurring at these reaction conditions.

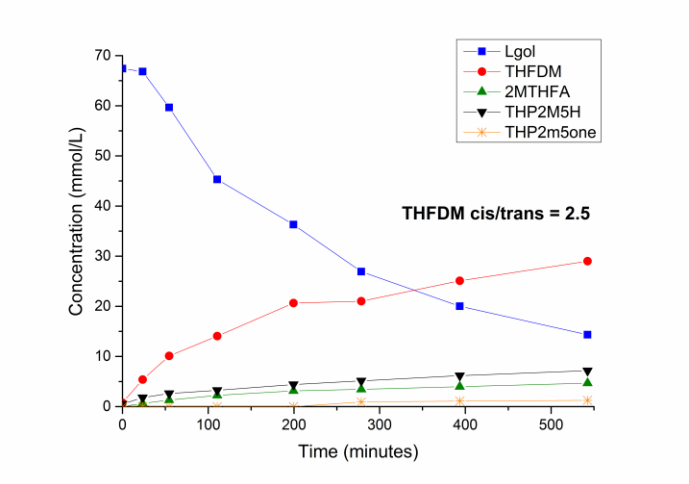

Figure 4.2. *Hydrogenolysis of Lgol (t/e = 1.7) over 450 mg 1 wt% Pd/SiAl in a batch reactor with dip-tube sampling. Conditions: 150°C, 500 psi H_2, 60 mL 60 mM Lgol in THF feed. Solid lines between points are visual aids.*

4.3.4. Effect of Lgol stereochemistry

We investigated the relationship between the Lgol feedstock stereoisomer ratio and the THFDM product stereoisomer ratio. We produced a Lgol feedstock containing a t/e ratio of 4.7 using 0.4 wt% Pd/Al_2O_3 catalyst (details described in Chapter 3). When the Lgol hydrogenolysis reaction was carried out using this feedstock (Figure 4.3), the THFDM product stereoisomer ratio was nearly equal to the ratio obtained in the experiment shown in Figure 4.2 (cis/trans = 2.5 vs

cis/trans = 2.6). This result indicates that the mechanism of Lgol hydrogenolysis to THFDM passes through an intermediate which erases the stereochemistry of the feed. Furthermore, when THFDM (cis/trans = 4.8) was fed over the Pd/SiAl catalyst at the same reaction conditions, the THFDM stereoisomer ratio did not change. This result indicates that THFDM production is irreversible, and the THFDM stereoisomer ratio is governed by kinetics rather than thermodynamics.

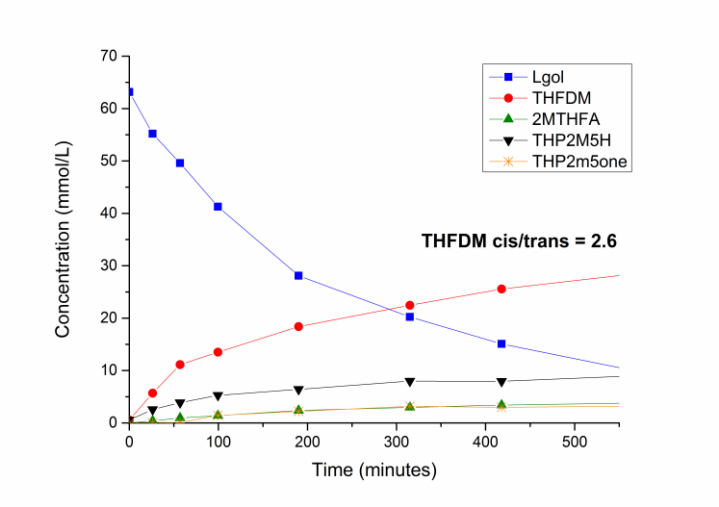

Figure 4.3. *Hydrogenolysis of Lgol (t/e = 4.5) over 450 mg 1 wt% Pd/SiAl in a batch reactor with dip-tube sampling. Conditions: 150°C, 500 psi H_2, 60 mL 60 mM Lgol in THF feed. Solid lines between points are visual aids.*

4.3.5. Determining whether THP2M5one is a THFDM precursor

THP2M5one can be produced from the acid-catalyzed isomerization of Lgol in the absence of a metal catalyst, via cleavage of the C-O bond of the anhydro-bridge. Amberlyst 70, a solid acid catalyst, was used to generate a product mixture containing 30.8 mM Lgol and 21.7 mM THP2M5one (Appendix, Section 8.3.2), and this mixture was fed over a Pd/SiAl catalyst (Figure 4.4) to determine whether THP2M5one is an intermediate between Lgol and THFDM. An additional experiment with pure Lgol at a similar initial concentration (29.8 mM) was conducted to provide a direct comparison (Figure 4.5).

The THFDM concentrations over time are comparable in Figures 4.4 and 4.5. If it is assumed that Lgol is the sole precursor to THFDM, the selectivity of Lgol to THFDM is nearly identical in Figure 4.4 (63%) versus Figure 6 (59%). In contrast, the THP2M5H concentration is significantly higher in Figure 4.4 than in Figure 4.5. If it is assumed that the THP2M5one present in Figure 4.4 is just hydrogenated to THP2M5H, and additionally that the Lgol in Figure 4.4 is converted to THP2M5H in 35% selectivity (as in Figure 4.5), then the selectivity of THP2M5one conversion to THP2M5H in Figure 4.4 is 88%. These results indicate that THP2M5one is hydrogenated to THPM2H and is not a THFDM precursor (Figure 4.1). We note that we cannot rule out the possibility of a second route from Lgol to THP2M5H which does not pass through THP2M5one. Because the 2MTHFA concentrations are comparable in Figures 4.4 and 4.5, 2MTHFA is not produced through THP2M5one or THP2M5H.

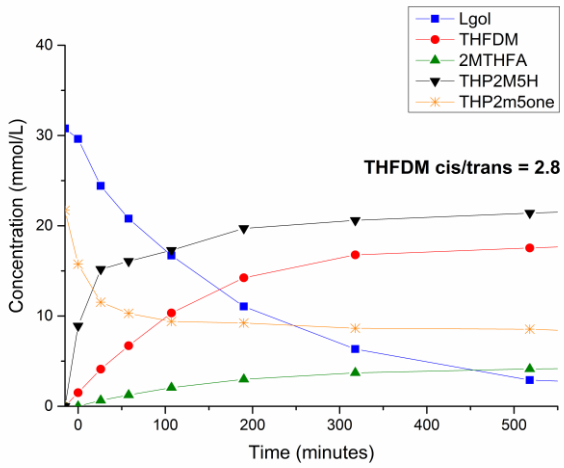

Figure 4.4. *Hydrogenolysis of a feedstock containing THP2M5one and Lgol, over 450 mg 1 wt% Pd/SiAl in a batch reactor with dip-tube sampling. Conditions: 150°C, 500 psi H_2, 60 mL feed containing 30.8 mM Lgol and 21.7 mM TH2m5one in THF. Time zero defined as time when the reaction temperature was reached. Solid lines between points are visual aids.*

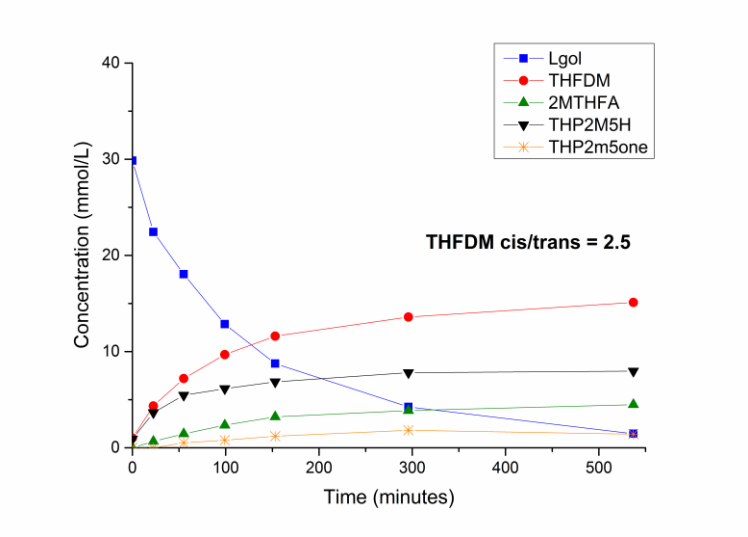

Figure 4.5. *Hydrogenolysis of Lgol (t/e = 1.7) over 450 mg 1 wt% Pd/SiAl in a batch reactor with dip-tube sampling. Conditions: 150°C, 500 psi H_2, 60 mL 30 mM Lgol in THF feed. Solid lines between points are visual aids.*

4.3.6. ^{13}C labeling study

Glucose containing a ^{13}C label at the anomeric carbon (C_1) position was converted to Lgol by first carrying out the acid-catalyzed dehydration of glucose to LGO in THF solvent over an Amberlyst 70 catalyst, followed by low-temperature hydrogenation of LGO over a 5% Ru/C catalyst to produce Lgol. This mixture contained the desired product Lgol as well as cis-THFDM from the hydrogenation of side-product HMF and THFA from hydrogenation of the side-product furfural. We then carried out the hydrogenolysis of Lgol to THFDM over a 1.1% Pt/SiAl catalyst in a batch reactor. Reaction conditions for these three steps are provided in the Appendix (Section 8.3.5). ^{13}C NMR was used to detect the location of the ^{13}C label on the THFDM product (Figure 4.6). The ^{13}C label is found solely at the hydroxymethyl position of THFDM, consistent with the mechanism proposed in this study.

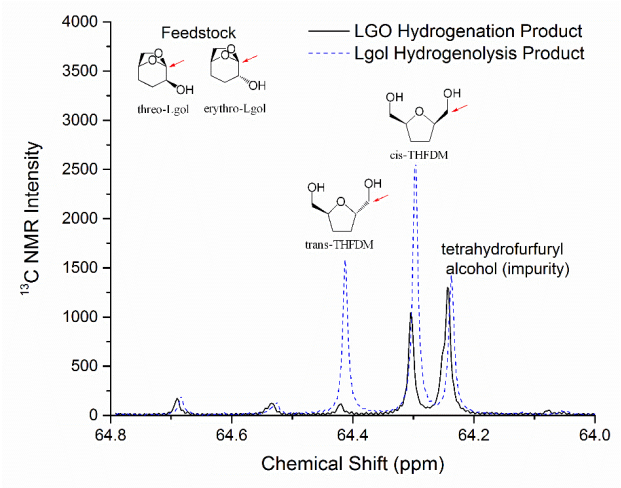

Figure 4.6. *^{13}C NMR of feedstock and product for $^{13}C_1$-labeled Lgol hydrogenolysis. Some cis-THFDM and THFA are present in the feedstock due to hydrogenation of HMF and furfural, respectively, produced during glucose dehydration. No major peaks were observed at the expected chemical shifts for the other carbon positions of cis-THFDM and trans-THFDM.*

4.3.7. Reactivity and stability of 1.1% Pt/SiAl in a continuous flow reactor

Next, we studied the reactivity, stability, and kinetics of a 1.1% Pt/SiAl catalyst for Lgol hydrogenolysis in a continuous flow reactor. The following experiments used Pt/SiAl rather than Pd/SiAl because Pt/SiAl does not produce the undesired side-product 2MTHFA. As shown in Figure 4.7, the 1.1% Pt/SiAl catalyst undergoes moderate deactivation with time on stream. Approximately 90% of the initial activity is recovered upon calcination and reduction, indicating that the deactivation is largely reversible. Additional catalyst regenerations resulted in similar reactivity. Therefore, deactivation is likely due to reversible deposition of carbonaceous species on the catalyst surface. Measurement of the CO_2 evolved during calcination of the spent catalyst (Figure 4.8) showed that only 12% of the missing carbon in the 25h time-on-stream experiment (Figure 4.7) was present on the catalyst surface, indicating that the majority of the missing carbon is likely in the form of soluble oligomeric humins. The regenerated catalyst showed no change in

the CO uptake and a moderate (35%) decrease in total acidity measured by NH_3-TPD relative to the fresh 1.1% Pt/SiAl (Table 4.1).

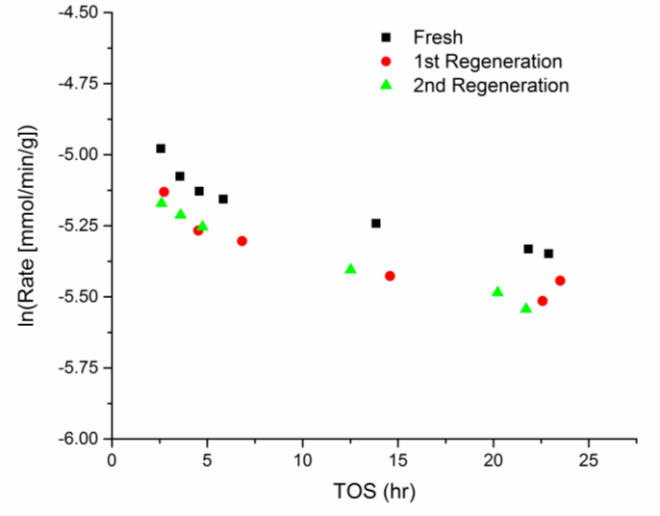

Figure 4.7: *Natural logarithm of Lgol consumption rate versus time on stream for fresh and regenerated 1.1% Pt/SiAl catalysts. Conditions: 150 mg cat, T = 129°C, P_{H2} = 750 psi, $C_{Lgol/THF}$ = 65 mM (t/e = 1.8), $F_{Lgol/THF}$ = 30 μL/min, F_{H2} = 6 mL/min.*

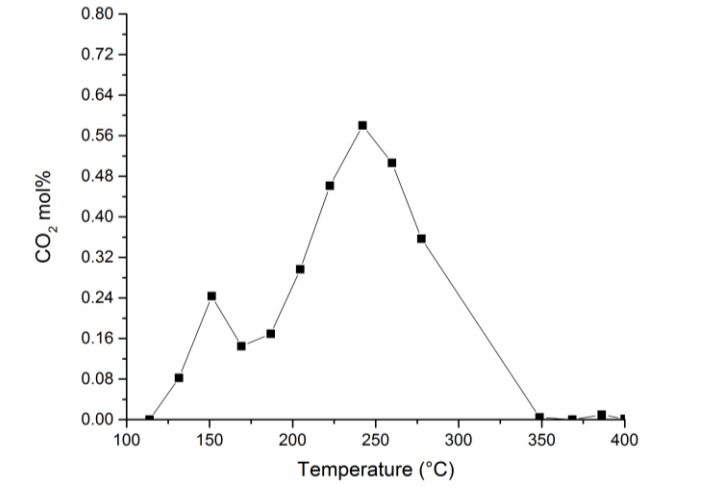

Figure 4.8: *CO_2 evolved during calcination of spent 1.1% Pt/SiAl catalyst (300 mg).*

Calcination conditions: 50 mL/min flowing air; 2 °C/min ramp to 400 °C, 1h hold. Solid lines between points are visual aids.

For the 1.1% Pt/SiAl catalyst, the product selectivities are as follows: 61% to THFDM (cis/trans = 1.0), 20% to THP2M5H, 5% to THP2M5one. The sum of selectivities is 86% (and is approximately constant with time-on-stream), indicating some degradation reactions are occurring under these conditions. The nearly 1:1 mixture of THFDM cis- and trans- isomers produced over 1.1% Pt/SiAl is notably different from the results obtained over 1% Pd/SiAl (cis/trans = 2.5), and from HMF hydrogenation to THFDM which generates predominantly the cis-THFDM isomer.[7] If THFDM is used as a polymer precursor, these variations in diastereoselectivity could have an impact on downstream polymer properties.[8]

4.3. Reaction kinetics over 1.1% Pt/SiAl

Reaction kinetics measurements were made in a continuous flow reactor operated at <30% conversion. The apparent activation energy was measured to be 105 kJ/mol in the range of 122-144° C (Figure 4.9A), comparable to reported activation energies for C-O hydrogenolysis of cyclic ethers[9]. We will also show that this value is in good agreement with the computed activation barrier from density functional theory (DFT). The total selectivity to observed products was roughly constant between 122°C and 144°C (Table 8.4 in the Appendix). At 144°C, 12% selectivity to unidentified GC products was observed.

The rate of Lgol consumption was found to be first order in Lgol in the range of 34-186 mM (Figure 4.9B), indicating that Lgol does not poison the catalyst surface. We note that the reaction order could potentially decrease at higher Lgol concentrations as site-blocking becomes relevant. As the Lgol concentration is increased from 34 mM to 186 mM, the total selectivity to observed products decreases from 94% to 74% (Table 8.4 in the Appendix).

A zero-order dependence in hydrogen between 500-1000 psi H_2 was measured (Figure 4.9C). This is in contrast to positive reaction orders typically measured for liquid-phase

hydrogenations at elevated pressure.[9-10] While for a conventional hydrogenation reaction the measured zero-order dependence could indicate that the surface is highly covered with hydrogen, we show in Section 4.3.8 that the reaction is rate-limited by acid sites for the 1.1% Pt/SiAl catalyst. Therefore, the zero-order dependence in hydrogen indicates that a fast (non-rate-determining) hydrogenation step follows a rate-limiting irreversible acid-catalyzed step. The product selectivity was not a function of H_2 pressure in this regime (Table 8.4 in the Appendix).

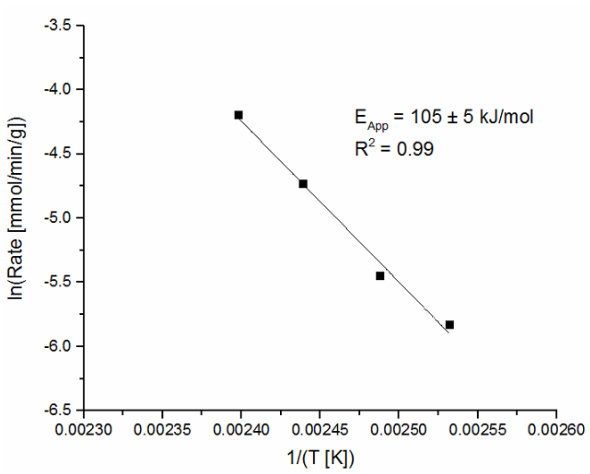

Figure 4.9A

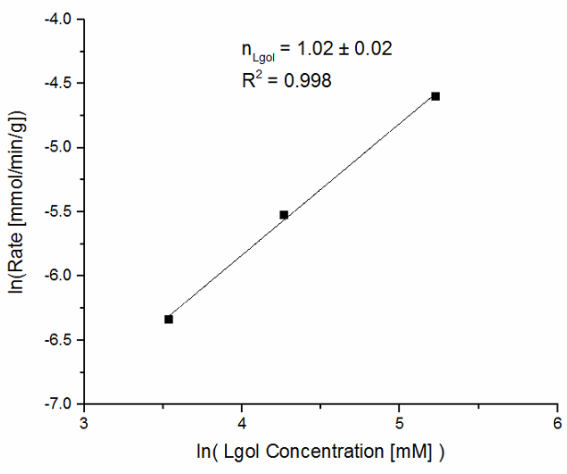

Figure 4.9B

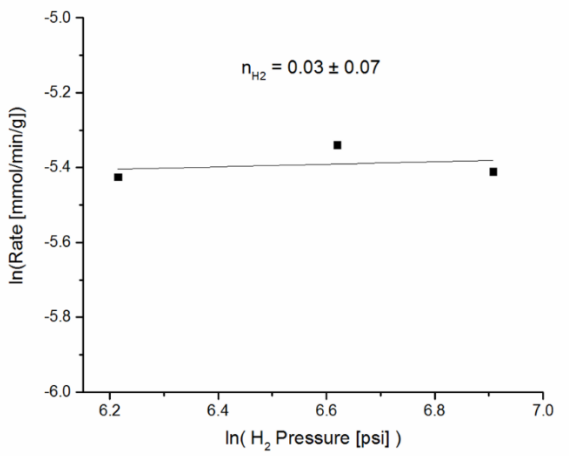

Figure 4.9C

Figure 4.9A-C: *Reaction kinetics measurements over 1.1% Pt/SiAl: (A) activation energy, (B) Lgol reaction order, and (C)* H_2 *reaction order. "Rate" refers to Lgol consumption rate. Base case conditions: 150 mg cat, T = 129°C,* P_{H2} *= 750 psi,* $C_{Lgol/THF}$ *= 65 mM (t/e = 1.7),* $F_{Lgol/THF}$ *= 30 μL/min,* F_{H2} *= 6 mL/min.* $F_{Lgol/THF}$ *= 60 μL/min was used for the T =137°C measurement, and* $F_{Lgol/THF}$ *= 100 μL/min was used for the T = 144°C measurement. Lgol conversion and product selectivities at each reaction condition are reported in the Appendix (Table 8.4).*

4.3.8. Effect of metal loading on rate and selectivity

The effect of the Pt metal loading on the rate and selectivity are shown in Figure 4.10. The acidity only decreased moderately between the SiAl support (Table 4.1; 670 μmol/g total acid sites), the 1.1% Pt/SiAl catalyst (530 μmol/g total acid sites), and the 5.3% Pt/SiAl catalyst (480 μmol/g total acid sites). Therefore, varying the metal loading in effect varies the ratio of metal to acid sites. In Figure 4.10B, the selectivity to THP2M5H and THP2M5one are summed together because these species constitute a parallel pathway to THFDM (Figure 4.1). Between these two products, THP2M5H is the major product at high metal loadings while THP2M5one is the major product at low metal loadings (see Table 8.4 in the Appendix).

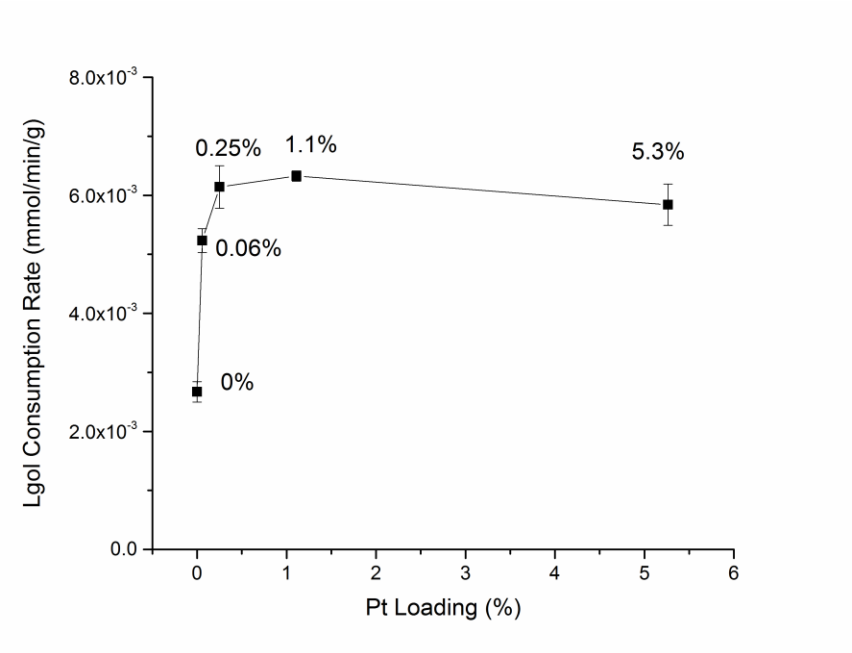

Figure 4.10A

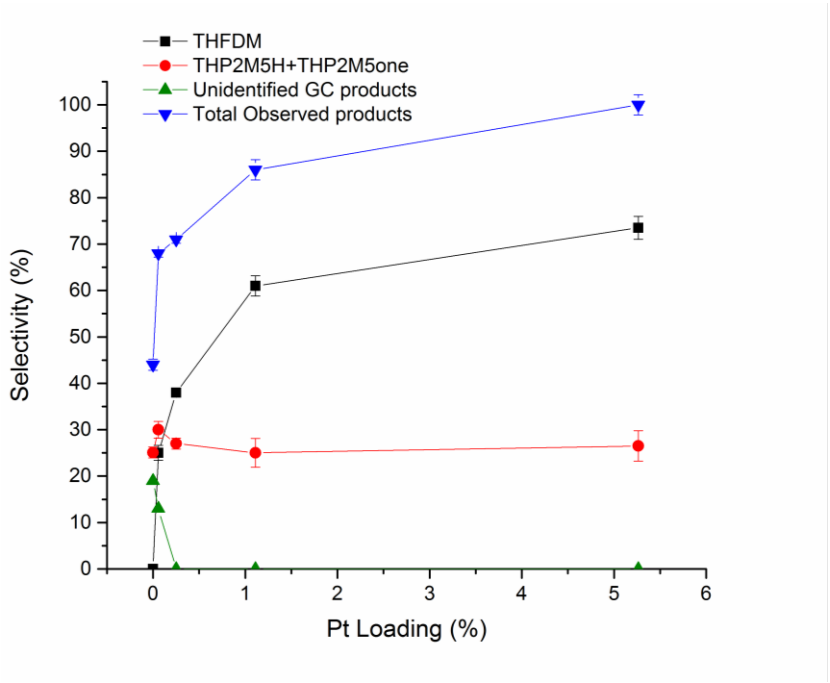

Figure 4.10B

Figure 4.10*: Initial Lgol Hydrogenolysis rate (A) & product selectivity (B) vs metal loading of Pt/SiAl Catalysts.*

Conditions: 150 mg cat (300 mg cat was used for 0% Pt), T = 129°C, PH2 = 750 psi, CLgol/THF = 65 mM (t/e = 1.6-2.1), FLgol/THF = 30 μL/min, FH2 = 6 mL/min. Solid lines between points are visual aids. In the case of 0% Pt, the selectivity to unidentified GC products increased with time-on-stream from 14% at 3.5h time-on-stream to 29% at 27h time-on-stream. The value of 19% shown in Figure 4B was measured at an intermediate time-on-stream of 15h.

The THFDM selectivity shown in Figure 4.10B refers to the sum of cis-THFDM and trans-THFDM. The THFDM cis/trans ratio is approximately constant as a function of Pt metal loading, at a value of 0.9-1.2. For the 5.3% Pt/SiAl catalyst, the selectivity was observed to change with time on stream for the first 25h before reaching a steady state value. The reported selectivity in all cases is the steady state value.

4.3.9. Role of metal and acid sites in kinetically relevant steps

The reaction rate and product selectivity are comparable between 1.1% and 5.3% Pt, indicating that above 1.1% Pt, the rate-limiting step is acid-catalyzed. Because hydrogenation can be assumed to occur only on metal sites, the hydrogenation step is therefore not rate-determining. In contrast, for a conventional hydrogenation reaction the reaction rate would be expected to scale linearly with the metal loading for catalysts with similar metal dispersion. The metal dispersions of the 1.1%, and 5.3% Pt catalysts are similar (Table 4.1), ruling out particle size effects. Based on the metal and Brønsted acid site densities of the 1.1% Pt/SiAl catalyst, each metal site has a turnover frequency (TOF) at least 25x higher than each Brønsted acid site for Lgol hydrogenolysis while remaining in the acid-limited regime. This rate of Lgol conversion is even maintained at

0.25% Pt, although the selectivity towards identifiable products decreases, as will be discussed in Section 4.3.10.

Based on our observation that Lgol hydrogenolysis is rate-limited by acid sites above 1.1% Pt loading, as well as the measured zero-order dependence on hydrogen (Figure 4.9C), we argue that the mechanism of Lgol hydrogenolysis proceeds through rate-determining, irreversible C-O cleavage and ring rearrangement of Lgol over acid sites, followed by desorption of a reactive intermediate which is then hydrogenated in a fast step over metal sites to form THFDM. If a quasi-equilibrated metal-catalyzed hydrogenation step preceded a rate-limiting acid-catalyzed step, a first-order dependence in H_2 pressure would be observed because the hydrogenated intermediate would be in equilibrium with the reactant and one equivalent of hydrogen. If the acid-catalyzed RDS was reversible rather than irreversible, a positive order dependence in H_2 would be observed.

The trend of reaction rate versus metal loading observed for Lgol hydrogenolysis (Figure 4.10A) is analogous to results in the alkane hydroisomerization literature over bifunctional Pt catalysts on acidic supports. The mechanism of alkane hydroisomerization proceeds via metal-catalyzed alkane dehydrogenation to form an alkene intermediate, followed by acid-catalyzed isomerization to form an isoalkene, followed by metal-catalyzed hydrogenation of the isoalkene to form isoalkanes.[11] The rate-limiting step for alkane hydroisomerization over Pt catalysts supported on Zeolite Y (Si/Al = 3) is also acid-catalyzed for Pt loadings above 0.4% (at reaction conditions of 200°C, 101 kPa, $P_{H2}/P_{n\text{-decane}} = 9$).[12] Based on the 0.4% Pt/Zeolite Y catalyst which has a metal/acid site ratio of 0.03, each metal site has at least a 33x higher TOF compared to each acid site (in this reference, accessible metal sites were measured based on transmission electron microscopy and/or H_2-O_2 titration; acid sites were defined as sites which adsorb NH_3 with a heat of adsorption greater than 24 kcal/mol measured by microcalorimetry). Similarly, in the

hydroisomerization of n-heptane over bifunctional Pt/SiAl catalysts (350°C, 101 kPa, $P_{H2}/P_{n\text{-heptane}}$ = 33), Samad, et al. found that each metal site has a TOF hundreds of times higher than each acid site.[13]

A hydrogen reaction order of -1 is observed for pentane hydroisomerization over bifunctional Pt/Al_2O_3 catalysts, because the presence of hydrogen inhibits the formation of the isoalkene intermediate.[11] The hydrogenation step following the acid-catalyzed step does not affect the hydrogen reaction order because the acid-catalyzed step is rate-limiting and irreversible. In contrast, a zero order dependence in H_2 for Lgol hydrogenolysis is observed because this reaction does not involve an initial metal-catalyzed dehydrogenation step.

4.3.10. Role of metal and acid sites in avoiding degradation reactions

As the metal loading is decreased in Figure 4.10B, the selectivity towards THFDM decreases and the selectivity towards THP2M5H + THP2M5one stays roughly constant. At low metal loadings (0-0.06% Pt), unidentified GC products were observed which may correspond to reactive intermediates. The selectivity to these unidentified products is 13% at 0.06% Pt and 19% at 0% Pt, as reported in the Appendix (Table 8.4). The total selectivity to observed liquid-phase products decreases as the metal loading is decreased, suggesting that degradation reactions are occurring under these conditions. We hypothesize that the concentration of reactive intermediates, which desorb from an acid site prior to being hydrogenated over a metal site, increases as the metal loading is decreased. These species are likely to be culprits for degradation reactions. At high metal loadings, the density of metal sites is sufficient to intercept and hydrogenate these reactive intermediates, thereby stabilizing them against degradation reactions. There is approximately one metal site for every four acid sites for the 5.3% Pt/SiAl catalyst and 100% of the product selectivity is accounted for, indicating that there are no degradation products with this catalyst.

In the conversion of Lgol to the side-product THP2M5H, we identified THP2M5one as a reactive intermediate formed over acid sites which is hydrogenated over metal sites. While we were not able to experimentally identify an intermediate in the pathway between Lgol and THFDM, the results in Section 4.3.11 provide further evidence for the existence of a reactive intermediate formed over acid sites which is hydrogenated to form THFDM. As the selectivity to THP2M5one + THP2M5H is roughly constant with decreasing metal loading, Figure 4.10B also suggests that the major culprit for degradation reactions is in the pathway between Lgol and THFDM rather than the pathway between Lgol and THP2M5H. We note that selectivity towards THFDM must approach zero as the metal loading approaches zero, since hydrogenation is required to form THFDM.

The selectivity versus metal loading trend in Figure 4.10B is also similar to the trend observed in the alkane hydroisomerization literature over Pt/H-Y catalysts. The selectivity towards mono-branched alkanes (versus poly-branched alkanes and cracking products) increases as the metal/acid site ratio is increased.[12a] Selectivity is governed by the sequential reaction of the mono-branched alkene intermediate either over metal or acid sites. At low metal loadings, this intermediate undergoes series reactions over acid sites, resulting in poly-branched products and cracking products. At high metal loadings, the metal intercepts and hydrogenates the mono-branched alkene intermediate, resulting in the mono-branched alkane product.

4.3.11. Effect of metal-acid site proximity

The bifunctional 1.1% Pt/SiAl catalyst was compared to a physical mixture of 1% Pt/SiO_2 and SiAl catalysts. The comparison shown in Table 4.3 is made on a basis of the same total number of metal and acid sites. While the reaction rate was found to be 1.6 times higher over the bifunctional catalyst compared to the physical mixture of metal and acid catalysts, the selectivity

to identified products was similar between the two cases (the physical mixture had 10% higher selectivity to THP2M5H and THP2M5one than the 1% Pt/SiAl catalyst). This indicates that high selectivity to desired products THFDM and THP2M5H can be achieved even with the physical mixture catalyst which has microscale proximity between metal and acid sites rather than nanoscale proximity in the case of the Pt/SiAl catalyst.[13b] In contrast, when SiAl alone is used, a low selectivity to THP2M5one (25%) is observed. If unidentified GC products are included, the total selectivity to observed products is approximately 44%.

Table 4.3. *Metal-acid site proximity effects*

		Selectivity [%]				
Catalyst	**Initial Rate (mmol/min /g_{SiAl})**	**THFDM (*cis/trans*)**	**THP2M-5one**	**THP2M-5H**	**Unidentified GC products**	**Total observed products**
1.1% Pt/SiAl	$6.3*10^{-3}$	61 (*1.0*)	5	20	0	86
SiAl only	$2.7*10^{-3}$	0	25	0	19**	44
Phys. Mixture*: 1% Pt/SiO_2 & SiAl	$3.9*10^{-3}$	57 (*1.2*)	3	32	0	93
Layered: SiAl, then 1% Pt/SiO_2	$2.5*10^{-3}$	34 (*2.1*)	12	15	0	61
Layered: 1% Pt/SiO_2, then SiAl	$3.3*10^{-3}$	0	23	0	23	46

*Conditions: 150 mg cat (for physical mixture and layered catalysts, 150 mg of each catalyst was used. For SiAl only, 300 mg cat was used), T = 129°C, P_{H2} = 750 psi, $C_{Lgol/THF}$ = 65 mM (t/e = 1.4-1.8), $F_{Lgol/THF}$ = 30 μL/min, F_{H2} = 6 mL/min. *For the physical mixture, the catalysts were ground together with a mortar and pestle to ensure the powders were well-mixed. **The selectivity to unidentified GC products increased with time-on-stream from 14% at 3.5h time-on-stream to*

29% at 27h time-on-stream. The value of 19% shown in Table 4.3 was measured at an intermediate time-on-stream of 15h.

In a layered configuration with a layer of SiAl catalyst followed by 3 cm of inert quartz wool followed by a layer of 1% Pt/SiO_2, a similar reaction rate was observed compared to the SiAl-only case, while the selectivity to identified products THFDM and THP2M5H was 61% (a layered configuration of metal sites followed by acid sites has similar reactivity to SiAl only, consistent with the fact that the metal catalyst alone has no reactivity). This suggests that when the metal and acid sites are completely separated, a greater fraction of the carbon is lost to degradation products. We hypothesize that this is because degradation reactions of reactive intermediates over acid sites are more prevalent when these intermediates cannot be rapidly hydrogenated over metal sites. Similarly, Samad, et al. found that in the case of n-heptane isomerization over Pt/SiAl catalysts, a physical mixture of Pt/SiO_2 and SiAl had comparable reactivity to the bifunctional Pt/SiAl catalyst, while catalysts comprised of layered metal and acid sites displayed a lower degree of bifunctionality (lower reaction rate and lower selectivity towards isoheptanes versus cracking products) compared to Pt/SiAl.[13b]

THFDM can be produced even when the metal and acid sites are completely separated. This confirms that the mechanism to produce THFDM proceeds through a reactive intermediate formed over acid sites which is then hydrogenated over metal sites. We were unable to experimentally identify intermediates between Lgol and THFDM, most likely because these species are rapidly hydrogenated at high metal loadings and are partially degraded at low metal loadings. It is possible that the unidentified GC products detected at low metal loadings are intermediates between Lgol and THFDM, however we could not identify these compounds using ^{13}C NMR due to their low concentration.

4.3.12. First principles simulations of Lgol conversion to THFDM and THP2M5H

First-principle calculations were performed starting from Lgol to complement the experimental findings and to determine the thermodynamic feasibility of the reaction intermediates in the formation of THFDM and THP2M5H. Erythro-Lgol was considered for this exploration of energy profiles (erythro-Lgol is marginally more stable than the threo-Lgol by ~2 kcal/mol). Computational details are provided in the Appendix, Section 8.3.9. The computed free energy profile (ΔG, 25°C in THF dielectric medium) and mechanistic steps associated with the acid-catalyzed transformation of erythro-Lgol to THFDM and THP2M5H are shown in Figure 4.11.

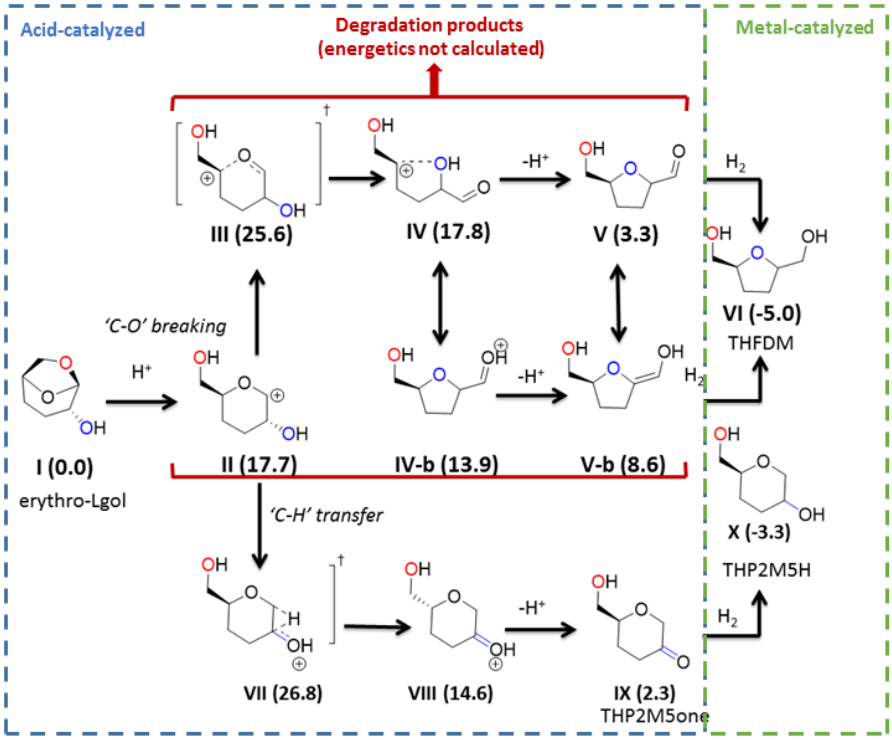

Figure 4.11. *Computed reaction mechanisms and relative free-energy profiles (kcal/mol) of Lgol-THFDM/THP2M5H pathways at the G4MP2 level of theory at 25°C. Solvation contributions from a THF dielectric (SMD model) computed at the B3LYP/6-31G(2df,p) level of theory are included*

in the relative free-energy profiles. All energies are respect to the free energy of neutral erythro-Lgol molecule in THF dielectric medium.

4.6.1. Formation of THFDM from Lgol

The proposed reaction steps associated with the formation of THFDM from erythro-Lgol is the following: I→ II→ III→ IV→ V→ VI. The erythro-Lgol (I) undergoes a preferred protonation at the anhydro-bridge oxygen atom, marginally preferred compared to the other 'O' sites. This C-O bond is expected to be most reactive towards acid-catalyzed cleavage. The initial protonation reaction (I→ II) is endergonic by 17.7 kcal/mol, suggesting that the protonation of erythro-Lgol is not spontaneous at room temperature in a tetrahydrofuran environment. The protonation of anhydro-bridge oxygen results in the cleavage of C-O bond forming a six-membered carbocation, denoted as 'II'. The $C\text{-}O_{ring}$ bond distances in this intermediate are 1.50 Å (left side of intermediate II) and 1.26 Å (right side of II), respectively, in the gas phase. Ab initio dynamic simulations performed for this cation suggests that the influence of explicit solvent molecules may cause further lengthening of the weakest C-O bond. The shortening of the reactive bond (1.26 Å, compared to ~1.40 Å for a C-O-C single bond[14]) indicates that the carbocation has an oxocarbenium resonance state which aids in its stabilization.[9]

The ring opening of the carbocation intermediate II occurs via a second C-O bond cleavage, which is facilitated by the oxocarbenium ion resonance state. The computed transition state (III) has a relative free energy of 25.6 kcal/mol. This value is in good agreement with the experimentally measured apparent activation energy barrier of 25.2 kcal/mol, although we note that the measured value is an apparent activation enthalpy while the DFT value is an activation Gibbs free energy. The potential energy scans also show that the C-O bond lengthening of species II does not require

a significant energy barrier from the protonated intermediates. Upon the C-O bond cleavage, the positive charge located at the C_5 position is stabilized by ring contraction resulting in the formation of a five-membered carbocation (IV: 17.8 kcal/mol). Formation of the acyclic intermediate (IV) results in erasure of the Lgol stereochemistry at the C_2 alcohol position, consistent with our finding that the THFDM cis/trans ratio is independent of the Lgol t/e ratio. The proposed ring rearrangement is also consistent with the C_1 radio-labeling results. Rearrangement of a proton from intermediate IV (central oxygen atom to the carbonyl group) would result in the formation of the IV-b intermediate (13.9 kcal/mol). The intermediates, IV and IV-b undergo deprotonation to form V (aldehyde, 3.3 kcal/mol) and V-b (enol, 8.6 kcal/mol), respectively. We expect that the rate of equilibration of aldehyde and enol tautomers is promoted under acidic conditions.

Experimentally, the identity of the metal (e.g. Pt vs Pd) has an effect on the THFDM cis/trans ratio. The Pt/SiAl catalysts displayed a cis/trans ratio of 0.9-1.2, while 1% Pd/SiAl has a THFDM cis/trans ratio of ~2.5 at similar reaction conditions. The fact that the metal identity affects the THFDM cis/trans ratio suggests that the metal participates in the step which forms the new stereocenter in THFDM. Direct hydrogenation of the aldehyde (V) would not affect the stereochemistry of THFDM. While the enol (V-b) is higher in energy than the aldehyde, even a small fraction of enol could be relevant to the hydrogenation reaction, as the rate of C=C hydrogenation can be orders-of-magnitude faster than the rate of C=O hydrogenation.[15] In the case of methyl pyruvate hydrogenation over Pd, Hall, et al. used tracer experiments with D_2 gas to show that the mechanism proceeds via keto-enol tautomerization followed by enol hydrogenation.[16] [17] In the hydrogenation of hydroxyacetone over 3 wt% Ru/TiO_2, Bergem and co-workers argued that the observed rate enhancement under acidic conditions may be due to acid-catalyzed formation of

the enol prop-2-ene-1,2-diol, which could then undergo rapid C=C hydrogenation to 1,2-propanediol.[18]

The computed energy profile for the THFDM indicate that the intermediates (II to V) all are higher in energy than the reactant species, making experimental observation of these species unlikely. Although the aldehyde intermediate V (or its tautomer V-b) is expected to desorb from acid sites prior to hydrogenation over metal sites, we could not detect these species experimentally, presumably due to their low concentration. While acid-catalyzed degradation of reaction intermediates in the pathway between Lgol and THFDM are expected to occur based on the results in Figure 4.10B, the energetics of these degradation reactions were not computed.

As shown in Figure 4.11, a competitive pathway from protonated erythro-Lgol (II) is the formation of THP2M5H (X). The reaction sequence is: I→ II→VII→ VIII→ IX→ X. Parallel to the C-O bond cleavage (II→ III), a hydrogen transfer from the C_2 to C_1 position of species II is possible, resulting in the formation of a six-membered cationic ketone species (VIII, 14. 6 kcal/mol). The computed free energy barrier for the hydrogen transfer is 26.8 kcal/mol at 25°C, indicating that the activation barriers for THFDM and THP2M5H production are comparable. Deprotonation of VIII results in THF2M5one (IX, 2.3 kcal/mol), which then undergoes exothermic hydrogenation to form THP2M5H (-3.3 kcal/mol).

4.4. Conclusions

The results in this study provide mechanistic insights into the hydrogenolysis of Lgol to THFDM and THP2M5H over bifunctional Pt and Pd-SiAl catalysts. The product THFDM cis/trans ratio is independent of the reactant Lgol t/e ratio, suggesting that the initial stereochemistry at the alcohol position of Lgol is erased during the reaction. Although THP2M5one can be produced

from the acid-catalyzed isomerization of Lgol, THP2M5one is hydrogenated to THP2M5H, and neither of these species are THFDM precursors. ^{13}C radio-labeling validated the proposed ring rearrangement of the 6-membered ring of Lgol to the 5-membered ring of THFDM. The 1.1% Pt/SiAl catalyst undergoes moderate deactivation with time-on-stream which is reversible upon calcination and reduction. The rate-limiting step for this reaction was found to be acid-catalyzed above 1.1% Pt loading. The zero-order dependence in hydrogen indicated that the metal participates in a fast hydrogenation step following an irreversible acid-catalyzed rate-determining step. The activation energy for the proposed rate-limiting acid-catalyzed C-O cleavage step is 25 kcal/mol, in agreement with the value from theoretical calculation. The selectivity towards THFDM increased with increasing metal loading, likely because degradation of reactive intermediates is minimized when these species are hydrogenated rapidly over metal sites. Using these insights, 73% THFDM selectivity and 100% overall selectivity to 16-HDO precursors was achieved using the 5.3% Pt/SiAl catalyst. A physical mixture of metal and acid sites displayed a comparable selectivity to the bifunctional Pt/SiAl catalyst, indicating that nanoscale proximity is not required to carry out Lgol hydrogenolysis selectively. However, when the metal and acid sites were completely separated using a dual-layered configuration with SiAl followed by Pt/SiO_2, a penalty in the overall selectivity is incurred. First-principles calculations revealed the energetics of the proposed reaction mechanism consistent with the experimental findings. This fundamental understanding of Lgol conversion provides a basis for the rational design of catalytic processes to convert biomass-derived levoglucosenone to high-value chemicals. As C-O hydrogenolysis reactions are ubiquitous in catalytic biomass conversion approaches, the insights gained in this work provide directions for controlling reactivity in the conversion biomass-derived intermediates over metal-acid bifunctional catalysts.

4.5. References

1. Allgeier, A. M.; Namal De Silva, W. I.; Korovessi, E.; Menning, C. A.; Ritter, J. C.; Sengupta, S. K.; Stauffer, C. S. Process for preparing 1,6-hexanediol. US 8865,940 B2, 2014.
2. (a) Buntara, T.; Melián-Cabrera, I.; Tan, Q.; Fierro, J. L. G.; Neurock, M.; de Vries, J. G.; Heeres, H. J., Catalyst studies on the ring opening of tetrahydrofuran–dimethanol to 1,2,6-hexanetriol. *Catalysis Today* **2013,** *210*, 106-116; (b) Buntara, T.; Noel, S.; Phua, P. H.; Melián-Cabrera, I.; de Vries, J. G.; Heeres, H. J., From 5-Hydroxymethylfurfural (HMF) to Polymer Precursors: Catalyst Screening Studies on the Conversion of 1,2,6-hexanetriol to 1,6-hexanediol. *Topics in Catalysis* **2012,** *55* (7), 612-619; (c) Buntara, T.; Noel, S.; Phua, P. H.; Melián-Cabrera, I.; de Vries, J. G.; Heeres, H. J., Caprolactam from Renewable Resources: Catalytic Conversion of 5-Hydroxymethylfurfural into Caprolactone. *Angewandte Chemie International Edition* **2011,** *50* (31), 7083-7087; (d) Nolan, M. R.; Sun, G.; Shanks, B. H., On the selective acid-catalysed dehydration of 1,2,6-hexanetriol. *Catalysis Science & Technology* **2014,** *4* (8), 2260-2266.
3. (a) Chheda, J. N.; Huber, G. W.; Dumesic, J. A., Liquid-Phase Catalytic Processing of Biomass-Derived Oxygenated Hydrocarbons to Fuels and Chemicals. *Angewandte Chemie International Edition* **2007,** *46* (38), 7164-7183; (b) Moreau, C.; Belgacem, M. N.; Gandini, A., Recent Catalytic Advances in the Chemistry of Substituted Furans from Carbohydrates and in the Ensuing Polymers. *Topics in Catalysis* **2004,** *27* (1), 11-30.
4. (a) 1,6-Hexanediol Market by Application (Polyurethanes, Coatings, Acrylates, Adhesives, Unsaturated Polyester Resins, Plasticizers, and Others) and By Geography (NA, Europe, Asia-Pacific, & ROW) - Trends and Forecasts to 2019. http://www.researchandmarkets.com/research/zs4gnb/16hexanediol (accessed January 22); (b) Van de Vyver, S.; Roman-Leshkov, Y., Emerging catalytic processes for the production of adipic acid. *Catalysis Science & Technology* **2013,** *3* (6), 1465-1479; (c) Werle, P.; Morawietz, M.; Lundmark, S.; Sörensen, K.; Karvinen, E.; Lehtonen, J., Alcohols, Polyhydric. In *Ullmann's Encyclopedia of Industrial Chemistry*, Wiley-VCH Verlag GmbH & Co. KGaA: 2000.
5. (a) Xiao, B.; Zheng, M.; Li, X.; Pang, J.; Sun, R.; Wang, H.; Pang, X.; Wang, A.; Wang, X.; Zhang, T., Synthesis of 1,6-hexanediol from HMF over double-layered catalysts of Pd/SiO2 + Ir-ReOx/SiO2 in a fixed-bed reactor. *Green Chemistry* **2016,** *18* (7), 2175-2184; (b) Tuteja, J.; Choudhary, H.; Nishimura, S.; Ebitani, K., Direct Synthesis of 1,6-Hexanediol from HMF over a Heterogeneous Pd/ZrP Catalyst using Formic Acid as Hydrogen Source. *ChemSusChem* **2014,** *7* (1), 96-100; (c) Alamillo, R.; Tucker, M.; Chia, M.; Pagan-Torres, Y.; Dumesic, J., The selective hydrogenation of biomass-derived 5-hydroxymethylfurfural using heterogeneous catalysts. *Green Chemistry* **2012,** *14* (5), 1413-1419.
6. NIST Standard Reference Database 69: NIST Chemistry WebBook. 2017.
7. Hu, X.; Westerhof, R. J. M.; Wu, L.; Dong, D.; Li, C.-Z., Upgrading biomass-derived furans via acid-catalysis/hydrogenation: the remarkable difference between water and methanol as the solvent. *Green Chemistry* **2015,** *17* (1), 219-224.
8. Young, R. J.; Lovell, P. A., *Introduction to Polymers*. 3 ed.; CRC Press: Boca Raton, FL, 2011.
9. Chia, M.; Pagán-Torres, Y. J.; Hibbitts, D.; Tan, Q.; Pham, H. N.; Datye, A. K.; Neurock, M.; Davis, R. J.; Dumesic, J. A., Selective Hydrogenolysis of Polyols and Cyclic Ethers over Bifunctional Surface Sites on Rhodium–Rhenium Catalysts. *Journal of the American Chemical Society* **2011,** *133* (32), 12675-12689.
10. (a) Ronzón, E.; Del Angel, G., Effect of rhodium precursor and thermal treatment on the hydrogenation of 2-cyclohexenone on Rh/SiO2 Catalysts. *Journal of Molecular Catalysis A: Chemical* **1999,** *148* (1–2), 105-115; (b) Schwartz, T. J.; Lyman, S. D.; Motagamwala, A. H.; Mellmer, M. A.; Dumesic, J. A., Selective Hydrogenation of Unsaturated Carbon–Carbon Bonds in Aromatic-Containing Platform Molecules. *ACS Catalysis* **2016,** *6* (3), 2047-2054.
11. Davis, M. E.; Davis, R. J., *Fundamentals of Chemical Reaction Engineering*. 1 ed.; McGraw-Hill: New York, NY, 2003.
12. (a) Alvarez, F.; Ribeiro, F. R.; Perot, G.; Thomazeau, C.; Guisnet, M., Hydroisomerization and Hydrocracking of Alkanes: 7. Influence of the Balance between Acid and Hydrogenating Functions on the Transformation ofn-Decane on PtHY Catalysts. *Journal of Catalysis* **1996,** *162* (2), 179-189; (b) Batalha, N.; Pinard, L.; Pouilloux, Y.; Guisnet, M., Bifunctional Hydrogenating/Acid Catalysis: Quantification of the Intimacy Criterion. *Catal Lett* **2013,** *143* (6), 587-591.
13. (a) Samad, J. E.; Blanchard, J.; Sayag, C.; Louis, C.; Regalbuto, J. R., The controlled synthesis of metal-acid bifunctional catalysts: Selective Pt deposition and nanoparticle synthesis on amorphous aluminosilicates. *Journal of Catalysis* **2016,** *342*, 213-225; (b) Samad, J. E.; Blanchard, J.; Sayag, C.; Louis, C.; Regalbuto, J. R., The controlled

synthesis of metal-acid bifunctional catalysts: The effect of metal:acid ratio and metal-acid proximity in Pt silica-alumina catalysts for n-heptane isomerization. *Journal of Catalysis* **2016,** *342*, 203-212.
14. Smith, M. B., *Organic Chemistry: An Acid-Base Approach*. 2 ed.; CRC Press: Boca Raton, FL, 2015.
15. Mäki-Arvela, P.; Hájek, J.; Salmi, T.; Murzin, D. Y., Chemoselective hydrogenation of carbonyl compounds over heterogeneous catalysts. *Applied Catalysis A: General* **2005,** *292*, 1-49.
16. Hall, T. J.; Johnston, P.; Vermeer, W. A. H.; Watson, S. R.; Wells, P. B., Enantioselective hydrogenation catalysed by palladium. *Studies in Surface Science and Catalysis* **1996,** *101*, 221-230.
17. Jeffery, E. L.; Mann, R. K.; Hutchings, G. J.; Taylor, S. H.; Willock, D. J., A density functional theory study of the adsorption of acetone to the (111) surface of Pt: Implications for hydrogenation catalysis. *Catalysis Today* **2005,** *105* (1), 85-92.
18. Bergem, H.; Xu, R.; Brown, R. C.; Huber, G. W., Low temperature aqueous phase hydrogenation of the light oxygenate fraction of bio-oil over supported ruthenium catalysts. *Green Chemistry* **2017,** *19* (14), 3252-3262.

Chapter 5. Levoglucosanol Hydrogenolysis to 1,2,5,6-Hexanetetrol over Metal-Acid Catalysts

5.1. Introduction

1,2,5,6-hexanetetrol (1256-HT) is a partially dehydrated C_6 sugar derivative with potential applications as a polymer precursor. Corma et al. noted that $>C_4$ reduced polyols have applications in the production of polyesters, alkyd resins, and polyurethanes.[1] 1256-HT is a symmetric molecule with terminal, vicinal hydroxyl groups, allowing for selective reactions at these functional groups. 1256-HT can also be dehydrated to the polymer precursor THFDM in up to 96% yield.[2] THFDM can further be converted into valuable polymer precursors, including 126-HT[3] and 16-HDO.[4] Potential uses of 1256-HT are currently limited by the lack of an efficient, high-yield route to 1256-HT. Archer Daniels Midland and others have shown that 1256-HT can be produced in up to 50% yields from sorbitol over a copper catalyst.[2a, 5] A variety of other polyols are produced along with 1256-HT, thus requiring a complex separation to purify 1256-HT.[6] 1256-HT has also been reported to be formed as a side-product of HMF hydrogenation in up to 28% selectivity, in which a mixture of polyols were also produced.[7] The lower carbon selectivity towards 1256-HT and the required separation from other polyols limit the viability of these technologies to produce 1256-HT.[2a]

In this chapter, we report a new catalytic route to produce 1256-HT in high yield from bio-renewable Lgol in water solvent. Experiments with different metal and acid catalysts are used to determine the reaction intermediates in the conversion between Lgol and 1256-HT. The relationship between the stereochemistry of the reactants, intermediates, and reaction products is

also analyzed. We propose a reaction network for Lgol conversion to 1256-HT, which is consistent with the experimental results obtained.

5.2. Experimental Methods

Lgol was prepared via quantitative hydrogenation of Cyrene (99%, Circa Group). Cyrene in water was hydrogenated at 60°C and 51.7 bar H_2 until complete conversion was achieved. To generate Lgol with a t/e ratio of 1.3, a 5% Ru/C (Strem Chemicals) catalyst was used and the Cyrene concentration in water was 20 wt%. To generate Lgol with a higher t/e ratio of 3.3, a 5% Pd/Al_2O_3 synthesized by incipient wetness impregnation was used, and the Cyrene concentration in water was 3 wt%. The Lgol in water samples were separated from the catalyst by filtration using a 0.22 μm PES syringe filter. When necessary, samples were additionally centrifuged using a 10kDa centrifugal filter (Merck Millipore) operated at 5200 rpm for 0.25h, to remove small particles. THFDM (98%, Alfa Chemicals), $Pt(NH_3)_4(NO_3)_2$ solution (99%, Strem Chemicals), and aluminum chloride hexahydrate (99%, Sigma Aldrich) were used as received. Grade 135 amorphous SiO_2-Al_2O_3 (SiAl) and Davisil grade SiO_2 were purchased from Sigma Aldrich. Sulfuric acid (96 wt%) was purchased from Fisher Chemical. Amberlyst 70 (possessing >2.55 mmol/g as reported by the vendor) was purchased from Dow Chemical, and was washed, crushed, and dried prior to use. Milli-Q water was used for all reactions and catalyst syntheses.

Pt/SiAl and Pt/SiO_2 catalysts were synthesized by incipient wetness impregnation of a $Pt(NH_3)_4(NO_3)_2$ solution in water. The catalysts were dried for >12h at 110°C in air, calcined at 400°C in flowing air (1°C/min ramp, 3 h hold), reduced at 260°C in flowing hydrogen (1°C/min ramp, 4 h hold), then passivated at room temperature with 1% O_2/Ar. When the SiAl support was

used directly in a reaction, it was calcined at 400^{o}C in flowing air prior to use. Pt/SiAl and SiAl catalysts were characterized in Chapter 4, Table 4.1.

A BioRad Aminex 87H column was used in a Shimadzu HPLC. The mobile phase was 5 mM H_2SO_4 (HPLC grade, Ricca Chemical) operated at a flow rate of 0.6 mL/min with a column temperature of 30^{o}C and an injection volume of 3 μL. Lgol, 1256-HT, 3,4-dideoxyglucose (34-Dglu), 3,4-dideoxymannose (34-Dman), and 3,4-dideoxyfructose (34-Dfru) were quantified by HPLC using a refractive index (RI) detector. The presence of 34-Dfru could also be monitored using a photodiode array (UV) detector at 206 nm. HPLC chromatograms of reaction products are provided in the Appendix (Section 8.2). Because THFDM is overlapping with Lgol in the HPLC, Lgol and THFDM were additionally quantified by GC when these species were both present. HPLC RI sensitivities for Lgol, 1256-HT, and 34-Dman/34-Dglu were measured by using quantitative ^{13}C NMR with a 110mM sorbitol internal standard to measure the concentration of these samples, which were then correlated to the HPLC refractive index signal. The HPLC RI sensitivity of 34-Dfru was assumed to be equal to that of 34-Dglu/34-Dman. The selectivity to a minor unknown product was approximated by assuming that this compound has the same HPLC RI sensitivity as 1256-HT.

Because 1256-HT, 34-Dfru, and 34-Dman are not separated by our HPLC method, experiments were run to completion to simplify analysis of the reaction product mixture. ^{13}C NMR was used to identify reaction products (details are provided in Section 8.4.1 of the Appendix). The Lgol conversion was defined as the change in the Lgol concentration divided by the initial Lgol concentration. The yield to a given product was defined as the concentration of that product divided

by the initial Lgol concentration. The selectivity to a given product was defined as the yield to that product divided by the Lgol conversion.

Lgol, THFDM, and THP2M5H were analyzed by a Shimadzu gas chromatograph (GC) equipped with a flame ionization detector with liquid injection. A Restek RTX-VMS capillary column (length: 30 m, inner diameter: 0.25 mm, film thickness: 1.4 μm) was used. The injection port and FID were maintained at 240°C. The injection volume was 1 μL and a split ratio of 50 was used. The column temperature ramp was as follows: hold 1 min at 40°C, ramp 10°C/min to 180°C, ramp 3°C/min to 240°C, hold 5 min at 240°C. Because THFDM and THP2M5H are partially overlapped in the GC, only the total yield to these two species is reported. The GC sensitivity of THP2M5H was assumed to be equal to that of THFDM.

Quantitative ^{13}C NMR spectra were collected on a Bruker Avance 500 MHz spectrometer at room temperature, using an inverse-gated decoupling pulse sequence with a 30° pulse. 10% D_2O was added to the samples prior to analysis. The ^{13}C NMR spectra were absolute-referenced to the associated ^{1}H NMR spectra. 112 Scans were used, with an acquisition time of 1 sec and a relaxation delay of 30 sec. ^{13}C NMR spectra for threo-Lgol, erythro-Lgol, cis-1256-HT, trans-1256-HT, cis-THFDM, and trans-THFDM were matched to those in the literature.[8] 34-Dglu, 34-Dman, and 34-Dfru were identified by ^{13}C NMR (see Section 8.4.1 in the Appendix). In some cases, ^{13}C NMR peaks could not be completely distinguished due to the similar chemical shifts between different carbon positions and between different tautomers. However, all chemical shifts, relative peak areas, and multiplicities of each carbon position are consistent with the assignments. Mestrenova (v. 12.01) was used for ^{13}C NMR prediction of reaction products. Electrospray ionization mass spectrometry (ESI-MS) was used to confirm the molecular weight of 34-Dfru.

Reactions of Lgol with SiAl, Pt/SiAl, and Pt/SiO_2 were carried out in a 45 mL Inconel Parr reactor. 10 mL of reaction solution and a magnetic stir bar were placed in the reactor. The reactor was purged 4x with 35.5 bar gas (H_2 or Ar), pressurized to 35.5 bar, then heated to the reaction temperature. The heat-up time was in the range of 10-15 minutes. Product concentrations from Parr reactor experiments were corrected for 2.3% evaporation of water from the reaction solution, which was measured based on an apparent increase in the carbon balance in the experiment with Lgol heated to 150°C in the absence of catalyst (Table 5.1, Entry 1). Reactions of Lgol with Amberlyst 70, H_2SO_4, and $AlCl_3$ were carried out were carried out in 10 mL thick-walled glass reactors (sealed by a PTFE cap) submerged in an oil bath. 3 mL of reaction solution and a magnetic stir bar were placed in the glass reactor. After reaction, products were cooled to room temperature using an ice bath, filtered with a 0.22 μm PES syringe filter prior to analysis. Reaction products at higher concentration (> 5 wt%) were diluted 5-10x in water prior to analysis.

5.3. Results and Discussion

Lgol conversion to 1256-HT was studied over different metal and acid catalysts to gain insights into the reaction network for this transformation. The proposed reaction network for Lgol conversion to 1256-HT is shown in Figure 5.1. The threo- and erythro- isomers of Lgol undergo acid-catalyzed hydrolysis to two diastereomers of a cyclic hemiacetal species, with threo-Lgol converted to 34-Dman and erythro-Lgol converted to 34-Dglu. At higher temperatures (i.e., 150°C) with no added catalyst, 34-Dman and 34-Dglu undergo aldose-ketose isomerization to a hemiketal-ketone species, 34-Dfru. Hydrogenation of 34-Dman forms cis-1256-HT; hydrogenation of 34-Dglu forms trans-1256-HT; and hydrogenation of 34-Dfru forms a nearly 1:1 mixture of cis- and

trans- 1256-HT. The following sections describe the experimental evidence for this reaction network.

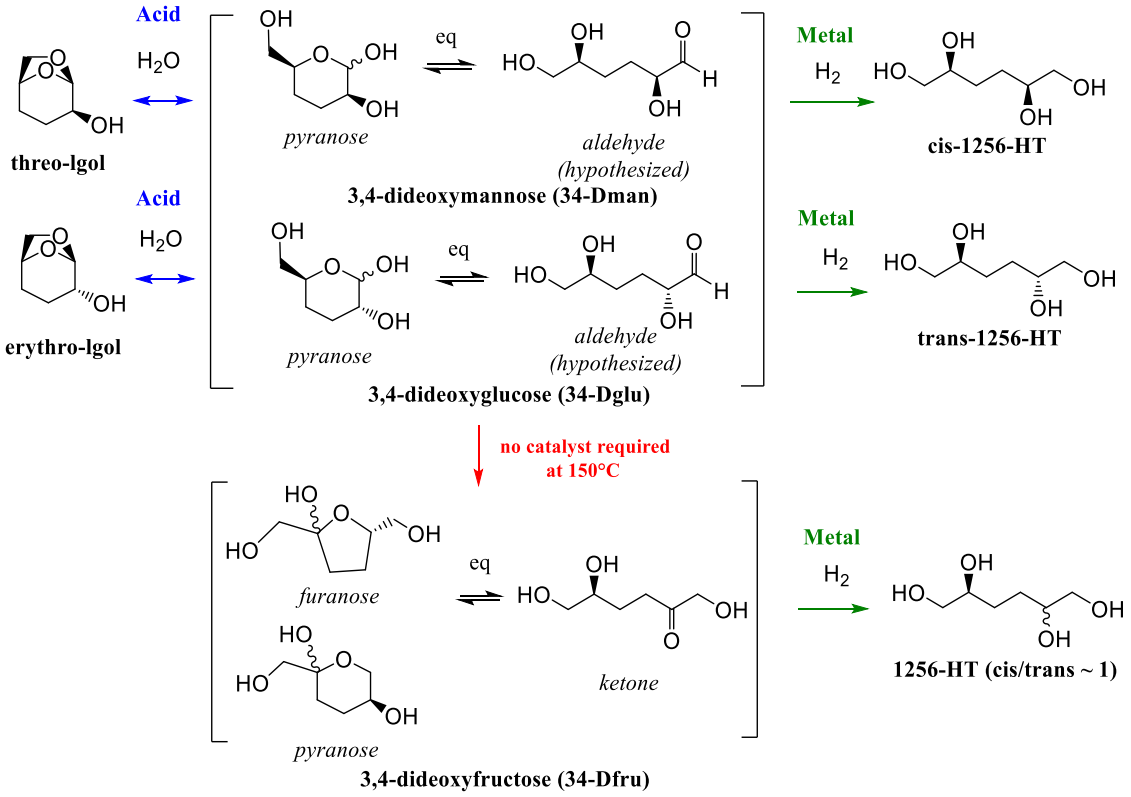

Figure 5.1: *Proposed reaction network for Lgol conversion to 1256-HT. "eq" indicates reactions which are assumed to be quasi-equilibrated.*

5.3.1. Lgol conversion over Pt & SiAl catalysts

In the absence of a catalyst, the conversion of Lgol at 150°C is less than 10% (Table 5.1, Entry 1). The conversion of Lgol is also less than 10% over a 5% Pt/SiO_2 catalyst in the absence of acid sites (Table 5.1, Entry 2) at 150°C, indicating that the first step in this reaction is acid-catalyzed rather than metal-catalyzed. Over a bifunctional 1.1% Pt/SiAl catalyst, containing metal (Pt) and acid (SiAl) sites, Lgol in water undergoes conversion to 1256-HT in 91% yield (Table

5.1, Entry 3). THFDM and THP2M5H are byproducts produced in a total yield of 5%. The product yields do not change when the reaction is run at a higher catalyst to feed ratio (Table 5.1, Entry 4), showing that 1256-HT is not reactive at these reaction conditions and that the observed THFDM is not formed via dehydration of 1256-HT. A physical mixture of SiAl and 5% Pt/SiO_2 shows comparable selectivity 1256-HT as the Pt/SiAl catalyst (Table 5.1, Entry 5), indicating that nanoscale proximity of metal and acid sites is not required for the selective conversion of Lgol to 1256-HT.

When Lgol is treated over SiAl in the absence of metal catalyst at 150^{o}C (Table 5.1, Entry 7), the major product is a hemiketal-ketone species, 34-Dfru (Figure 5.1), produced in 80% selectivity. Similar to fructose,[9] this species exhibits five tautometric forms in water, which were observed by ^{13}C NMR: α and β pyranose, α and β furanose, and an acyclic ketone form (Table 8.8 in the Appendix). In Section 5.3.2, we will show that 34-Dfru is produced via aldose-ketose isomerization of 34-Dglu and 34-Dman.

Hydrogenation of 34-Dfru (Table 5.1, Entry 8) over Pt/SiO_2 results in 77% selectivity to 1256-HT with THFDM + THP2M5H as the major side-product (15% yield). The 1256-HT yield is lower, at the expense of a higher THFDM + THP2M5H yield, compared to the 1.1% Pt/SiAl catalyst. A similar decrease in the 1256-HT yield is observed at lower H_2 pressures (Figure 5.2). These results suggest that when the SiAl sites are separated from the Pt metal sites, or when the rate of hydrogenation is lower (at lower H_2 pressures), reaction intermediates can be converted to THFDM precursors over SiAl acid sites prior to hydrogenation over Pt metal sites. In Chapter 4, we reported that THFDM and THP2M5H are the main hydrogenolysis products over Pt/SiAl catalysts in THF solvent. Lgol cannot be converted to 1256-HT in an organic solvent, because

water is a stoichiometric reactant in the formation of 1256-HT. The reaction mechanism to form THFDM in THF solvent was proposed to proceed via a series of carbocation intermediates. Some of the intermediates in the pathway to produce 1256-HT from Lgol in water are the hydrated versions of these carbocation intermediates. A comparison of the proposed reaction intermediates in the production of 1256-HT, THFDM, and THP2M5H are shown in Figure 5.4. Precursors to THFDM and THP2M5H could not be identified in the product mixture of Lgol conversion over SiAl due to the low concentration of these species.

Table 5.1. *Lgol conversion (t/e = 1.3) over Pt/SiAl, SiAl, and Pt/SiO_2 catalysts.*

					Selectivity (%)				
Entry	**Feed**	**Catalyst (cat/feed ratio)**	**Conditions**	**Lgol Conversion (%)**	**1256-HT (c/t)**	**34-Dman + 34-Dglu**	**34-Dfru**	**THFDM + THP2M5H**	**Unknown**
1	Lgol	None	150^{o}C, 3h, 35.5 bar H_2	8	0	8	94	0	0
2	Lgol	5% Pt/SiO_2 (10 mg/g)	150^{o}C, 3h, 35.5 bar H_2	3					
3	Lgol	1.1% Pt/SiAl (10 mg/g)	150^{o}C, 6h, 35.5 bar H_2	100	91 (1.07)	0	0	5	2
4	Lgol	1.1% Pt/SiAl (20 mg/g)	150^{o}C, 6h, 35.5 bar H_2	100	91 (1.06)	0	0	6	2
5	Lgol	SiAl + 5% Pt/SiO_2 (10 mg/g each)	150^{o}C, 6h, 35.5 bar H_2	99	92 (1.06)	0	0	3	2
6	Lgol	SiAl (10 mg/g)	100^{o}C, 3h, 35.5 bar Ar	1					

7	Lgol	SiAl (10 mg/g)	150°C, 6h, 35.5 bar Ar	95	0	3	80	0	2
8	Product of (7)	5% Pt/SiO_2 (10 mg/g)	150°C, 9h, 35.5 bar H_2	100	77 (1.00)	0	0	15	0

Conditions: *1.9 wt% Lgol in water (t/e = 1.3), 750 rpm stir rate.*

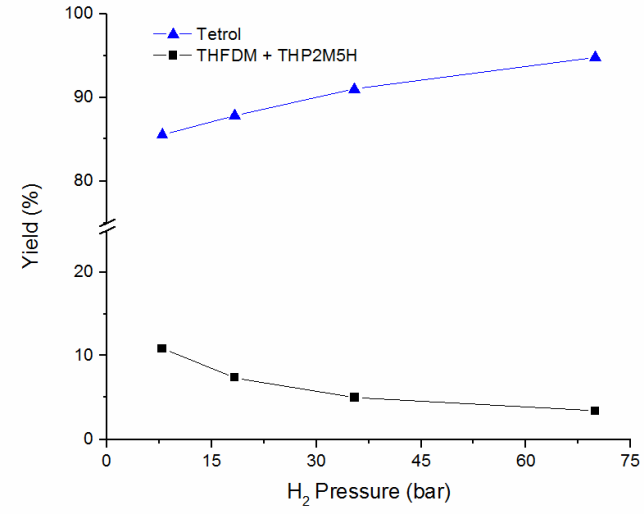

Figure 5.2. *Effect of H_2 pressure on 1256-HT yield from Lgol over 1.1% Pt/SiAl*

Conditions*: 150°C, 10mg catalyst per g feed, 1.9 wt% Lgol in water (t/e = 1.3). Reaction time was chosen such that 100% conversion of Lgol and all reaction intermediates was achieved (6h for experiments at 18.2 bar and above; 12h for the experiment at 7.9 bar). A minor unidentified product (2% selectivity) was observed in all experiments. Solid lines are visual aids.*

The conversion of Lgol to 1256-HT over Pt/SiAl catalysts was investigated at different Lgol concentrations (Figure 5.3). 1256-HT yields of up to 86% were also achieved at Lgol concentrations up to 21 wt% in water over a 5.3% Pt/SiAl catalyst, demonstrating that this reaction can be carried out at more industrially relevant reactant concentrations.

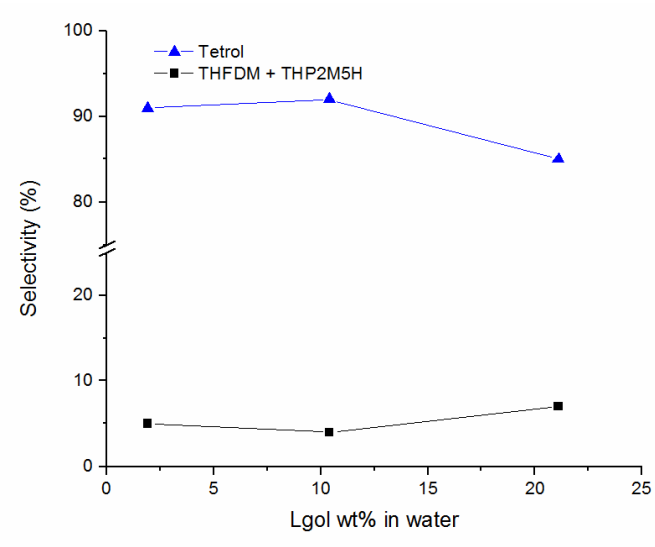

Figure 5.3. *Effect of Lgol concentration on 1256-HT selectivity over Pt/SiAl catalysts.*

Conditions*: 150°C, 35.5 bar H_2, Lgol in water (t/e = 1.3), 10mg catalyst per g feed, 750 rpm. Catalyst metal loading and reaction time were selected to reach >95% conversion of Lgol and reaction intermediates (1.1% Pt/SiAl and t=6h for 1.9 wt% Lgol; 5.3% Pt/SiAl and t=6h for 10 wt% Lgol; 5.3% Pt/SiAl and t=17h for 21 wt% Lgol). The experiment at 21 wt% Lgol was carried out in a 75 mL Parr reactor to maintain a stoichiometric excess of H_2. Solid lines are visual aids.*

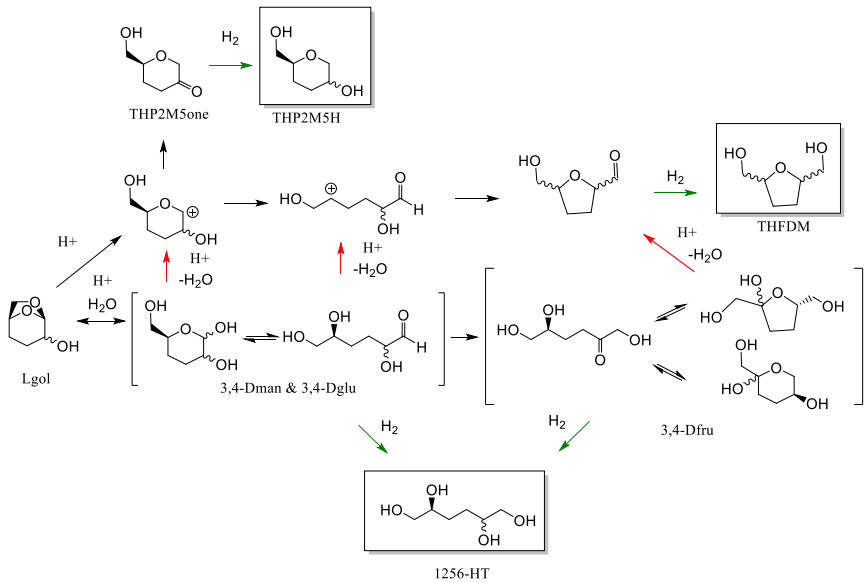

Figure 5.4. *Proposed pathways to form 1256-HT, THFDM, and THP2M5H from Lgol. The pathway to form THFDM and THP2M5H from Lgol in THF solvent was reported in Chapter 4. Red arrows indicate hypothetical dehydration reactions which could connect the 1256-HT and THFDM production pathways. Green arrows indicate hydrogenation reactions occurring on metal sites.*

5.3.2. Lgol conversion over different acid catalysts

At a lower temperature of 100°C, SiAl has negligible reactivity for Lgol conversion (Table 5.1, Entry 6). In contrast, when Lgol is treated over Amberlyst 70 at 100°C, the threo- and erythro-isomers of Lgol are hydrated to 34-Dman and 34-Dglu, respectively, in 86% selectivity (Table 5.2, Entry 2). This reaction is similar to the hydrolysis of LGA to glucose (see Figure 8.11 in the Appendix), in that water is added to the anhydro-bridge facilitated by an acid catalyst.[10] In the case of Lgol hydrolysis, both C_2 epimers (i.e., the 3,4-dideoxy- versions of glucose and mannose) are produced because both the erythro- and threo- isomers of Lgol are present. This reaction reaches equilibrium at 83% conversion of erythro-Lgol and 58% conversion of threo-Lgol, indicated by the fact that the Lgol conversion and product yields do not change significantly between 30-120 min (Figure 5.5). Nearly identical results are achieved with H_2SO_4 catalyst (Table 5.2, Entry 6), verifying that the results in Figure 5.5 are not due to catalyst deactivation. No conversion of Lgol is observed at 100°C in the absence of catalyst (Table 5.2, Entry 1).

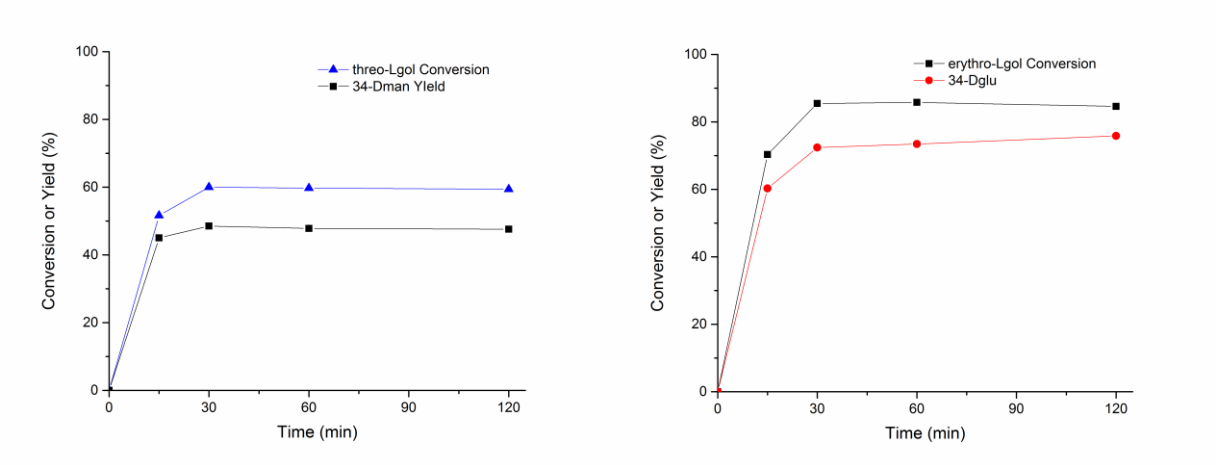

Figure 5.5A: *threo-Lgol conversion*

Figure 5.5B*: erythro-Lgol conversion*

Figure 5.5. *threo- and erythro- Lgol conversion to 34-Dman and 34-Dglu over Amberlyst 70. 16.7 mg catalyst per g feed, 1.9 wt% Lgol in water (t/e = 1.3), T = 100°C, 500 rpm. Solid lines are visual aids.*

Treating 34-Dglu and 34-Dman (formed over Amberlyst 70 or H_2SO_4) at 150°C in the absence of catalyst (Table 5.2, Entries 4 and 7) results in isomerization to 34-Dfru, with similar selectivity as the reaction of Lgol over SiAl at the same temperature (Table 5.1, Entry 7). While the Brønsted acid sites of SiAl are expected to catalyze the hydrolysis of Lgol to 34-Dman and 34-Dglu, it is not clear whether the isomerization of 34-Dman and 34-Dglu to 34-Dfru occurs on the catalyst surface or in solution. SiAl possesses both Brønsted and Lewis acid sites, whereas Amberlyst 70 contains only Brønsted acid sites.[11] A Lewis acid catalyst, namely $AlCl_3$, was able to isomerize 34-Dman and 34-Dglu to 34-Dfru (Table 5.2, Entry 5) at 100°C, under conditions at which this reaction does not proceed in the absence of a catalyst (Table 5.2, Entry 3). This result shows that the isomerization of 34-Dman and 34-Dglu to 34-Dfru is promoted by Lewis acid sites, similar to glucose isomerization to fructose (see Figure 8.11 in the Appendix).[12] It should be noted

that there are multiple possible mechanisms of aldose-ketose isomerization which could be taking place in the transformation of 34-Dman and 34-Dglu to 34-Dfru.

Hydrogenation of 34-Dglu + 34-Dman over Pt/SiO_2 at 100°C forms 1256-HT in high selectivity (89%) (Table 5.2, Entry 8). The reaction was carried out at 100°C to avoid possible isomerization of 34-Dman and 34-Dglu to 34-Dfru. We hypothesize that hydrogenation of 34-Dman and 34-Dglu proceeds via ring-opening to the acyclic aldehyde tautomer (Figure 5.1) as is the case with other cyclic hemiacetals, such as glucose and 2-hydroxytetrahydropyran.[9, 13]

Table 5.2. *Lgol conversion (t/e = 1.3) over Amberlyst 70, H_2SO_4, and $AlCl_3$ catalysts.*

					Selectivity (%)			
Entry	**Feed**	**Catalyst (cat/feed ratio)**	**Conditions**	**Lgol Conversion (%) (t/e*)**	**1256-HT (c/t)**	**34-Dman + 34-Dglu (34-Dman/34-Dglu)**	**34-Dfru**	**THFDM + THP2M5H**
1	Lgol	None	100°C, 2h, air	0				
2	Lgol	Amberlyst 70 (16.7 mg/g)	100°C, 0.5h, air	68 (0.92)	0	87 (0.89)	0	0
3	Product of (2)	None	100°C, 2h, air	68 (0.94)	0	88 (0.87)	0	0
4**	Product of (2)	None	150°C, 3h, 35.5 bar Ar	73 (1.0)	0	3	76	0
5	Product of (2)	$AlCl_3$ (50mM)	100°C, 0.5h, air	76 (0.81)	0	2	78	0
6	Lgol	H_2SO_4 (50mM)	100°C, 0.5h, air	66 (0.98)	0	89 (0.86)	0	0
7***	Product of (6)	None	150°C, 3h, 35.5 bar Ar	67 (0.99)	0	2	82	0

8	Product of (2)	5% Pt/SiO_2 (10 mg/g)	100°C, 9h, 35.5 bar H_2	73 (0.95)	89 (0.93)	0	0	1

Conditions: *1.9 wt% Lgol in water (t/e = 1.3). Entries 4, 7, and 8 carried out in 45 mL Parr reactor (750 rpm stir rate). Entries 1, 2, 3, 5, and 6 carried out in 10mL thick-walled glass reactor (500 rpm stir rate). *threo-erythro ratio of converted Lgol. **Feedstock treated with Amberlyst 21 basic anion exchange resin (0.12 g per g solution) to remove trace anions prior to reaction. *** neutralized using Amberlyst 21 basic anion exchange resin and diluted 1.4x in water prior to reaction.*

5.3.3. Relationship between Lgol and 1256-HT stereochemistry

To gain further insight into the reaction network, the effect of the Lgol t/e ratio on the 1256-HT c/t ratio was studied. The t/e ratio of Lgol can be varied by hydrogenating Cyrene with different metal catalysts, as shown in Chapter 3. Different c/t ratios of 1256-HT could impact the physico-chemical properties of chiral products derived from 1256-HT.[14] The results of Lgol conversion with a higher t/e ratio (t/e = 3.3) are summarized in Table 5.3.

The t/e stereochemistry of Lgol is partially preserved upon conversion to 1256-HT over Pt/SiAl catalysts. When starting with Lgol with a t/e ratio of 3.3, the 1256-HT c/t ratio is 1.47, corresponding to 35% preservation of the t/e stereochemistry of Lgol (Table 5.3, Entry 1). Using a higher metal loading of 5.3% Pt/SiAl (Table 5.3, Entry 2) results in a 1256-HT c/t ratio of 2.00 (64% preservation of the t/e stereochemistry of Lgol), suggesting that using a higher Pt loading promotes the rapid hydrogenation of 34-Dman and 34-Dglu prior to isomerization to 34-Dfru. On the other hand, when the acid (SiAl) and metal (Pt) sites are separated, 34-Dglu and 34-Dman are

isomerized to 34-Dfru prior to hydrogenation (Table 5.3, Entry 3). Hydrogenation of 34-Dfru at 150ºC over Pt/SiO_2 presumably occurs via the acyclic ketone tautomer, and produces nearly equal amounts of cis- and trans-1256-HT (Table 5.3, Entry 4). Similarly, hydrogenation of fructose has been reported to result in a 1:1 mixture of sorbitol and mannitol (see Figure 8.11 in the Appendix) when the acyclic ketone form of fructose is hydrogenated.[15] The yield of 1256-HT over separated SiAl and Pt/SiO_2 catalysts is lower, at the expense of a higher yield of THFDM + THP2M5H, compared to the reaction with the bifunctional 1.1% Pt/SiAl catalyst.

When Lgol is hydrolyzed using Amberlyst 70 at 100ºC (Table 5.3, Entry 5), the conversions of erythro- and threo-Lgol are nearly equal to the case in which the t/e ratio is 1.3 (Table 5.2, Entry 2). This result is consistent with the finding that the Lgol hydrolysis reaction has reached equilibrium (Figure 5.5). The ratio of the two diastereomers of the product, 34-Dglu and 34-Dman, is nearly equal to the ratio of converted threo- and erythro-Lgols. Hydrogenation of the mixture of 34-Dman and 34-Dglu and Lgol over 5% Pt/SiO_2 at 100ºC results in nearly complete retention of the Lgol t/e stereochemistry in the formation of cis and trans-1256-HT (Table 5.3, Entry 6). Similarly, hydrogenation of glucose and mannose does not alter the C_2 stereocenter and therefore produces sorbitol and mannitol, respectively (see Figure 8.11 in the Appendix).[9, 16]

Table 5.3: *Lgol conversion (t/e = 3.3) over metal and acid catalysts.*

					Selectivity (%)				
Entry	**Feed**	**Catalyst (cat/feed ratio)**	**Conditions**	**Lgol Conversion (%) (t/e*)**	**1256-HT (c/t)**	**34-Dman + 34-Dglu (34-Dman/34-Dglu)**	**34-Dfru**	**THFDM + THP2M5H**	**Unknown**
1	Lgol	1.1% Pt/SiAl (10 mg/g)	150°C, 6h, 35.5 bar H_2	100	94 (1.47)	0	0	5	2
2	Lgol	5.3% Pt/SiAl (10 mg/g)	150°C, 3h, 35.5 bar H_2	99	89 (2.00)	0	0	3	2
3	Lgol	SiAl (10 mg/g)	150°C, 6h, 35.5 bar Ar	95	0	3	74	0	2
4	Product of (3)	5% Pt/SiO_2 (10 mg/g)	150°C, 9h, 35.5 bar H_2	98	69 (1.08)	0	0	19	2
5	Lgol	Amberlyst 70** (16.7mg /g)	100°C, 0.5h, air	63% (2.25)	0	88 (2.10)	0	0	0
6	Product of (5)	5% Pt/SiO_2 (10 mg/g)	100°C, 9h, 35.5 bar H_2	70% (2.48)	84 (2.30)	1	0	0	2

Conditions: *2 wt% Lgol in water (t/e = 3.3), 750 rpm. *threo-erythro ratio of converted Lgol. **Carried out in a thick-walled glass reactor, 500 rpm*

These experiments show that the c/t ratio of 1256-HT can be controlled by varying i) the Lgol t/e ratio, ii) the type of the acid catalyst, which in turn affects the required reaction temperature, and iii) the metal-acid ratio and proximity (e.g. different metal loadings, or using separated metal and acid sites).

5.3.4. Comparison of catalytic pathways to produce 1256-HT

Figure 5.6 compares the pathways to produce 1256-HT via sorbitol and Lgol. Previous approaches to produce 1256-HT from hydrogenolysis of sorbitol (derived from glucose or R-glycosides) over Cu-based catalysts showed a maximum 1256-HT yield of < 50%, and required harsher reaction conditions (≥ 200°C).[2a, 5] The lower 1256-HT yield is due to the difficulty of selectively dehydrating the C_3 and C_4 positions of sorbitol without catalyzing dehydration reactions at other carbon positions. In contrast, the route to produce 1256-HT from Lgol is inherently more selective to 1256-HT because the precursor, LGO, is dehydrated at the C_3 and C_4 positions during its formation from LGA.[17] The pathway from LGO to 1256-HT involves hydrogenation of C=C and C=O bonds over a metal catalyst, C-O cleavage of an anhydro-bridge ether bond over an acid catalyst, ring-opening of a cyclic hemiacetal, and optional aldose-ketose isomerization. Because these reactions can be carried out selectively at milder conditions (≤ 150°C), LGO can be converted to 1256-HT without catalyzing undesired side reactions. Furthermore, the ability to alter the Lgol t/e ratio, via stereoselective hydrogenation of the ketone group of Cyrene (Chapter 3), offers control over the 1256-HT c/t ratio which is not available with the sorbitol conversion route.

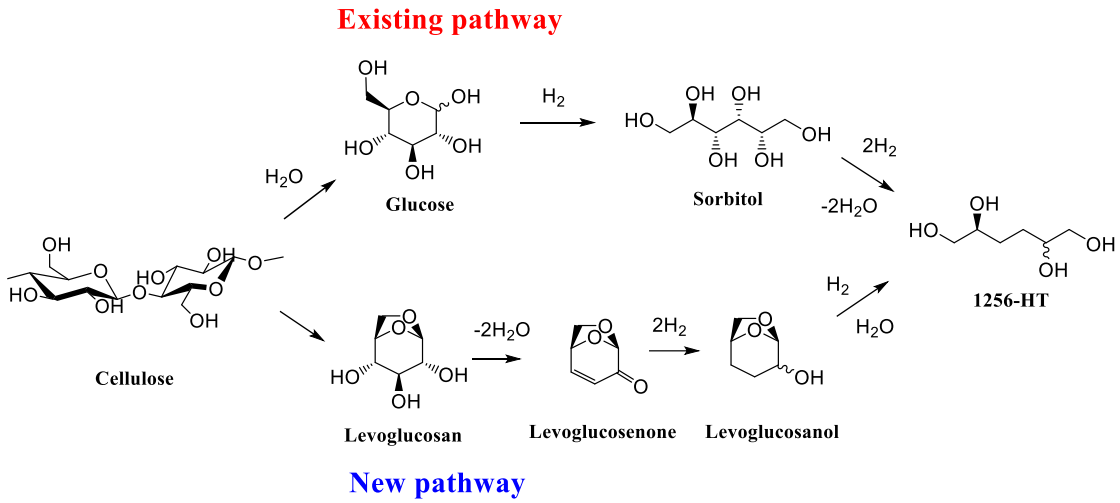

***Figure 5.6**: 1256-HT production from cellulose via sorbitol and via levoglucosenone.*

When comparing these two routes from cellulose to 1256-HT, it should be noted that the maximum reported yield of LGO from cellulose is about 50%, due to humin formation and other side-reactions.[18] One benefit of the route to 1256-HT via LGO is that the high selectivity to 1256-HT avoids the need to separate 1256-HT from numerous other polyols.[6]

5.4. Conclusions

We have elucidated a new route to convert bio-renewable Lgol into 1256-HT in water solvent over metal and acid catalysts in up to 90% yield. High 1256-HT yields are maintained at Lgol concentrations of up to 21 wt% in water. This route is significantly more selective than previously reported sorbitol hydrogenolysis routes, and offers control over the 1256-HT c/t ratio. The choice of acid catalyst (Amberlyst 70 or SiAl) and reaction temperature (100^{o}C or 150^{o}C) can be used to control which reaction intermediates (34-Dman and 34-Dglu, or 34-Dfru) are formed in the conversion of Lgol to 1256-HT. The 1256-HT c/t ratio can be altered by varying the Lgol t/e ratio, and by selecting the reaction conditions to determine whether the stereocenter at the C_2

position is preserved or erased prior to hydrogenation. This new approach to produce 1256-HT from cellulose-derived levoglucosenone opens the door to new, sustainable chemicals derived from 1256-HT.

5.5. References

1. Corma, A.; Iborra, S.; Velty, A., Chemical Routes for the Transformation of Biomass into Chemicals. *Chemical Reviews* **2007,** *107* (6), 2411-2502.
2. (a) Strensrud, K.; Ma, C.-C. Synthesis of R-glucosides, sugar alcohols, reduced sugar alcohols, and furan derivatives of reduced sugar alcohols (patent application). 2017; (b) Moreau, C.; Belgacem, M. N.; Gandini, A., Recent Catalytic Advances in the Chemistry of Substituted Furans from Carbohydrates and in the Ensuing Polymers. *Topics in Catalysis* **2004,** *27* (1), 11-30.
3. (a) Buntara, T.; Melián-Cabrera, I.; Tan, Q.; Fierro, J. L. G.; Neurock, M.; de Vries, J. G.; Heeres, H. J., Catalyst studies on the ring opening of tetrahydrofuran–dimethanol to 1,2,6-hexanetriol. *Catalysis Today* **2013,** *210*, 106-116; (b) Buntara, T.; Noel, S.; Phua, P. H.; Melián-Cabrera, I.; de Vries, J. G.; Heeres, H. J., From 5-Hydroxymethylfurfural (HMF) to Polymer Precursors: Catalyst Screening Studies on the Conversion of 1,2,6-hexanetriol to 1,6-hexanediol. *Topics in Catalysis* **2012,** *55* (7), 612-619.
4. (a) 1,6-Hexanediol Market by Application (Polyurethanes, Coatings, Acrylates, Adhesives, Unsaturated Polyester Resins, Plasticizers, and Others) and By Geography (NA, Europe, Asia-Pacific, & ROW) - Trends and Forecasts to 2019. http://www.researchandmarkets.com/research/zs4gnb/16hexanediol (accessed January 22); (b) He, J.; Burt, S. P.; Ball, M.; Zhao, D.; Hermans, I.; Dumesic, J. A.; Huber, G. W., Synthesis of 1,6-Hexanediol from Cellulose Derived Tetrahydrofuran-Dimethanol with Pt-WOx/TiO2 Catalysts. *ACS Catalysis* **2018,** *8* (2), 1427-1439; (c) He, J.; Huang, K.; Barnett, K. J.; Krishna, S.; Martin Alonso, D.; Brentzal, Z.; Burt, S. P.; Walker, T. W.; Banholzer, W.; Maravelias, C. T.; Hermans, I.; Dumesic, J.; Huber, G., New catalytic strategies for alpha-omega diol production from lignocellulosic biomass. *Faraday Discussions* **2017**; (d) Chia, M.; Pagán-Torres, Y. J.; Hibbitts, D.; Tan, Q.; Pham, H. N.; Datye, A. K.; Neurock, M.; Davis, R. J.; Dumesic, J. A., Selective Hydrogenolysis of Polyols and Cyclic Ethers over Bifunctional Surface Sites on Rhodium–Rhenium Catalysts. *Journal of the American Chemical Society* **2011,** *133* (32), 12675-12689; (e) Allgeier, A. M.; Namal De Silva, W. I.; Korovessi, E.; Menning, C. A.; Ritter, J. C.; Sengupta, S. K.; Stauffer, C. S. Process for preparing 1,6-hexanediol. US 8865,940 B2, 2014.
5. Urbas, B. Process for the production of 3,4-dideoxyhexitol. US 1989/4,820,880, 1989.
6. Smith, B.; Ma, C.-c. Process for the isolation of 1,2,5,6-hexanetetrol from sorbitol hydrogenolysis reaction mixtures using simulated moving bed chromatography. 2017.
7. Alamillo, R.; Tucker, M.; Chia, M.; Pagan-Torres, Y.; Dumesic, J., The selective hydrogenation of biomass-derived 5-hydroxymethylfurfural using heterogeneous catalysts. *Green Chemistry* **2012,** *14* (5), 1413-1419.
8. (a) Miftakhov, M. S.; Gaisina, I. N.; Valeev, F. A.; Shitikova, O. V., Synthesis of 1,6-anhydro-3-bromo-3,4-dideoxy-β-d-threo-hex-3-enopyranose. *Russ Chem Bull* **1995,** *44* (12), 2350-2352; (b) Maier, M. E.; Reuter, S., Double Asymmetric Dihydroxylation of 1,5-Hexadiene. *Liebigs Annalen* **1997,** *1997* (10), 2043-2046; (c) Connolly, T. J.; Considine, J. L.; Ding, Z.; Forsatz, B.; Jennings, M. N.; MacEwan, M. F.; McCoy, K. M.; Place, D. W.; Sharma, A.; Sutherland, K., Efficient Synthesis of 8-Oxa-3-aza-bicyclo[3.2.1]octane Hydrochloride. *Organic Process Research & Development* **2010,** *14* (2), 459-465.
9. L.G. Wade, J., *Organic Chemistry*. 7 ed.; Prentice Hall: Upper Saddle River, NJ, 2010.
10. (a) Helle, S.; Bennett, N. M.; Lau, K.; Matsui, J. H.; Duff, S. J. B., A kinetic model for production of glucose by hydrolysis of levoglucosan and cellobiosan from pyrolysis oil. *Carbohydrate Research* **2007,** *342* (16), 2365-2370; (b) Abdilla, R. M.; Rasrendra, C. B.; Heeres, H. J., Kinetic Studies on the Conversion of Levoglucosan to Glucose in Water Using Brønsted Acids as the Catalysts. *Industrial & Engineering Chemistry Research* **2018,** *57* (9), 3204-3214.
11. Weingarten, R.; Tompsett, G. A.; Conner Jr, W. C.; Huber, G. W., Design of solid acid catalysts for aqueous-phase dehydration of carbohydrates: The role of Lewis and Brønsted acid sites. *Journal of Catalysis* **2011,** *279* (1), 174-182.

12. (a) Román-Leshkov, Y.; Moliner, M.; Labinger, J. A.; Davis, M. E., Mechanism of Glucose Isomerization Using a Solid Lewis Acid Catalyst in Water. *Angewandte Chemie International Edition* **2010,** *49* (47), 8954-8957; (b) Delidovich, I.; Palkovits, R., Catalytic Isomerization of Biomass-Derived Aldoses: A Review. *ChemSusChem* **2016,** *9* (6), 547-561.
13. Brentzel, Z. J.; Barnett, K. J.; Huang, K.; Maravelias, C. T.; Dumesic, J. A.; Huber, G. W., Chemicals from Biomass: Combining Ring-Opening Tautomerization and Hydrogenation Reactions to Produce 1,5-Pentanediol from Furfural. *ChemSusChem* **2017,** *10* (7), 1351-1355.
14. Young, R. J.; Lovell, P. A., *Introduction to Polymers*. 3 ed.; CRC Press: Boca Raton, FL, 2011.
15. Heinen, A. W.; Peters, J. A.; van Bekkum, H., Hydrogenation of fructose on Ru/C catalysts. *Carbohydrate Research* **2000,** *328* (4), 449-457.
16. Mishra, D. K.; Hwang, J.-S., Selective hydrogenation of d-mannose to d-mannitol using NiO-modified TiO2 (NiO-TiO2) supported ruthenium catalyst. *Applied Catalysis A: General* **2013,** *453*, 13-19.
17. Greatrex, B. W.; Meisner, J.; Glover, S. A.; Raverty, W., Support for a Dioxyallyl Cation in the Mechanism Leading to (−)-Levoglucosenone. *The Journal of Organic Chemistry* **2017,** *82* (23), 12294-12299.
18. Cao, F.; Schwartz, T. J.; McClelland, D. J.; Krishna, S. H.; Dumesic, J. A.; Huber, G. W., Dehydration of cellulose to levoglucosenone using polar aprotic solvents. *Energy & Environmental Science* **2015,** *8* (6), 1808-1815.

Chapter 6. Methyl Glycoside Conversion to Hexanetetrols and Hexanetriols over Metal Catalysts

6.1. Introduction

Sugars are a valuable feedstock for the production of oxygenated commodity chemicals because they can be sourced from renewable carbon sources, and due to their inherent oxygenated functional groups.[1] They are also ideal precursors for chiral synthesis due to their well-defined stereochemistry.[2] The feedstocks in this work include the methyl glycosides of D-galactose, a food additive derived from milk sugar[3]; D-mannose, a food additive found in plant sources or produced from glucose epimerization[4]; L-rhamnose is a 6-deoxy sugar predominantly found in plant pectin;[5] L-fucose is a 6-deoxy-sugar predominantly found in algae.[6] Sugars as well as lignocellulosic biomass can be hydrodeoxygenated to partially reduced polyols over heterogeneous metal-acid catalysts.[1, 7] However, these processes are typically not regio-selective, due to indiscriminate cleavage of C-OH groups, which results in a complex mixture of polyols.[8] These catalytic steps are also typically not stereoselective, destroying the stereocenters present in the original sugar feedstock.

Tomishige and co-workers recently reported on a route to selectively deoxygenate cis-vicinal OH groups from a variety of methyl glycosides feedstocks in 82-92% yield using a ReO_x-Pd/CeO_2 catalyst, resulting in stereopure methyl dideoxy-glycosides.[9] Methyl glycosides can be produced from sugars in nearly quantitative yields in methanol solvent over an acid catalyst.[10] In one example, a 3,4-dideoxyarabinoside feedstock was further converted to (2R)-1,2,5-pentanetriol with high stereoselectivity using methoxy bond hydrolysis followed by hydrogenation.[9a] Control

over product stereochemistry can be critical for applications such as pharmaceuticals, fine chemicals, and polymer synthesis.[2, 11]

Partially reduced polyols are valuable intermediates in the chemical industry, with applications as polymer precursors (e.g. in alkyd resins), surfactants, and hydrophilic solvents.[1] For example, 126-HT can be produced from petroleum via acrolein dimerization[12] or from biomass via HMF.[13] 126-HT has applications as a surfactant, non-toxic solvent, and cross-linker in alkyd resins.[12, 14] Derivatives of 126-HT are used in hydraulic fluids, corrosion inhibitors[15], and plasticizers.[12] The synthesis of another partially reduced polyol, 1256-HT, has been reported in up to 50% yield from hydrogenolysis of sugars over a Cu catalyst, along with a mixture of other polyols.[8b] In Chapter 5, we showed that 1256-HT can be produced from biomass-derived Lgol in up to 90% yield**,** via the intermediates 34-Dman and 34-Dglu. Further work is needed to synthesize materials from biomass-derived polyols in order to assess their properties.[16]

In this work, we show that the methyl-dideoxyglycosides can be converted, with high regio- and stereo-selectivity, to hexanetriols and hexanetetrols over a supported Pt catalyst. We propose a reaction mechanism involving methoxy bond hydrolysis and hydrogenation. Our results demonstrate a selective catalytic approach to produce hexanetetrols and hexanetriols as valuable feedstocks for the chemical industry.

6.2. Experimental Methods

$Pt(NH_3)_4(NO_3)_2$ solution (99%, Strem Chemicals) were used as received. Grade 135 amorphous SiO_2-Al_2O_3 (SiAl) and Davisil grade SiO_2 were purchased from Sigma Aldrich. Milli-Q water was used for all reactions and catalyst syntheses. The synthesis of dideoxy-methyl-glycosides from methyl-glycosides was reported in previous work[9a].

Pt/SiAl and Pt/SiO_2 catalysts were synthesized by incipient wetness impregnation of a $Pt(NH_3)_4(NO_3)_2$ solution in water. The catalysts were dried at 110^{o}C in air, calcined at 400^{o}C in flowing air (1^{o}C/min ramp, 3 h hold), reduced at 260^{o}C in flowing hydrogen (1^{o}C/min ramp, 4 h hold), then passivated at room temperature with 1% O_2/Ar. When the SiAl support was used directly in a reaction, it was calcined at 400^{o}C in flowing air prior to use. Pt site densities measured by CO chemisorption, and the acid site density of the 5.3% Pt/SiAl catalyst measured by NH_3-temperature programmed desorption, are reported in Chapter 4, Table 4.1.

A BioRad Aminex 87H column was used in a Shimadzu HPLC. The mobile phase was 5 mM H_2SO_4 (HPLC grade, Ricca Chemical) operated at a flow rate of 0.6 mL/min with a column temperature of 30^{o}C and an injection volume of 3 μL. Reaction products were quantified by HPLC using an RI detector. Chemical standards of the reaction products in this work are not commercially available. 1256-HT was prepared from Cyrene as described in Chapter 5. The RI sensitivity of 1,2,3,6-hexanetetrol (1236-HT) was assumed to be equal to that of 1256-HT. For quantification of 1,4,5-hexanetriol (145-HT) and 1,2,5-hexanetriol (125-HT), the RI sensitivity of these species was assumed to be equal to that of 126-HT.

^{13}C NMR spectra were collected on a Bruker Avance 500 MHz spectrometer at room temperature, using a Bruker DCH CryoProbe for increased sensitivity. 10% D_2O was added to the samples prior to analysis. The ^{13}C NMR spectra were absolute-referenced to the associated ^{1}H NMR spectra. Normal ^{13}C spectra were collected using 1H-decoupling using a 30° pulse, 128 scans, an acquisition time of 1 sec, and a relaxation delay of 2 sec. Quantitative ^{13}C NMR spectra were collected using inverse-gated decoupling, using a 30° pulse, 112 scans, an acquisition time

of 1 sec and a relaxation delay of 30 sec. NMR, HPLC, and polarimetry analysis of the reaction products and intermediates are provided in the Appendix (Sections 8.5.1 and 8.5.2).

Reactions were carried out in a 45 mL Inconel Parr reactor. 10-15 mL of reaction solution and a magnetic stir bar were placed in the reactor. The reactor was purged 4x with 35.5 bar gas (H_2 or Ar), pressurized to the desired pressure, then heated to the desired temperature. The heat-up time was in the range of 10-15 minutes. After reaction, products were cooled to room temperature using an ice bath, filtered with a 0.22 μm PES syringe filter prior to analysis. Product concentrations were corrected for 2.3% evaporation of water during the reaction.

6.3. Results and Discussion

6.3.1. Conversion of methyl- 2,3-dideoxy –glycosides

The reaction networks for the conversion of methyl-2,3-dideoxy-mannopyranoside (MDM) and methyl-2,3-dideoxy-rhamnopyranoside (MDR) are shown in Figure 6.1. Using a 5% Pt/SiO_2 catalyst at 120^oC in water, MDM is converted to (2R, 3S)-1236-HT in 95% yield and 100% stereoselectivity (Table 6.1, Entry 1; NMR, HPLC, and polarimetry provided in Supplementary Information, Section 8.5.1A). Incorporating the 96% yield of MDM from methyl-mannopyranoside,[9a] the overall yield of 1236-HT from methyl-mannopyranoside is 91%. Similarly, MDR is converted to (4R, 5S)-145-HT , in 92% yield and 100% stereoselectivity (Table 6.1, Entry 3; NMR, HPLC, and polarimetry provided in Supplementary Information, Section 8.5.1B). Incorporating the 92% yield of MDR from methyl-rhamnopyranoside,[9a] the overall yield of 145-HT from methyl-rhamnopyranoside is 85%.

Carrying out the reaction without any catalyst demonstrates that the first step is methoxy bond hydrolysis. For MDM conversion, 36 ^{13}C NMR peaks are observed at complete reactant conversion (Table 6.1, Entry 2A). These intermediates are tentatively identified as the alpha- and beta pyranose, alpha- and beta- furanose, anhydro-furanose, and anhydro-pyranose forms of 3,4-dideoxymannose/mannosan (23-Dman), based on ^{13}C NMR chemical shifts, multiplicities, and ESI-MS data (Appendix, Section 8.5.2A). Some of these intermediates may exist in equilibrium in water at room temperature. Hydrogenation of this mixture (Table 6.1, Entry 2B) results in an identical yield of 1236-HT to the one-pot case, showing that 23-Dman is an intermediate to 1236-HT. Cyclic hemiacetals exist in equilibrium with an aldehyde form.[17] While the aldehyde forms of these intermediates are not observed experimentally at room temperature by ^{13}C NMR, the aldehyde is expected to be the reactive form towards hydrogenation.

For the MDR case, 24 ^{13}C NMR peaks are observed at 100% reactant conversion (Table 6.1, Entry 4A). These intermediates are tentatively identified as four C_6 species, namely the alpha and beta pyranose, and alpha and beta furanose of 2,3-dideoxy-rhamnose (34-Drha), based on ^{13}C NMR chemical shifts, multiplicities, and ESI-MS data (Appendix, Section 8.5.2B). Some of these intermediates may exist in equilibrium in water at room temperature. 23-Drha cannot convert to the anhydro- form due to lack of a C_6-OH group. Over Pt/SiO_2, these intermediates are hydrogenated to 145-HT in 80% selectivity (Table 6.1, Entry 4B). The decrease in selectivity from the one-step case to the two-step case could be due to side-reactions which occur when the metal is not present to rapidly hydrogenate intermediates. Small unknown peaks are observed in the HPLC, whose yield sums to 9% (assuming they have the same RI sensitivity as 145-HT).

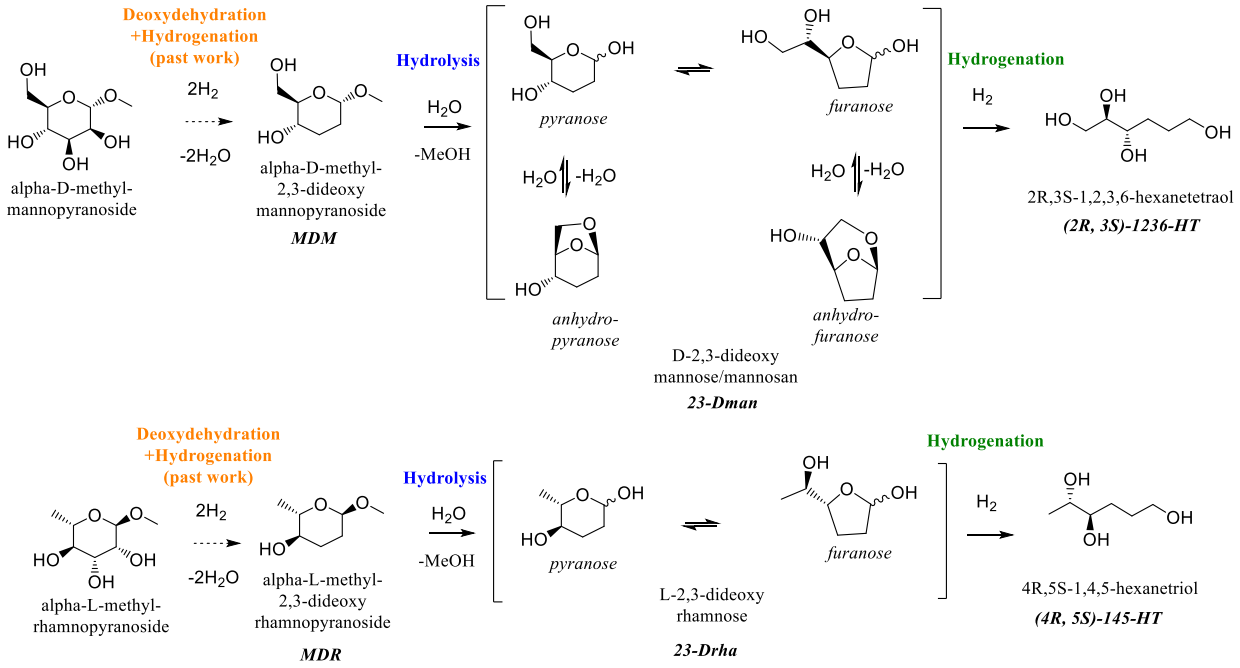

Figure 6.1. *Conversion of methyl-2,3-dideoxy-glycosides*

Table 6.1. *Conversion of 2,3-dideoxy sugars to hexane-triols and hexanetetrols*

Entry	Feed	Catalyst	Conditions	Conversion (%)	Major Product	HPLC Selectivity (%)	Diastereomer Selectivity
1	MDM	5% Pt/SiO_2	120^oC, 21h	100	1236-HT	95	100% (2R, 3S)
2A	MDM	None	120^oC, 21h	100	23-Dman	____	____
2B	Product of 2A	5% Pt/SiO_2	120^oC, 21h	100	1236-HT	96	100% (2R, 3S)
3	MDR	5% Pt/SiO_2	120^oC, 21h	100	145-HT	92	100% (4R, 5S)
4A	MDR	None	120^oC, 21h	100	23-Drha	____	____
4B	Product of 4A	5% Pt/SiO_2	120^oC, 21h	96	145-HT	76	100% (4R, 5S)

Conditions: *2 wt% feed in water (10-15 ml), 0.01 g cat/ g solution, 1000 psi* H_2

6.3.2. Conversion of methyl-3,4-dideoxy-glycosides

The reaction networks for conversion of methyl-3,4-dideoxy-glycosides are shown in Figure 6.2. Hydrogenation of these feedstocks at 120^{o}C for 21h over 5% Pt/SiO_2 results in low (10%) conversion, under conditions where the two methyl-2,3-dideoxy-glycosides achieve 100% conversion. A higher temperature of 150^{o}C was therefore used for the methyl-3,4-dideoxy-glycosides. The lower reactivity of methyl-3,4-dideoxy-glycoside (MDG, MDF) compared to methyl-2,3-dideoxy-glycosides (MDM, MDR) is consistent with the fact that the hydrolysis rate of methyl-2-deoxy-glucopyranoside has been reported to be three orders of magnitude greater than that of methyl-glucopyranoside. This effect is due to the electron-withdrawing nature of the C_2-OH group which destabilizes the carbocation transition state.[10]

Over 5% Pt/SiO_2 at 150^{o}C, methyl-3,4-dideoxy-galactopyranoside (MDG) is converted to 2R, 5S-1256-HT with 81% selectivity and 95% stereoselectivity [(2R, 5S) / (2S, 5S)] (Table 6.2, Entry 1). Incorporating the 88% yield of MDG from methyl-galactopyranoside,[9a] the overall selectivity of 1256-HT from methyl-galactopyranoside is 71%. Similarly, methyl-3,4-dideoxy-fucopyranoside is converted to 2S, 5S-125-HT in 90% selectivity and 82% stereoselectivity [(2S, 5S) / (2R, 5S)] (Table 6.2, Entry 4). Incorporating the 82% yield of MDF from methyl-fucopyranoside,[9a] the overall selectivity of 125-HT from methyl-fucopyranoside is 74%.

While 2,3-dideoxy feedstocks both show 100% stereoselectivity, 3,4-dideoxy feedstocks display non-zero selectivity towards C_2-OH stereo-inversion products (Table 6.2). In Chapter 5, we reported that 3,4-Dglu and 3,4-Dman can undergo aldose-ketose isomerization to form a hemiketal-ketone species, 3,4-dideoxyfructose. This reaction occurs in the absence of catalyst at

150°C, but is largely suppressed at a lower temperature of 100°C. Formation of the ketone group at the C_2 position erases the original C_2 stereocenter, and hydrogenation results in a 1:1 mixture of diastereomers of 1256-HT. Therefore, we expect that the partial loss of stereoselectivity in MDG and MDF conversion is due to aldose-ketose isomerization prior to hydrogenation (Figure 6.2). The isomerization is only possible for sugars containing a C_2-OH group, and is not possible for MDM or MDR.

To investigate the reaction network for MDG and MDF conversion, we treated these feedstocks with an Amberlyst 70 acid catalyst at 100°C to hydrolyze the methoxy group while avoiding aldose-ketose isomerization (Table 6.2, Entries 2A and 5A). MDG is hydrolyzed to form a mixture of 3,4-dideoxy-glucopyranose (34-Dglu) and erythro-Lgol (i.e., the anhydro version of 34-Dglu) intermediates (Table 6.2, Entry 2A). In Chapter 5, we reported that erythro-Lgol is hydrolyzed to 34-Dglu with an equilibrium conversion of 83% at 100°C over an acid catalyst in water. The same equilibrium distribution is observed here (Appendix, Section 8.5.2C). Unlike 23-Dman and 23-Drha, 34-Dglu cannot form a furanose tautomer due to lack of a C_4-OH group. Hydrogenation of 34-Dglu results in the formation of 2R, 5S-1256-HT with high selectivity (77%) and stereoselectivity (95%), (Table 6.2, Entry 2B), confirming that these are key intermediates between MDG and 1256-HT. The 16% residual erythro-Lgol is not converted in this second step over Pt/SiO_2, as hydrolysis of this intermediate requires an acid catalyst. It is noteworthy that a fraction of the dideoxy sugars 34-Dglu and 23-Dman can be dehydrated to anhydro- species in water at 100°C, whereas for regular sugars such as glucose, the equilibrium heavily favors glucose over levoglucosan in water.[18] This suggests that the removal of hydroxyl groups from sugar molecules changes the relative stabilities of sugar and anhydro- sugar in water.

Similarly to MDG, MDF is hydrolyzed to intermediates which are tentatively identified as the alpha and beta pyranose forms of 3,4-dideoxyfucose (34-Dfuc), based on ^{13}C NMR chemical shifts and multiplicities, and ESI-MS data (Table 6.2, Entry 5A) (Appendix, Section 8.5.2D). Some of these intermediates may exist in equilibrium in water at room temperature. A furanose tautomer cannot be formed due to the lack of a C_4-OH group, and an anhydro species cannot be formed due to the lack of a C_6-OH group. Hydrogenation of 34-Dfuc produces 125-HT in high yield and stereoselectivity (Table 6.2, Entry 5B), confirming that 34-Dfuc are intermediates between MDF and 125-HT.

To further increase the stereoselectivity of MDG and MDF conversion, we used a bifunctional metal-acid catalyst, 5% Pt/SiO_2-Al_2O_3. The acid sites facilitate methoxy bond hydrolysis at lower temperature (100^oC) where the aldose-ketose isomerization is suppressed, while the metal sites rapidly hydrogenate the 34-Dglu/34-Dfuc intermediates. Using this approach, the stereoselectivity for MDG conversion to 1256-HT increases from 95% (2R, 5S) to 98% (Table 6.2, Entry 3) with 87% total selectivity to 1256-HT (NMR, HPLC, and polarimetry described in the Appendix, Section 8.5.1C). Incorporating the 88% yield of MDG from methyl-galactopyranoside,[9a] the overall selectivity of 1256-HT from methyl-galactopyranoside is 77%. The stereoselectivity for MDF conversion to 125-HT increases from 82% (2S, 5S) to 90% (Table 2, Entry 6) with 84% overall selectivity to 125-HT (NMR, HPLC, and polarimetry provided in Appendix, Section 8.5.2D). Incorporating the 82% yield of MDF from methyl-fucopyranoside,[9a] the overall selectivity of 125-HT from methyl-fucopyranoside is 69%.

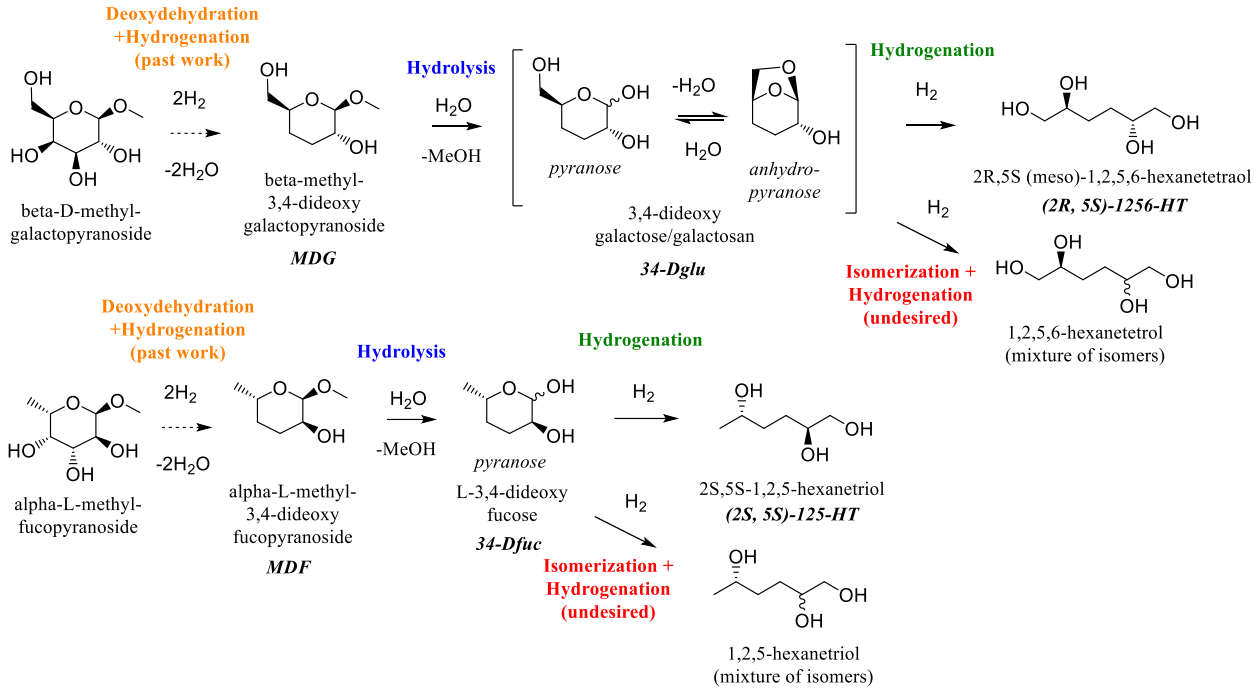

Figure 6.2. *Conversion of methyl-3,4-dideoxy-glycosides*

Table 6.2. *Conversion of 3,4-dideoxy sugars to hexane-triols and hexanetetrols*

Entry	Feed	Catalyst	Conditions	Conversion (%)	Major Product	HPLC Selectivity (%)	Diastereomer Selectivity
1	MDG	5% Pt/SiO_2	150°C, 15h*	95	1256-HT	81	95% 2R, 5S 5% 2S, 5S
2A	MDG	Amberlyst 70	100°C, 2h	100	34-Dglu	____	____
2B	Product of 2A	5% Pt/SiO_2	100°C, 32h	100	1256-HT	77**	95% 2R, 5S 5% 2S, 5S
3	MDG	5.3% Pt/SiAl	100°C, 62 h	94	1256-HT	87	98% 2R, 5S 2% 2S, 5S
4	MDF	5% Pt/SiO_2	150°C, 15h*	100	125-HT	90	82% 2S, 5S 18% 2R, 5S

5A	MDF	Amberlyst 70	100°C, 2h	100	34-Dfuc	____	____
5B	Product of 5A	5% Pt/SiO_2	100°C, 32h	100	125-HT	79	93% 2S, 5S 7% 2R, 5S
6	MDF	5.3% Pt/SiAl	100°C, 62 h	100	125-HT	84	92% 2S, 5S 8% 2R, 5S

Conditions: *2 wt% feed in water (10-15 mL), Experiments with Pt catalysts conducted with 10 mg solution/g cat and 1000 psi H2. Experiments with Amberlyst 70 catalysts conducted with 8.33 mg solution/g cat and 500 psi Ar.*Experiment at 120°C for 21h resulted in ~10% conversion. **16% yield of erythro-Lgol, which would only be converted to 1256-HT in the presence of a metal-acid catalyst.*

6.4. Conclusions

We have demonstrated the regio- and stereo – selective synthesis of hexane-tetrols and triols from methyl glycoside feedstocks and investigated the reaction network for these transformations. First, methyl glycosides are subjected to deoxydehydration and hydrogenation of cis-vicinal OH groups over a ReO_x-Pd/CeO_2 catalyst in 82-92% yield. Next, the resulting dideoxy-glycoside feedstocks are converted over Pt-based catalysts with selectivities of 80-95% and stereoselectivities of 90-100%. MDM is converted to (2R,3S)-1256-HT; MDR is converted to 4R,5S-145HT; MDG is converted 2R,5S-1256HT; and MDF is converted to 2S,5S-125HT. Each of the four dideoxy glycoside feedstocks is first hydrolyzed to a set of tentatively identified intermediates consistent with the structure of the feedstocks, followed by hydrogenation to hexane-triols and -tetrols. 2,3-dideoxy feedstocks (MDM and MDR) are more reactive than 3,4-dideoxy feedstocks (MDG and MDF). Furthermore, only 3,4-dideoxy feedstocks can undergo aldose-

ketose isomerization at the C_2-OH position which decreases the stereoselectivity. Inversion of the C_2-OH stereocenter can be suppressed by introduction of a bifunctional metal-acid catalyst. This work provides insights into controlling reactivity and stereoselectivity in the hydrogenation of carbohydrates over supported metal catalysts. By demonstrating a new route to produce targeted polyols from sugar glycosides with high regio- and stereo- selectivity, this report lays the groundwork for further research into the applications of these molecules in the chemical industry.

6.5. References

1. Corma, A.; Iborra, S.; Velty, A., Chemical Routes for the Transformation of Biomass into Chemicals. *Chemical Reviews* **2007,** *107* (6), 2411-2502.
2. Jarosz, S.; Magdycz, M.; Lewandowski, B., Sugars as chiral synthons in the preparation of fine chemicals. In *Carbohydrate Chemistry: Volume 35*, The Royal Society of Chemistry: 2009; Vol. 35, pp 232-259.
3. Williams, C. A., GALACTOSE. In *Encyclopedia of Food Sciences and Nutrition (Second Edition)*, Caballero, B., Ed. Academic Press: Oxford, 2003; pp 2843-2846.
4. Hu, X.; Shi, Y.; Zhang, P.; Miao, M.; Zhang, T.; Jiang, B., d-Mannose: Properties, Production, and Applications: An Overview. *Comprehensive Reviews in Food Science and Food Safety* **2016,** *15* (4), 773-785.
5. Khosravi, C.; Benocci, T.; Battaglia, E.; Benoit, I.; de Vries, R. P., Chapter One - Sugar Catabolism in Aspergillus and Other Fungi Related to the Utilization of Plant Biomass. In *Advances in Applied Microbiology*, Sariaslani, S.; Gadd, G. M., Eds. Academic Press: 2015; Vol. 90, pp 1-28.
6. Wijesinghe, W. A. J. P.; Jeon, Y.-J., Biological activities and potential industrial applications of fucose rich sulfated polysaccharides and fucoidans isolated from brown seaweeds: A review. *Carbohydrate Polymers* **2012,** *88* (1), 13-20.
7. (a) Tomishige, K.; Nakagawa, Y.; Tamura, M., Selective hydrogenolysis and hydrogenation using metal catalysts directly modified with metal oxide species. *Green Chemistry* **2017,** *19* (13), 2876-2924; (b) Chheda, J. N.; Huber, G. W.; Dumesic, J. A., Liquid-Phase Catalytic Processing of Biomass-Derived Oxygenated Hydrocarbons to Fuels and Chemicals. *Angewandte Chemie International Edition* **2007,** *46* (38), 7164-7183.
8. (a) Amada, Y.; Watanabe, H.; Hirai, Y.; Kajikawa, Y.; Nakagawa, Y.; Tomishige, K., Production of Biobutanediols by the Hydrogenolysis of Erythritol. *ChemSusChem* **2012,** *5* (10), 1991-1999; (b) Strensrud, K.; Ma, C.-C. Synthesis of R-glucosides, sugar alcohols, reduced sugar alcohols, and furan derivatives of reduced sugar alcohols (patent application). 2017; (c) Kühne, B.; Vogel, H.; Meusinger, R.; Kunz, S.; Kunz, M., Mechanistic study on –C–O– and –C–C– hydrogenolysis over Cu catalysts: identification of reaction pathways and key intermediates. *Catalysis Science & Technology* **2018,** *8* (3), 755-767.
9. (a) Tamura, M.; Yuasa, N.; Cao, J.; Nakagawa, Y.; Tomishige, K., Transformation of Sugars into Chiral Polyols over a Heterogeneous Catalyst. *Angewandte Chemie International Edition* **2018,** *57* (27), 8058-8062; (b) Ota, N.; Tamura, M.; Nakagawa, Y.; Okumura, K.; Tomishige, K., Performance, Structure, and Mechanism of ReOx–Pd/CeO2 Catalyst for Simultaneous Removal of Vicinal OH Groups with H2. *ACS Catalysis* **2016,** *6* (5), 3213-3226; (c) Ota, N.; Tamura, M.; Nakagawa, Y.; Okumura, K.; Tomishige, K., Hydrodeoxygenation of Vicinal OH Groups over Heterogeneous Rhenium Catalyst Promoted by Palladium and Ceria Support. *Angewandte Chemie International Edition* **2015,** *54* (6), 1897-1900.
10. Bochkov, A. F.; Zaikov, G. E., *Chemistry of the O-Glycosidic Bond: Formation and Cleavage*. Elsevier: 2016.
11. Young, R. J.; Lovell, P. A., *Introduction to Polymers*. 3 ed.; CRC Press: Boca Raton, FL, 2011.
12. Ballard, S. A.; Whetstone, R. R. 1, 2, 6-hexanetriol. 1956.

13. (a) Alamillo, R.; Tucker, M.; Chia, M.; Pagan-Torres, Y.; Dumesic, J., The selective hydrogenation of biomass-derived 5-hydroxymethylfurfural using heterogeneous catalysts. *Green Chemistry* **2012,** *14* (5), 1413-1419; (b) Buntara, T.; Melián-Cabrera, I.; Tan, Q.; Fierro, J. L. G.; Neurock, M.; de Vries, J. G.; Heeres, H. J., Catalyst studies on the ring opening of tetrahydrofuran–dimethanol to 1,2,6-hexanetriol. *Catalysis Today* **2013,** *210*, 106-116.
14. Tess, R. W.; Harline, R. D.; Mika, T. F., 1,2,6-Hexanetriol in Alkyd Resins. *Industrial & Engineering Chemistry* **1957,** *49* (3), 374-378.
15. Sullivan, P. B., Borate corrosion inhibitors (US3403104 A). Union Carbide Corp. : 1968.
16. H., K. S.; Kefeng, H.; J., B. K.; Jiayue, H.; T., M. C.; A., D. J.; W., H. G.; Mario, D. b.; M., W. B., Oxygenated commodity chemicals from chemo-catalytic conversion of biomass derived heterocycles. *AIChE Journal* **2018,** *64* (6), 1910-1922.
17. L.G. Wade, J., *Organic Chemistry*. 7 ed.; Prentice Hall: Upper Saddle River, NJ, 2010.
18. Helle, S.; Bennett, N. M.; Lau, K.; Matsui, J. H.; Duff, S. J. B., A kinetic model for production of glucose by hydrolysis of levoglucosan and cellobiosan from pyrolysis oil. *Carbohydrate Research* **2007,** *342* (16), 2365-2370.

Chapter 7. Conclusions and Future Directions

7.1. Conclusions

We have investigated the catalytic conversion of biomass-derived intermediates to a variety of renewable chemicals over metal and acid catalysts, with an emphasis on the cellulose-derived platform molecule LGO. In the acid-catalyzed isomerization of LGO, we developed a reaction kinetics model to describe the experimental data across a range of concentrations and temperatures. LGO is isomerized to HMF in the presence of a Brønsted acid catalyst, and HMF is further converted to LA and FA. LGO exists in equilibrium with a dihydrated species at reaction conditions. The main sources of carbon loss are thermal and catalytic degradation of HMF. Within the range of experimental conditions studied, the yield of HMF from LGO can be maximized at higher temperatures and shorter reaction times. The yields of HMF and LA decrease monotonically as the THF/water solvent ratio increases, suggesting that water plays a role in the LGO isomerization reaction. Using a mixed THF/water solvent system and lower temperature to slow the equilibration of LGO and DH, analysis of the initial rate of HMF production showed that HMF is produced primarily from LGO and is not produced from DH. These results are consistent with a mechanism for LGO isomerization which proceeds via hydration of the anhydro–bridge, followed by ring rearrangement analogous to the isomerization of glucose to fructose.

In the metal-catalyzed hydrogenation of LGO to Cyrene and Lgol, we have shown that the C=C bond of LGO can be selectively hydrogenated to Cyrene at low temperature (40°C), with the C=O bond further hydrogenated to two stereoisomers of Lgol at higher temperatures (100°C). An excess of the threo-Lgol isomer is favored over supported Pd catalysts across multiple particle sizes and temperatures, and the stereoisomer ratio is kinetically controlled. The excess of threo-

Lgol over erythro-Lgol is likely due to a steric hindrance effect induced by the prochiral anhydro-bridge group.

In the hydrogenolysis of Lgol to THFDM and THP2M5H over bifunctional metal-acid catalysts in THF solvent, the product THFDM cis/trans ratio is independent of the reactant Lgol t/e ratio, suggesting that the initial stereochemistry at the alcohol position of Lgol is erased during the reaction. Although THP2M5one can be produced from the acid-catalyzed isomerization of Lgol, THP2M5one is hydrogenated to THP2M5H, and neither of these species are THFDM precursors. ^{13}C radio-labeling validated the proposed ring rearrangement of the 6-membered ring of Lgol to the 5-membered ring of THFDM. The 1.1% Pt/SiAl catalyst undergoes moderate deactivation with time-on-stream which is reversible upon calcination and reduction. The rate-limiting step for this reaction was found to be acid-catalyzed above 1.1% Pt loading. The zero-order dependence in hydrogen indicated that the metal participates in a fast hydrogenation step following an irreversible acid-catalyzed rate-determining step. The activation energy for Lgol conversion is 25 kcal/mol, in agreement with the value from theoretical calculation. The selectivity towards THFDM increased with increasing metal loading, likely because degradation of reactive intermediates is minimized when these species are hydrogenated rapidly over metal sites. Using these insights, 73% THFDM selectivity and 100% overall selectivity to 16-HDO precursors was achieved using the 5.3% Pt/SiAl catalyst. A physical mixture of metal and acid sites displayed a comparable selectivity to the bifunctional Pt/SiAl catalyst, indicating that nanoscale proximity is not required to carry out Lgol hydrogenolysis selectively. However, when the metal and acid sites were completely separated using a dual-layered configuration with SiAl followed by Pt/SiO_2, a penalty in the overall selectivity is incurred. First-principles calculations revealed the energetics of the proposed reaction mechanism consistent with the experimental findings.

In the hydrogenolysis of Lgol to 1256-HT in water, we elucidated a new route to produce 1256-HT in 90% yield over metal and acid catalysts. High 1256-HT yields are maintained at Lgol concentrations of up to 21 wt% in water. This route is significantly more selective than previously reported sorbitol hydrogenolysis routes, and offers control over the 1256-HT c/t ratio. The choice of acid catalyst (Amberlyst 70 or SiAl) and reaction temperature (100^{o}C or 150^{o}C) can be used to control which reaction intermediates (34-Dman and 34-Dglu, or 34-Dfru) are formed in the conversion of Lgol to 1256-HT. The 1256-HT c/t ratio can be altered by varying the Lgol t/e ratio, and by selecting the reaction conditions to determine whether the stereocenter at the C_2 position is preserved or erased prior to hydrogenation.

In the conversion of methyl glycosides, we demonstrated the regio- and stereo – selective synthesis of hexane-tetrols and triols from these feedstocks and investigated the reaction network. First, methyl glycosides are subjected to deoxydehydration and hydrogenation of cis-vicinal OH groups over a ReO_x-Pd/CeO_2 catalyst in 82-92% yield. Next, the resulting dideoxy-glycoside feedstocks are converted over Pt-based catalysts with selectivities of 80-95% and stereoselectivities of 90-100%. MDM is converted to (2R,3S)-1256-HT; MDR is converted to 4R,5S-145HT; MDG is converted 2R,5S-1256HT; and MDF is converted to 2S,5S-125HT. Each of the four dideoxy glycoside feedstocks is first hydrolyzed to a set of tentatively identified intermediates consistent with the structure of the feedstocks, followed by hydrogenation to hexane-triols and -tetrols. 2,3-dideoxy feedstocks (MDM and MDR) are more reactive than 3,4-dideoxy feedstocks (MDG and MDF). Furthermore, only 3,4-dideoxy feedstocks can undergo aldose-ketose isomerization at the C_2-OH position which decreases the stereoselectivity. Inversion of the C_2-OH stereocenter can be suppressed by introduction of a bifunctional metal-acid catalyst.

Overall, we have demonstrated how a fundamental understanding of the catalytic chemistry of biomass conversion processes over metal and acid catalysts enables the tuning of reactivity towards desired products in high yield and stereoselectivity, aiding in the economical production of renewable chemicals from biomass.

7.2. Future Directions and Outlook

7.2.1. Future Directions

i) Rational Catalyst Design for LGO conversion

In this thesis, the reaction chemistry for LGO conversion to high-value chemicals was studied using conventional metal and acid catalysts such as Pd/Al_2O_3 and Pt/SiAl. An important next step is the design of novel, well-defined catalysts to carry out these transformations with higher activity, selectivity, stability, and lower cost. For example, in Chapter 3 we studied the stereoselective hydrogenation of Cyrene to Lgol, showing that an excess of the threo- isomer of the erythro- isomer is formed due to steric hindrance effects. In Chapter 5, we showed how the diastereomer ratio of Lgol translates to the diastereomer ratio of 1256-HT. Controlling stereochemistry in hydrogenation reactions can be critical for product applications such as polymer synthesis and pharmaceuticals. The Lgol t/e ratio from Cyrene hydrogenation was observed to change with the catalyst support, but the underlying reason for this effect was not fully understood. Future work should elucidate how to control the t/e ratio as a function of the catalyst properties (electronic and geometric properties of the metal, support, and their interface). Designing a catalyst which further biases the adsorption mode of Cyrene towards a less hindered configuration could further improve the stereoselectivity. This could be accomplished by locating metal nanoparticles within a confined environment – for example in a zeolite pore,[1] or by using atomic layer deposition

of a metal oxide to encapsulate metal nanoparticles within a 'nanobowl' configuration.[2] Another approach to improve stereoselectivity would be to use chiral modifiers which adsorb to the catalyst surface and influence adsorbate orientations, as has been demonstrated by Baiker and co-workers.[3]

Another key area for rational catalyst design is the synthesis of bifunctional metal-acid catalysts with controlled metal-acid site configurations. In Chapters 4 and 5, we varied the bulk metal/acid site ratio (by varying the Pt loading on an acidic SiAl support) and proximity (by studying a bifunctional catalyst versus a physical mixture of metal and acid catalysts, or two separate catalyst beds). We found that increasing the metal/acid site ratio and proximity improves the selectivity to desired products in hydrogenolysis processes by rapidly hydrogenating intermediates formed over acid sites before they can undergo undesired reactions. In Lgol hydrogenolysis to THFDM, higher selectivity was achieved by avoiding acid-catalyzed degradation reactions of unsaturated intermediates. In Lgol conversion to 1256-HT, higher stereoselectivity was achieved by avoiding aldose-ketose isomerization of hemiacetal intermediates. However, the catalysts used in these studies were synthesized by a conventional incipient wetness impregnation approach, likely resulting in a wide distribution of metal-acid site configurations. Designing novel catalysts with controlled orientations of metal and acid sites would aid in understanding these bifunctionality effects and also lead to improved performance. This could potentially be achieved with a 'controlled surface reactions' synthesis approach, wherein a small amount of an oxophilic promoter metal is deposited selectively on a reduced metal nanoparticle, without adsorption onto the support.[4] Then, all acid sites (formed at the oxophilic metal) would be surrounded by reduced metal sites; reaction intermediates formed over acid sites would be immediately hydrogenated over metal sites before they can migrate to other acid sites.

Designing such a material could allow for improved selectivity, or allow one to maintain high selectivity at lower metal loadings (and therefore lower cost).

ii) Scale up of LGO Conversion Technologies

Numerous practical challenges relevant to scale-up of LGO conversion technologies should be addressed. Most of the reactivity studies in this thesis were conducted in batch reactors, which are amenable to reaction network elucidation but where catalyst stability is difficult to measure. Future work should study these reactions in continuous flow reactors to assess stability, mechanisms of deactivation, and regenerability. The work in this thesis was carried out with pure feedstocks; future work should upgrade realistic feedstocks derived from biomass and assess the effect of organic and impurities on catalyst activity, selectivity, and stability. Operation at high reactant concentrations and at high conversion will decrease separations costs of solvent and reactants. Pd and Pt were used as model metal catalysts in this thesis. Replacing these expensive metals with non-noble metals such as Cu and Ni would decrease catalyst cost, although challenges such as metal leaching in the liquid phase will need to be addressed. O'Neill, et al showed that atomic layer deposition of Al_2O_3 overcoats stabilized base-metal Cu catalysts against irreversible deactivation by selectively covering the under-coordinated sites which are susceptible to sintering and leaching in the liquid phase.[5] Similar approaches could be applied in this project to develop stable, low-cost base metal catalysts. A full techno-economic model for the production of these new biomass-derived chemicals would provide insight into the major cost drivers in these processes, and reveal which aspects of the technology require further research to aid in commercialization.

iii) Synthesis and Evaluation of Materials from Biomass-derived Monomers

Most of the biomass-derived molecules described in this thesis are not commercially available, and experimental demonstrations of their applications in the chemical industry are either limited or non-existent. Therefore, a key next step is to demonstrate the applications of these biomass-derived monomers in the chemical industry. α,ω-diols such as THFDM should be tested as replacements for 16-HDO in paints, coatings, adhesives, nylon, and plastics.[6] Recent patents have shown that polyesters and polyethers can be synthesized from THFDM (produced from HMF hydrogenation) coupled with di-acids, and noted that the THFDM cis/trans ratio affects downstream polymer properties.[7] In Chapter 4, we showed that different THFDM cis/trans ratios can be produced from Lgol (cis/trans ~1 to ~2.5) in contrast to the high (>5:1) ratios produced from HMF hydrogenation.[8] Monomer stereochemistry can have a significant influence on the physico-chemical properties of polymers.[9] Hexane-tetrols and –triols with controlled stereochemistry, produced in Chapters 5 and 6, should be studied as hydrophilic cross-linking agents in polyesters similar to 126-HT.[10] Another application of these polyols is in non-ionic surfactants, where the number, positions, and stereochemistry of hydroxyl groups are known to influence surfactant properties.[11] Demonstrating the applicability of these biomass-derived monomers in real-world applications is a critical requirement for industrial adoption.

7.2.2. Outlook

An overarching theme in this thesis is that a fundamental understanding of the reaction network and mechanism in biomass conversion reactions is necessary for the rational design of catalytic systems to tune selectivity to desired products. Biomass conversion studies which are conducted with a purely empirical ‘trial-and-error’ approach, without an understanding of the underlying reaction mechanisms, can overlook key insights which could lead to transformational

improvements in biomass conversion processes. To this end, I recommend that future biomass conversion keep the following two details in mind:

i) The majority of previous biomass conversion studies over heterogeneous catalysts have not paid close attention to the stereochemistry of reactants and products. Investigation of stereochemistry was an important part of this thesis due to the chiral nature of the feedstocks. We investigated a case in which the prochiral nature of the feedstock resulted in a stereoselective hydrogenation (Chapter 3); a case in which the product stereochemistry is independent of the reactant stereochemistry, indicating that an achiral intermediate is formed during this process (Chapter 4); and cases in which stereocenters in prochiral reactants can be preserved or destroyed upon formation of reaction products, depending on the reaction conditions and mechanism (Chapters 5-6). Investigation of stereochemistry is common in organic synthesis, but not in biomass conversion research. I therefore recommend that future biomass conversion research study the stereochemistry of reactants and products as both a useful mechanistic tool and an important property for downstream applications.

ii) Some studies of biomass hydrogenolysis processes have not paid close attention to possible effects of the metal-acid site ratio and proximity. Investigation of the effect of metal and acid sites on series and parallel reactions in hydrogenolysis processes has traditionally been done in the alkane hydroisomerization catalysis literature. In Chapters 4-5, we showed that these parameters have a critical influence on activity and selectivity for hydrogenolysis reactions of biomass-derived oxygenates. For example: in Lgol hydrogenolysis to THFDM (Chapter 4), if this reaction was treated as a simple hydrogenation reaction, then one would assume that increasing the metal loading would result in higher per-mass activity. However, we showed that acid sites control the

rate above 1% Pt loading. As another example, if different acid catalysts had been screened for this reaction without a mechanistic understanding, highly active acid catalysts would likely display low product selectivity due to acid-catalyzed degradation reactions. Such an investigation would miss the fact that the metal-acid site balance controls the selectivity; if the acid catalyzed activity is increased, the metal-catalyzed activity should be proportionally increased to maintain high selectivity. I recommend that future biomass conversion research utilizes insights from the hydrocarbon conversion literature in understanding bifunctional catalysis effects.

More broadly, the biomass-derived molecules synthesized in this thesis provide opportunities for sustainable new products with potentially unique properties that can be used in the polymer, solvent and surfactant industries. The processes for producing these compounds have potential advantages including using oxygenated functionalities present in biomass, avoiding the use of harmful reagents, and in some cases offering a high yield route utilizing heterogeneous catalysts. The current market price of the majority of these chemicals is high (> $10,000/ton) because they are currently not produced commercially, or only produced in small-scale batch processes. The cost of these molecules could be brought down to $1,000-$5,000/ton if they are produced at larger scale (>10 kton/yr). The sale of higher-value, lower-volume bio-chemicals could significantly lower the selling price of lower-value, high-volume biofuels in an integrated biorefinery.

Scale-up of a new technology requires a major capital investment. There is a chicken-and-egg problem with development of these new technologies, as major capital investment in a new technology is inherently risky, while end-users will not adopt these new products unless they are already produced at economical scale and their properties can be tested. Therefore, the properties

of end-products made from these molecules are often unknown. Materials made from these chemicals could have similar properties to petroleum-derived products, or could even have unique properties with performance advantages over petroleum-derived products. The question of which party in the supply chain (producers of these molecules, polymer manufacturers, formulators, or end-users) is willing to adopt the risk to develop these new technologies remains a major roadblock to industrial adoption. Collaboration between potential producers and users of these biomass-derived molecules is critical to overcoming this problem. Successfully demonstrating the applications of new biomass-derived products in their proposed applications decreases the risk involved in adopting these technologies.

In spite of the challenges with implementing new renewable chemicals technologies, the numerous societal benefits of these technologies should be kept in mind. These benefits include: i) providing long term value and creating manufacturing jobs in rural communities, ii) lowering the carbon footprint of materials, and iii) reducing the dependence on non-renewable fossil fuels as feedstocks for the chemical industry. The chemical industry is one of the few industries that can create long term wealth by converting low value products into materials that society needs to maintain our standard of living. It is critical that our field continues to use our knowledge of chemical engineering to create new chemicals and materials from renewable biomass sources.

7.3. References

1. Csicsery, S. M., Shape-selective catalysis in zeolites. *Zeolites* **1984,** *4* (3), 202-213.

2. (a) Shang, Z.; Patel, R. L.; Evanko, B. W.; Liang, X., Encapsulation of supported metal nanoparticles with an ultra-thin porous shell for size-selective reactions. *Chemical Communications* **2013,** *49* (86), 10067-10069; (b) Canlas, C. P.; Lu, J.; Ray, N. A.; Grosso-Giordano, N. A.; Lee, S.; Elam, J. W.; Winans, R. E.; Van Duyne, R. P.; Stair, P. C.; Notestein, J. M., Shape-selective sieving layers on an oxide catalyst surface. *Nat Chem* **2012,** *4* (12), 1030-1036.

3. Meemken, F.; Hungerbühler, K.; Baiker, A., Monitoring Surface Processes During Heterogeneous Asymmetric Hydrogenation of Ketones on a Chirally Modified Platinum Catalyst by Operando Spectroscopy. *Angewandte Chemie International Edition* **2014,** *53* (33), 8640-8644.
4. Hakim, S. H.; Sener, C.; Alba-Rubio, A. C.; Gostanian, T. M.; O'Neill, B. J.; Ribeiro, F. H.; Miller, J. T.; Dumesic, J. A., Synthesis of supported bimetallic nanoparticles with controlled size and composition distributions for active site elucidation. *Journal of Catalysis* **2015,** *328*, 75-90.
5. O'Neill, B. J.; Jackson, D. H. K.; Crisci, A. J.; Farberow, C. A.; Shi, F.; Alba-Rubio, A. C.; Lu, J.; Dietrich, P. J.; Gu, X.; Marshall, C. L.; Stair, P. C.; Elam, J. W.; Miller, J. T.; Ribeiro, F. H.; Voyles, P. M.; Greeley, J.; Mavrikakis, M.; Scott, S. L.; Kuech, T. F.; Dumesic, J. A., Stabilization of Copper Catalysts for Liquid-Phase Reactions by Atomic Layer Deposition. *Angewandte Chemie International Edition* **2013,** *52* (51), 13808-13812.
6. 1,6-Hexanediol Market by Application (Polyurethanes, Coatings, Acrylates, Adhesives, Unsaturated Polyester Resins, Plasticizers, and Others) and By Geography (NA, Europe, Asia-Pacific, & ROW) - Trends and Forecasts to 2019. http://www.researchandmarkets.com/research/zs4gnb/16hexanediol (accessed January 22).
7. (a) Jeol, S. Polyesters from aromatic carboxylic diacid and 2,5-bis(hydroxymethyl)tetrahydrofuran (WO2016102361A1). 2016; (b) Stensrud, K. Diallyl ethers of 2,5-bis(hydroxymethyl)tetrahydrofuran and processes for making the same (WO2013188252A2). 2013; (c) Jacquel, N.; Degand, G.; Saint-Loup, R. Thermoplastic aromatic polyesters comprising tetrahydrofuran-dimethanol and furandicarboxylic acid motifs (US20170145153A1). 2017.
8. Hu, X.; Westerhof, R. J. M.; Wu, L.; Dong, D.; Li, C.-Z., Upgrading biomass-derived furans via acid-catalysis/hydrogenation: the remarkable difference between water and methanol as the solvent. *Green Chemistry* **2015,** *17* (1), 219-224.
9. Young, R. J.; Lovell, P. A., *Introduction to Polymers*. 3 ed.; CRC Press: Boca Raton, FL, 2011.
10. Tess, R. W.; Harline, R. D.; Mika, T. F., 1,2,6-Hexanetriol in Alkyd Resins. *Industrial & Engineering Chemistry* **1957,** *49* (3), 374-378.
11. Miyake, M.; Yamashita, Y., Molecular Structure and Phase Behavior of Surfactants. 2017; pp 389-414.

Chapter 8. Appendices

8.1. Appendix for Chapter 2

8.1.1. Derivation of HMF production rate in terms of the combined concentration of LGO and DH

Because LGO and DH are in equilibrium at our experimental conditions, it is possible to express the rate of HMF production in terms of a lumped kinetic parameter multiplied by the combined concentration of LGO and DH. Accordingly, the rate of HMF formation can be modeled as being first order in the combined concentration of LGO and DH, without needing to determine which species is the reactant. This is done by first defining a constant K_1, which represents the equilibrium ratio of the concentrations of LGO and DH in the aqueous solvent system at a given temperature.

$$K_1 = \frac{[DH]}{[LGO]}$$

In the general case, HMF can be produced from both DH and LGO. Assuming that the reaction is first-order in LGO with rate constant k_1, first-order in DH with rate constant k_2, and first order in the free proton concentration, the rate of HMF production from LGO and DH can be expressed as follows:

$$r = k_1[LGO][H^+] + k_2[DH][H^+]$$

Equation S1 can be manipulated to express the concentrations of LGO and DH in terms of the combined concentration of LGO and DH. Combining this with the equation above, we can write the rate of HMF production in terms of the combined concentration of LGO and DH:

$$r = \left(k_1 \frac{1}{1+K_1}\right)[LGO + DH][H^+] + \left(k_2 \frac{K_1}{1+K_1}\right)[LGO + DH][H^+]$$

Finally, all of the constant terms in Equation S3 can be lumped into a single kinetic parameter (k_*) multiplied by the combined concentration of LGO and DH:

$$r = k_*[LGO + DH][H^+]$$

The above equation also applies in the case in which LGO or DH are the sole reactant (in the limit of $k_1 \rightarrow 0$ or $k_2 \rightarrow 0$, respectively). Thus, in any of the three cases, the rate of HMF production can be expressed in terms of the combined concentration of LGO and DH.

8.1.2. Differential Equations for Kinetic Model

In a batch reactor system, the time derivatives for the concentrations of all species in the network are given below:

$$\frac{d}{dt}[LGO + DH] = -r_1$$

$$\frac{d}{dt}[HMF] = r_1 - r_2 - r_3 - r_4$$

$$\frac{d}{dt}[LA] = r_2$$

$$\frac{d}{dt}[FA] = r_2$$

8.1.3. NMR of LGO-dihydrate

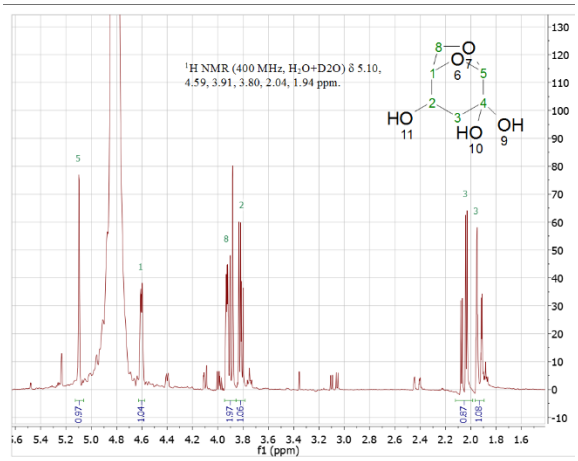

Figure 8.1. *^{1}H NMR of DH (water suppression)*

8.2. Appendix for Chapter 3

8.2.1. ^{13}C NMR of Lgol

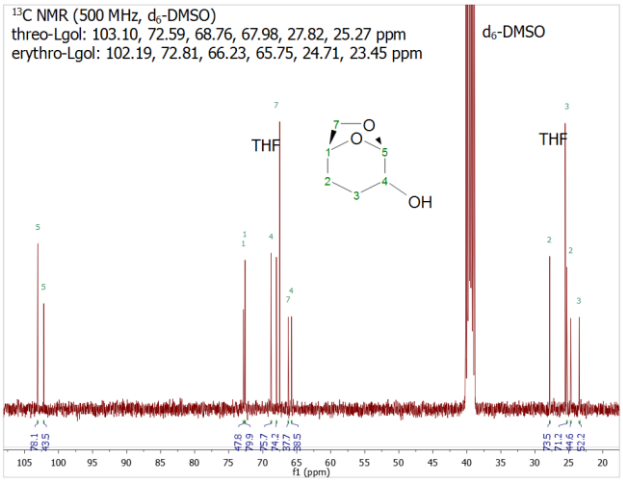

Figure 8.2: *Quantitative ^{13}C NMR spectrum of Cyrene hydrogenation containing threo-Lgol and erythro-Lgol (d_6-DMSO and residual THF solvent are also present). Multiplicities were confirmed using polarization transfer (DEPT) experiments. 480 Scans were used with a relaxation delay of 20 sec.*

Measured chemical shifts agree with the literature.[1]

8.2.2. CO Chemisorption

CO chemisorption was used to count the number of active sites for supported Pd catalysts, as shown in Table 8.1. For Pd/Al_2O_3 catalysts, the dispersion decreased as a function of increasing Pd loading, (53% dispersion at 0.4 wt%, 11% dispersion at 5 wt%). The 1% Pd/SiAl and Pd/Al_2O_3 catalysts have similar dispersions (37% vs 42%), indicating that they have approximately similar particle sizes (3.0 nm vs 2.6 nm).

Table 8.1. *CO Chemisorption*

Catalyst	**Site Density [µmol/g]***	**Dispersion (%)**	**Approx. Particle Size (nm)****
1% Pd/C	9.7	10.4	11
5% Pd/C	104.5	22.2	5.0
0.4% Pd/Al_2O_3	21.0	53.2	2.1
1% Pd/Al_2O_3	39.1	41.6	2.6
5% Pd/Al_2O_3	51.6	11.0	10
1% Pd/SiAl	34.5	36.7	3.0

**Assuming a stoichiometry of 1.5 Pd/CO*

*** Approximated as 1.1/D, using the CO chemisorption data and assuming spherical particles*

8.3. Appendix for Chapter 4

8.3.1. ^{13}C NMR of reaction products

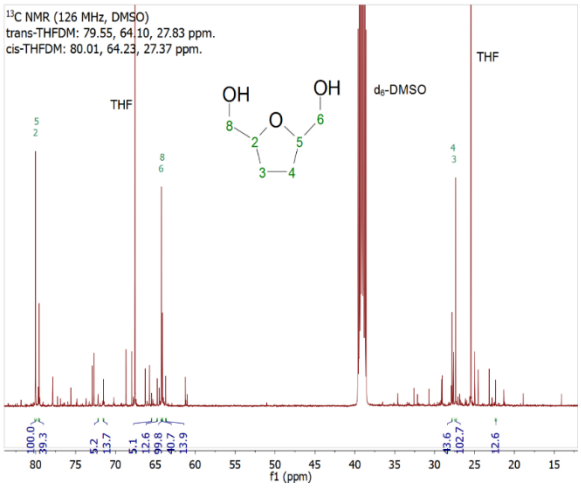

Figure 8.3. *Quantitative ^{13}C NMR spectrum of THFDM-rich product, produced via Lgol hydrogenolysis in Figure 3. (d_6-DMSO, residual THF solvent, Lgol, other side-products are also present). Multiplicities were confirmed using polarization transfer (DEPT) experiments.*

Measured chemical shifts agree with the literature.[2]

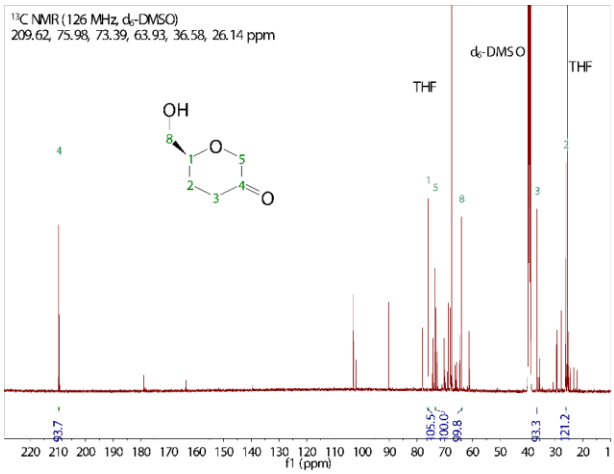

Figure 8.4. *Quantitative ^{13}C NMR spectrum of THP2M5one-rich product, produced via acid-catalyzed Lgol isomerization (d_6-DMSO, Lgol, residual THF solvent, and other side-products are also present). Multiplicities were confirmed using polarization transfer (DEPT) experiments.*

Measured chemical shifts agree with the literature.[3]

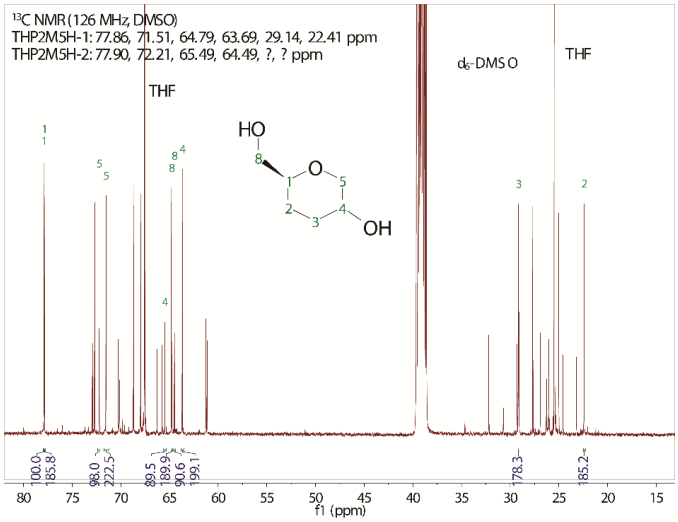

Figure 8.5: *Quantitative ^{13}C NMR spectrum of THP2M5one hydrogenation final product (d_6-DMSO, Lgol, residual THF solvent, and other side-products are also present). The two isomers of THP2M5H were identified using this spectrum. Multiplicities were assigned using polarization transfer (DEPT) experiments. The two up-field carbons present in THP2M5H-2 could not be assigned due to the presence of impurity peaks.*

The Mestrenova-predicted ^{13}C NMR spectrum of THP2M5H predicts the following chemical shifts: 77.19, 70.29, 67.06, 65.72, 30.08, 28.71 ppm. These are in good agreement with the chemical shifts in our measured spectrum.

8.3.2. Synthesis of THP2M5one and THP2M5H

Lgol Isomerization to THP2M5one

The acid-catalyzed isomerization of 65 mM Lgol in THF solvent (60 mL) was carried out in a batch reactor at 100°C for 3h over 400 mg Amberlyst 70 acid catalyst under inert atmosphere.

54% Lgol conversion and 61% THP2M5one selectivity were observed, with no other identifiable products.

THP2M5one hydrogenation to THP2M5H

A solution containing Lgol and THP2M5one (15 mL) was generated using the acid-catalyzed isomerization of Lgol described above. This mixture was then hydrogenated at 100℃ for 3h over a Pd/Al_2O_3 catalyst under 500 psi H_2 atmosphere. The Lgol was unreactive, while the THP2M5one was quantitatively hydrogenated to the two isomers of THP2M5H.

8.3.3. Product Peak deconvolution

Quantification of cis-THFDM, trans-THFDM, THP2M5one, and the two isomers of THP2M5H is made challenging by the fact that these compounds are chemically very similar. As shown in Figure 8.6, trans-THFDM is overlapped with one isomer of THP2M5H in the GC, while cis-THFDM is overlapped with THP2M5one.

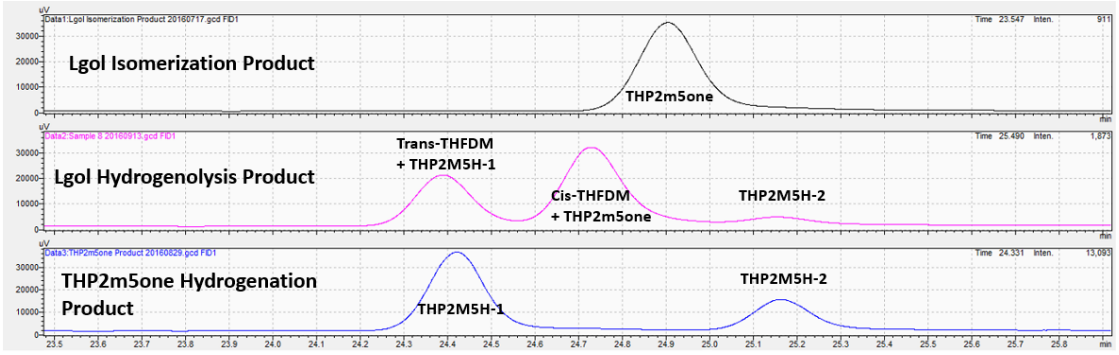

Figure 8.6: *GC-FID chromatograms of Lgol isomerization product, Lgol hydrogenolysis product, and THP2M5one hydrogenation product.*

A combination of GC, HPLC, and NMR was used to quantify these species. For experiments with concentrations over time, NMR of the final product solution was used to correct the data at earlier reaction times. An example of these calculations is shown below, for Lgol hydrogenolysis to THFDM over 1% Pd/SiAl (from Figure 4.2):

i) Using the HPLC-UV detector at 206 nm, the THP2M5one concentration in the final product solution was calculated as 1.1 mM.

ii) The concentration of cis-THFDM in the final product was calculated by examining the GC peak corresponding to (cis-THFDM + THP2M5one) and subtracting the concentration of THP2M5one found in (i). This resulted in a cis-THFDM concentration of 20.6 mM.

iii) Quantitative ^{13}C NMR of the final product solution was used to acquire the THFDM cis/trans ratio. It was found to be cis/trans = 2.45. The concentrations of trans-THFDM, THP2M5H-1, and THP2M5H-2 were found by using the known concentration of cis-THFDM (by GC) and the relative peak areas by NMR (Table 8.2). Note that the peak area of cis-THFDM and trans-THFDM must be divided by two because each peak corresponds to two C nucleii. The NMR peaks used for quantification were selected as peaks which were isolated in the NMR and therefore easily integrated. The concentration of THP2M5H-2, and the combined concentration of trans-THFDM and THP2M5H-1, can be measured by GC. The concentrations of these products measured by NMR can be compared to those measured by GC, and show reasonable agreement, as shown in Table 8.2. ^{13}C NMR spectra were run with a relaxation delay of D_1 = 15 sec. All NMR peaks used for integration displayed reasonable agreement in the integrated peak area. A longer relaxation delay, D_1 = 30 sec, was used in one case and the relative peak areas did not change, verifying that the NMR quantitation is accurate.

iv) For dip-tube experiments, the concentrations of all products at earlier reaction times were corrected by assuming that the THFDM cis/trans ratio is not a function of conversion. This assumption was validated by running the Lgol hydrogenolysis reaction to intermediate conversion (53%) and verifying by NMR that the cis/trans ratio remained 2.45. Using this assumption, the

true concentrations of trans-THFDM, THP2M5H-1, and THP2M5H-2 could be calculated at all reaction times. Then, the total concentrations of THFDM and THP2M5H could be calculated.

Table 8.2. *Product Concentrations in Final Product Solution from Figure 4.2*

Species	**NMR Peaks used (ppm)**	**Average Relative NMR Peak Area**	**NMR Concentration (mM)**	**GC Concentration (mM)**
Cis-THFDM	80.0, 64.3, 27.4	100.8	-	20.6
Trans-THFDM	79.6, 64.2, 27.9	41.2	8.4	-
THP2M5H-1	72.2, 65.5	12.9	5.3	-
THP2M5H-2	71.5, 64.8, 63.7, 22.4	5.2	2.1	2.7
Trans-THFDM + THP2M5H-1	-		13.7	12.9

8.3.4. NH3-TPD and IPA-TPD Plots

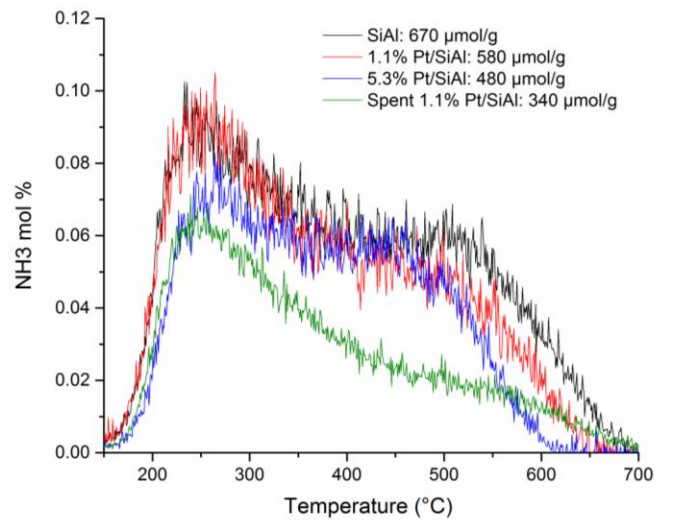

Figure* 8.7: NH_3-TPD of Pt/SiAl catalysts (100 mg). NH_3 was adsorbed at 150°C. The temperature was ramped to 700°C at a rate of 10°C/min.*

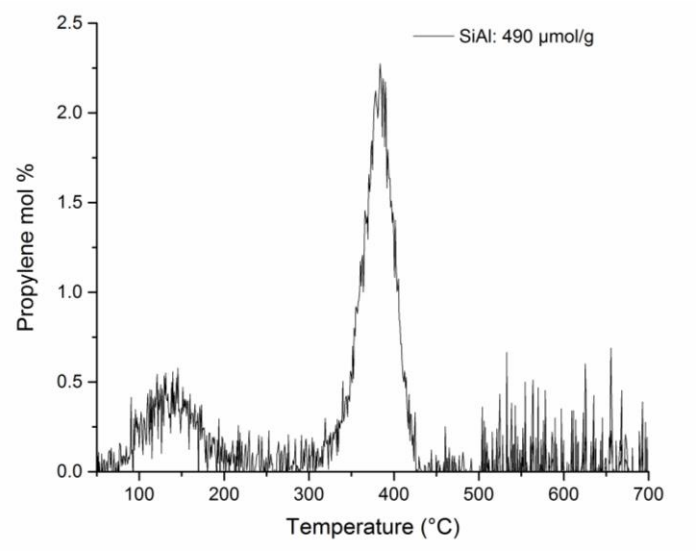

Figure 8.8: *IPA-TPD of SiAl (500 mg). IPA was adsorbed at 50°C. The temperature was ramped to 700°C at a rate of 10°C/min.*

8.3.5. Reaction conditions (45 mL Parr batch reactor) for ^{13}C radio-labeling experiment:

Step i) Glucose dehydration: 60 mg Amberlyst 70, 125 mg $^{13}C_1$-glucose, 20 mL THF, T = 170°C, P_{Argon} = 300 psi, t = 25 min (heat-up time: 15 min).

Step ii) LGO hydrogenation: 200 mg 5% Ru/C (Strem Chemicals), 18.25 mL product from Step (i), T = 100°C, P_{H2} = 500 psi, t = 3h.

Step iii) Lgol hydrogenolysis: 50 mg 1.1% Pt/SiAl, 10 mL product from Step (ii), T = 150°C, P_{H2} = 500 psi, t = 6h. This was followed by addition of 50 mg 1.1% Pt/SiAl catalyst and reaction for an additional 6h to reach high conversion. A longer reaction time and more catalyst was likely needed due to the presence of humins and other impurities in the cellulose-derived Lgol feed which could result in catalyst deactivation.

8.3.6. Details concerning reaction kinetics measurements, selectivity measurements, and calculation of experimental error:

The catalyst undergoes an initial deactivation period over approximately 15h followed by relatively stable activity. Reaction kinetics measurements to calculate the reaction orders and activation barrier were made in this stable regime at <35% conversion. For reaction kinetics measurements over the 1.1% Pt/SiAl catalyst, the experiment was started at the baseline conditions (65 mM Lgol, 129°C, 750 psi H_2), then a single parameter (temperature, pressure, or concentration) was varied to study the effect of these parameters on the reaction rate. Once the new steady state was reached, three consecutive time-on-stream samples were taken prior to changing the conditions again. In a given experiment, the relevant parameter were varied in non-monotonic order. At the end of each run, the reactor was brought back to the initial conditions to re-measure the rate and account for possible deactivation over the course of the measurements.

For the activation energy measurement, the feed flow rate was varied in order to maintain the conversion in the range of 10-30% at different temperatures. The reaction rate was found to be independent of the feed flow rate between 30-60 μL/min, which rules out effects of external transport limitations on the reaction kinetics. In order to correct for the effect of a small amount of THF evaporation on the measured concentrations in the product effluent samples, the GC peak of butylated hydroxytoluene (BHT) present as a stabilizer in the THF solvent was used as an internal standard.

For the investigation of reaction rate and selectivity versus metal loading and metal-acid proximity effects, the initial reaction rate was found by extrapolating the natural logarithm of the rate versus time on stream to zero time. The reactant conversion was ~45% at the earliest time-on-stream point and decreased to ~30% over 25h time-on-stream. The total selectivity to identified

products was found from the average of ~5 steady-state measurements. The selectivities towards individual products THFDM, THP2M5H, and THP2M5one were measured by ^{13}C NMR analysis of a reaction sample after ~15h time-on-stream.

Reported experimental errors in the reaction rate measurements are based on the standard error calculated from the linear fit of the ln(rate) versus time-on-stream data. Error in the overall selectivity to identified products was calculated using the standard error from the variance between multiple steady-state points. Error in the selectivity towards individual products was propagated from the standard error in integrals of different peaks in the ^{13}C spectrum. We note that this error analysis does not account for possible systematic error in the assumption that certain compounds have the same GC-FID sensitivity as similar compounds (THP2M5H was assumed to have the same sensitivity as THFDM, while Lgol and THP2M5one were assumed to have the same sensitivity as Cyrene).

8.3.7. Effect of trace water on product selectivity

During this study we discovered that trace amounts of water in the THF solvent have an effect on the product selectivity, as shown in Table 8.3. The reaction rate and total selectivity to identified products are not affected. The water content specification on the THF from Sigma Aldrich is < 0.05% (< 500 ppm). We found that when comparing the selectivity from Lgol/THF feedstocks made from different bottles of THF, it was sometimes necessary to add 500 ppmv water (0.05 vol%). Bottle 1 was used for the majority of the experiments in the paper. Bottle 2 showed a difference in selectivity (e.g. THFDM selectivity dropped from 61% to 47%) than Bottle 1, but when 500 ppmv water was added to Bottle 2, the product selectivities were comparable to those observed with Bottle 1. Trace amounts of water have previously been observed to affect the

reactivity of SiAl catalysts for acid-catalyzed reactions.[4] Water is known to adsorb to aluminum sites in aluminosilicate materials such as zeolites and affect their coordination environment.[5]

Table 8.3: *Effect of trace water on product selectivity*

		Selectivity [%]			
THF source	**Rate (mmol/min/ g_{SiAl})**	**THFDM (*cis/trans*)**	**THP2M5one**	**THP2M5H**	**Total identified products**
Bottle 1	$6.3*10^{-3}$	61 (*1.0*)	5	20	86
Bottle 2	$5.5*10^{-3}$	47 (*0.8*)	13	26	86
Bottle 2 + 500 ppmv water	$6.1*10^{-3}$	57 (*0.9*)	7	23	86

Conditions: 150 mg cat, T = 129°C, P_{H2} = 750 psi, $C_{Lgol/THF}$ = 65 mM (t/e = 1.7), $F_{Lgol/THF}$ = 30 µL/min, F_{H2} = 6 mL/min.

8.3.8. Conversion and selectivities to all products for continuous flow experiments

Table 8.4. *Conversion and selectivities to all products for continuous flow experiments*

		Selectivities (%)						
Experiment	**Conversion (%)**	**cis-THFDM**	**trans-THFDM**	**THP2M5H-1**	**THP2M5H-2**	**THP2M5one**	**Unidentified GC Products**	**Total Observed Products**
1.1% Pt/SiAl	32%	30%	31%	4%	17%	5%	0%	86%
Activation Energy (T = 122° C)	18%	28%	34%	0%	15%	7%	0%	84%
Activation Energy (T = 137° C)	31%	22%	27%	3%	15%	11%	8%	86%
Activation Energy (T = 144° C)	32%	19%	24%	1%	12%	14%	12%	82%
H_2 Order (P_{H2} = 500 psi)	27%	27%	29%	3%	16%	5%	0%	81%
H_2 Order (P_{H2} = 1000 psi)	27%	29%	32%	3%	16%	5%	0%	86%

Lgol Order (Conc = 34 mM)	26%	33%	34%	3%	19%	5%	0%	94%
Lgol Order (Conc = 185 mM)	24%	23%	26%	3%	12%	6%	5%	74%
SiAl	25%	0%	0%	0%	0%	25%	19%	45%
0.06% Pt/SiAl	28%	12%	13%	6%	9%	16%	13%	68%
0.25% Pt/SiAl	33%	19%	19%	6%	12%	9%	~0%	71%
5.3% Pt/SiAl	20%	40%	33%	5%	17%	5%	0%	100%
Phys. Mix (1% Pt/SiO_2 + SiAl)	24%	31%	26%	7%	25%	3%	0%	93%
Layered: SiAl , then 1% Pt/SiO_2	11%	23%	11%	2%	13%	12%	0%	61%
Layered: 1% Pt/SiO_2, then SiAl	18%	0%	0%	0%	0%	23%	24%	46%

8.3.9. Computational Details

In this work, we have employed the CCSD(T)-based G4MP2[6] level of theory to investigate the reaction mechanism and the energy landscape of the hydrogenolysis of Lgol in acidic non-aqueous media. The G4MP2 level of theory enables accurate prediction of protonation affinities of the biomass derived molecules compared to standard density functional methods.[7] The geometries, zero-point energies, and temperature corrections for this method are evaluated at the B3LYP/6-31G(2df,p) level of theory. To account for the solvation from a non-aqueous medium, a single point energy evaluation was performed in a tetrahydrofuran dielectric (ε=7.4) by employing the SMD solvation model[8] at the B3LYP/6-31G(2df,p) level of theory. The proton solvation energy in tetrahydrofuran is taken as -255.9 kcal/mol to compute the energies of protonated species (~10 kcal/mol lower than the proton solvation energy by an aqueous acidic medium at 25°C). The Gibbs free energy (ΔG at 25°C) is computed as the sum of the gas phase G4MP2 free energies (ΔG_{gas}) and the solvation energy ($E_{solv} = E_{SMD}-E_{gas}$). Selected ab initio dynamics calculations of protonated intermediates in the presence of a limited number of explicit solvent molecules were also performed using the ADMP formalism[9] to understand the steric interactions of cations with the solvent molecules. This approach is also used to generate initial

configurations for selected G4MP2 calculations. All calculations were carried out using the Gaussian 09 software.[10]

8.4. Appendix for Chapter 5

8.4.1. ^{13}C NMR of reaction products

To assign the ^{13}C NMR spectra of 34-Dglu and 34-Dman, we first determined that there were four different chemical species (based on comparison of peak areas in the quantitative ^{13}C NMR; see Table 8.5). These compounds are assigned as α and β anomers of 34-Dglu and 34-Dman. Different ratios of 34-Dglu and 34-Dman were generated by converting Lgol feedstocks over Amberlyst 70 at 100^{o}C with t/e ratios of 1.3 (Table 5.2, Entry 2) and 3.3 (Table 5.3, Entry 5). We calculated the peak area ratios of different pairs of these four peaks (e.g. [34-Dman_1 + 34-Dman+2]/[34-Dglu_1 + 34-Dglu_2]) and found that only one of these ratios matched the ratio of the two peaks observed in the HPLC, as well as the t/e ratio of the converted Lgols (Table 8.6). We cannot rule out the possibility that the stereochemistry at the C_2 position is completely inverted upon Lgol hydrolysis, but there is no chemical reason to expect this to occur. The α and β anomers were not distinguished in this study; these species are expected to exist in equilibrium in water. All assignments are in reasonable agreement with the Mestrenova ^{13}C NMR-predicted chemical shifts for 34-Dman/34-Dglu (Table 8.7), noting that 34-Dman and 34-Dglu are not distinguished by the NMR prediction software. The multiplicities of each ^{13}C peak are consistent with the assignments. The C_2 and C_5 carbon positions were not distinguished due to their similar chemical shifts and multiplicities. The C_3 and C_4 positions were also not distinguished due to their similar chemical shifts and multiplicities.

Table 8.5: *Quantitative ^{13}C NMR chemical shifts, relative peak areas, and multiplicities of reaction products of Lgol conversion over Amberlyst 70 with two different t/e ratios at 100°C. "34-Dglu_1" and "34-Dglu_2" refer to the two anomers of 34-Dglu, and "34-Dman_1" and 34-Dman_2" refer to the two anomers of 34-Dman. Residual Lgol peaks were excluded from this table. Multiplicities were assigned based on ^{13}C DEPT135 and DEPT90 NMR experiments.*

#	Chemical Shift (ppm)	Lgol t/e = 1.3 Feed Normalized Area	Lgol t/e= 3.3 feed Normalized Area	Multiplicity	Assignment	Carbon Position
1	98.19 .. 98.12	100	100	C-H	DDG_1	C1
2	94.97 .. 94.93	45	127	C-H	DDM_2	C1
3	93.45 .. 93.39	63	183	C-H	DDM_1	C1
4	91.90 .. 91.84	31	36	C-H	DDG_2	C1
5	76.79 .. 76.74	47	129	C-H	DDM_2	C2 or C5
6	76.68 .. 76.61	100	101	C-H	DDG_1	C2 or C5
7	70.39 .. 70.34	96	106	C-H	DDG_1	C2 or C5
8	69.47 .. 69.41	62	177	C-H	DDM_1	C2 or C5
9	68.73 .. 68.69	28	25	C-H	DDG_2	C2 or C5
10	67.84 .. 67.79	30	32	C-H	DDG_2	C2 or C5
11	66.14 .. 66.09	46	129	C-H	DDM_2	C2 or C5
12	65.73 .. 65.68	64	184	C-H	DDM_1	C2 or C5
13	64.39 .. 64.32	61	192	C-H2	DDM_1	C6
14	64.27 .. 64.22	44	135	C-H2	DDM_2	C6
15	63.98 .. 63.94	27	30	C-H2	DDG_2	C6
16	63.90 .. 63.83	101	110	C-H2	DDG_1	C6
17	29.45 .. 29.37	100	114	C-H2	DDG_1	C3 or C4
18	27.92 .. 27.85	39	140	C-H2	DDM_2	C3 or C4
19	25.81 .. 25.75	100	102	C-H2	DDG_1	C3 or C4
20	25.45 .. 25.41	31	38	C-H2	DDG_2	C3 or C4
21	24.37 .. 24.33	27	30	C-H2	DDG_2	C3 or C4
22	23.53 .. 23.47	64	177	C-H2	DDM_1	C3 or C4
23	20.42 .. 20.36	66	181	C-H2	DDM_1	C3 or C4
24	20.06 .. 20.00	48	134	C-H2	DDM_2	C3 or C4

Species	Lgol t/e = 1.3 Feed		Lgol t/e= 3.3 feed	
	Average Peak Area	Standard Error (%)	Average Peak Area	Standard Error (%)
DDG_1	99	1%	106	2%
DDG_2	29	3%	32	6%
DDM_1	63	1%	182	1%
DDM_2	45	3%	132	1%

Table 8.6: *Ratio of 34-Dman (i.e., DDM) to 34-Dglu (i.e., DDG) by ^{13}C NMR and by HPLC, and ratio of converted threo- and erythro- Lgol isomers, for hydrolysis of Lgol using two different Lgol diastereomer ratios (1.3 and 3.3).*

t/e Lgol Feed	DDM/DDG (NMR)	DDM/DDG (HPLC)	t/e Converted Lgol
1.3	0.82	0.89	0.92
3.3	2.3	2.2	2.4

Table 8.7**:** *Mestrenova ^{13}C NMR-predicted chemical shifts (ppm) for 34-Dman/34-Dglu (which are not distinguished in the NMR prediction). The carbon numbering convention is also provided.*

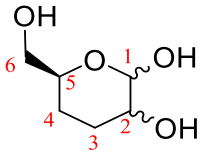

DDM & DDG

Carbon Position	DDM & DDF
1	97.3
2	70.3
3	26.7
4	25.2
5	73.3
6	65.3

34-Dfru was produced from treatment of Lgol in water over SiAl at 150°C (Table 5.1, Entry 7). The quantitative ^{13}C NMR assignments of the different tautomers of 34-Dfru are shown in Table 8.8. Similar to fructose, five tautomers are observed by ^{13}C NMR: acyclic ketone, α and β-furanose, and α and β-pyranose. The ketone tautomer was assigned based on the observation a ketone peak at 213.7 ppm (quaternary), and the C_5 carbon position ("C-H" multiplicity) at 71.1 ppm. The α and β furanose tautomers were assigned based on the two peaks at 106.4 and 106.0 ppm (C_2 anomeric carbon; quaternary), and two peaks at 81.5 and 79.6 ppm (C_5 hydroxymethyl-ether carbon; "C-H" multiplicity). The C_5 hydroxymethyl-ether carbon position is only present in the furanose tautomer, allowing the furanose and pyranose tautomers to be distinguished. The C_2 anomeric carbon positions of the α and β pyranose tautomers were assigned as the two peaks at 95.7 and 95.1 ppm. The α and β anomers were not distinguished in this study.

Concerning the region of the ^{13}C NMR spectrum of 34-Dfru up-field of 70 ppm, peaks corresponding to the different tautomers of 34-Dfru could not be completely distinguished due to the similar chemical shifts between different carbon positions. As shown in Table 8.8, the chemical shift, relative peak area, and multiplicity of each carbon position are consistent with the assignments; all assignments are also in reasonable agreement with the Mestrenova ^{13}C NMR predicted chemical shifts (Table 8.9). In the region of the spectrum between 63-68 ppm, the expected number of "pyranose (C_1 or C_6)" peaks (four), "pyranose (C_5)" peaks (two), and "ketone or furanose (C_1 or C_6)" peaks (six) are observed. The C_5 pyranose peak was assigned based on the "C-H" multiplicity of this carbon position. The C_1 and C_6 carbon positions of the ketone and furanose tautomers were not distinguished because the peaks had similar chemical shifts, peak areas, and multiplicities. In the region of the spectrum between 23-34 ppm, the expected number of "ketone or furanose (C_3 or C_4)" peaks (six) and the expected number of pyranose (C_3 or C_4) peaks (four) are observed. The C_3 and C_4 carbon positions of the ketone and furanose tautomers were not distinguished because the peaks had similar chemical shifts, peak areas, and multiplicities.

Table 8.8: *Quantitative ^{13}C NMR chemical shifts, normalized peak areas, multiplicities, and assignments from quantitative-^{13}C NMR of reaction products of Lgol conversion over SiAl at 150^{o}C. Multiplicities were assigned based on ^{13}C DEPT135 and DEPT90 NMR experiments. "Assignments" refers to the assignment of the carbon position for a given tautomer (ketone, furanose, or pyranose) of 34-Dfru. Minor peaks from residual Lgol were excluded from this table.*

#	Chemical Shift (ppm)	Normalized Area	Multiplicity	Assignment
1	213.78 .. 213.73	100.0	Quaternary	Ketone (C2)
2	106.41 .. 106.33	111.7	Quaternary	Furanose (C2)
3	106.01 .. 105.96	79.2	Quaternary	Furanose (C2)
4	95.68 .. 95.64	44.4	Quaternary	Pyranose (C2)
5	95.15 .. 95.11	38.4	Quaternary	Pyranose (C2)
6	81.55 .. 81.50	78.5	C-H	Furanose (C5)
7	79.60 .. 79.55	94.8	C-H	Furanose (C5)
8	71.11 .. 71.05	94.1	C-H	Ketone (C5)
9	67.68 .. 67.62	40.6	C-H2	Pyranose (C1 or C6)
10	67.20 .. 67.13	89.1	C-H2	Ketone or furanose (C1 or C6)
11	67.02 .. 66.97	35.4	C-H2	Pyranose (C1 or C6)
12	65.35 .. 65.28	92.7	C-H2	Ketone or furanose (C1 or C6)
13	65.24 .. 65.16	99.0	C-H2	Ketone or furanose (C1 or C6)
14	65.14 .. 65.07	81.9	C-H2	Ketone or furanose (C1 or C6)
15	65.07 .. 65.02	42.4	C-H	Pyranose (C5)
16	64.90 .. 64.84	75.5	C-H2	Ketone or furanose (C1 or C6)
17	64.69 .. 64.64	42.6	C-H2	Pyranose (C1 or C6)
18	64.24 .. 64.19	35.9	C-H2	Pyranose (C1 or C6)
19	63.69 .. 63.62	142.3 (two peaks)	Larger peak: C-H2 Smaller peak: C-H	Larger peak: Ketone or furanose (C1 or C6) Smaller peak: Pyranose (C5)
20	33.97 .. 33.91	93.4	C-H2	Ketone or furanose (C3 or C4)
21	33.42 .. 33.36	81.6	C-H2	Ketone or furanose (C3 or C4)
22	33.07 .. 33.01	96.8	C-H2	Ketone or furanose (C3 or C4)
23	28.71 .. 28.65	46.4	C-H2	Pyranose (C3 or C4)
24	26.46 .. 26.41	47.6	C-H2	Pyranose (C3 or C4)
25	26.28 .. 26.21	95.7	C-H2	Ketone or furanose (C3 or C4)
26	25.86 .. 25.79	85.2	C-H2	Ketone or furanose (C3 or C4)
27	25.66 .. 25.58	104.8	C-H2	Ketone or furanose (C3 or C4)
28	24.10 .. 24.04	48.0	C-H2	Pyranose (C3 or C4)
29	23.89 .. 23.84	48.1	C-H2	Pyranose (C3 or C4)

Table 8.9: *Mestrenova ^{13}C NMR-predicted chemical shifts (ppm) for furanose, ketone, and pyranose tautomers of 34-Dfru. The carbon numbering convention is also provided.*

Carbon Position	Pyranose	Furanose	Ketone
1	66.4	66.8	69.1
2	95.4	103.9	212.1
3	30.0	32.1	36.6
4	27.4	27.4	29.0
5	67.2	74.5	71.6
6	66.7	65.9	66.8

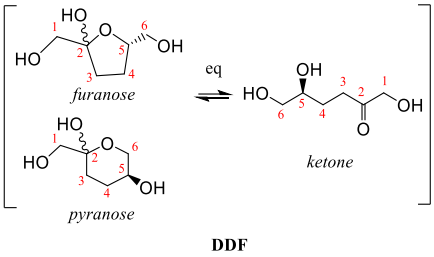

DDF

Electrospray ionization mass spectrometry (ESI-MS) analysis of 34-Dfru was done on a Bruker maXis ultra-high resolution, time-of-flight mass spectrometer using infusion in positive ion mode. Samples were diluted 1:60,000 in 85% methanol/15% water (v/v) prior to analysis. Samples were infused at 3 uL/min with a source voltage of 3500V. The source temperature was set to 180^{o}C while the nebulizer pressure was 0.4 bar and the drying gas flow was 4 L/min. The mass range measured was 75 to 1550 m/z. The ESI-MS shows a single major peak at m/z = 171, consistent with the molecular weight of 34-Dfru (148 g/mol) plus a sodium ion (23 g/mol). This result rules out the presence of a hydrated geminal diol (which would have molecular weight 166 g/mol), a compound which could also show a quaternary ^{13}C NMR peak in the 90-110 ppm region of the ^{13}C NMR spectrum. A smaller peak at m/z = 131 was observed, which could correspond to a protonated isomer of Lgol (e.g. a THFDM precursor, 130 g/mol).

Cis- and trans- tetrol were assigned using reported ^{13}C NMR chemical shifts from the literature.[1] The c/t ratio was calculated based on the ratio of these peaks measured by quantitative ^{13}C NMR.

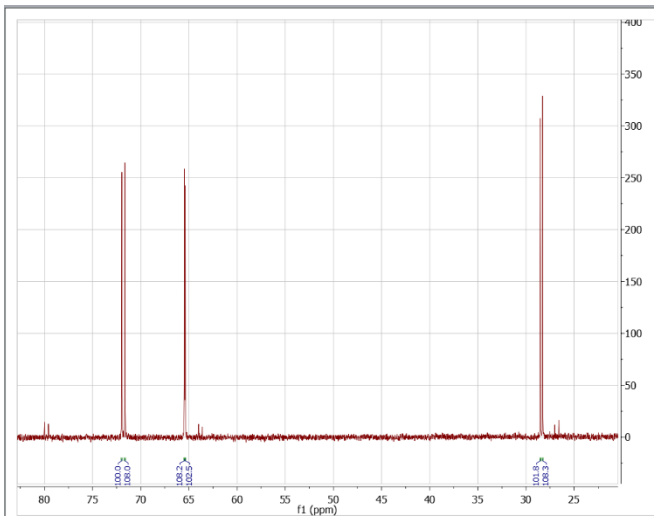

***Figure 8.9**: Quantitative ^{13}C NMR of product of Tetrol. cis-tetrol: 71.7, 65.5, 28.3 ppm. trans-tetrol: 72.0, 65.4, 28.6 ppm. A small amount of side-product THFDM is also present in this spectrum, consistent with the GC results.*

8.2. HPLC Chromatograms of Reaction Products

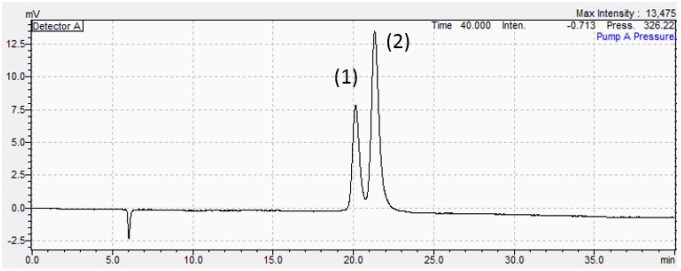

***Figure 8.10A:** Lgol (t/e = 1.3) feedstock. (1) = erythro-Lgol. (2) = threo-Lgol.*

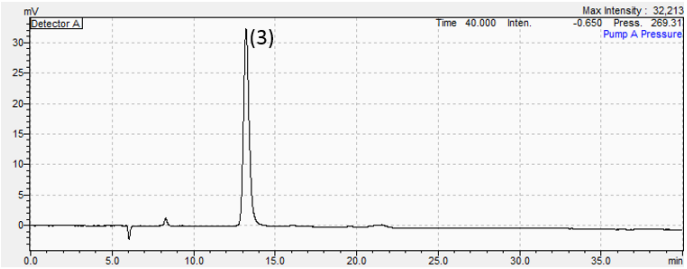

Figure 8.10B: *Product of Table 5.1, Entry 3. (3) = mixture of cis- and trans-Tetrol. Minor unknown compound also observed at a retention time of 8 min.*

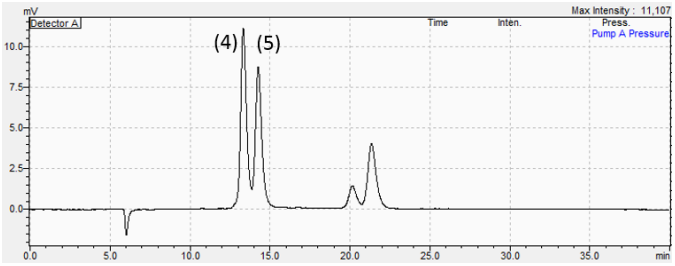

Figure 8.10C**:** *Product of Table 5.3, Entry 2. (4) = 34-Dglu. (5) = 34-Dman.*

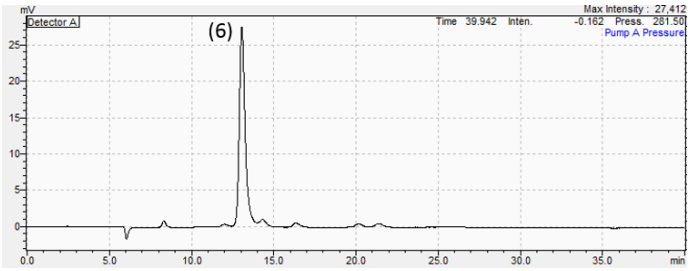

Figure 8.10D: *Product of Table 5.1, Entry 7. (6) = 34-Dfru.*

Figure 8.10: *HPLC chromatograms of reaction products. Compounds in the HPLC were assigned based on comparison with* ^{13}C *NMR spectra. 34-Dglu, 34-Dfru, cis-tetrol, and trans-tetrol are all overlapped in the HPLC.*

8.4. Reaction network for metal- and acid- catalyzed conversions of levoglucosan, mannose, glucose, and fructose

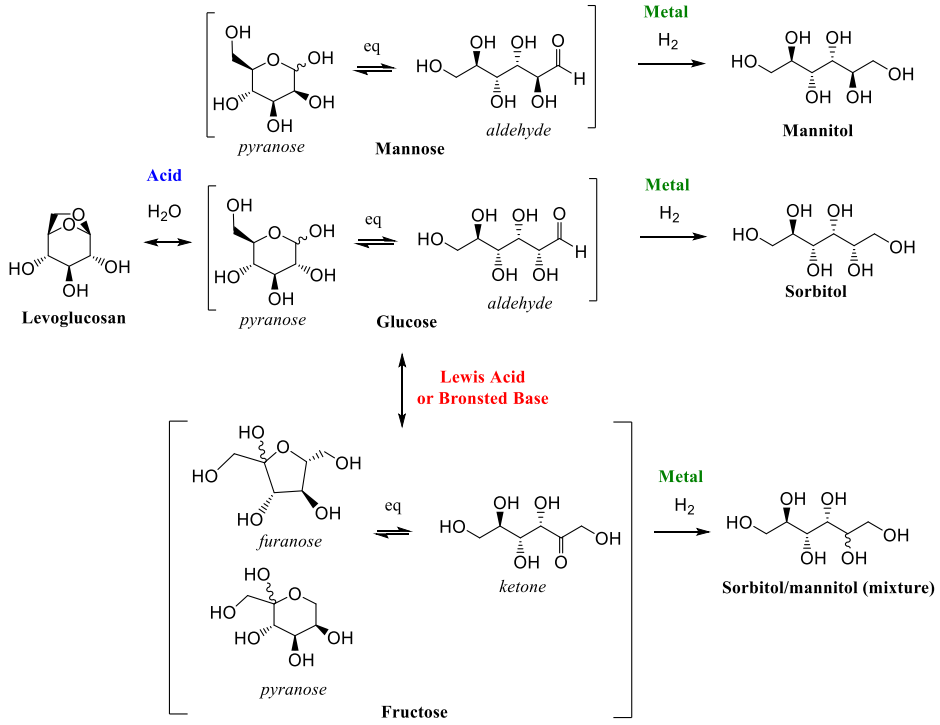

Figure 8.11: *Relevant acid-catalyzed and metal-catalyzed reactions of levoglucosan, glucose, mannose, and fructose. "eq" indicates reactions which are assumed to be quasi-equilibrated.*

8.5. Appendix for Chapter 6

8.5.1. NMR, HPLC, and Polarimetry Analyses of hexane-tetrols and –triols

A) 2R, 3S-1236-HT

i) NMR

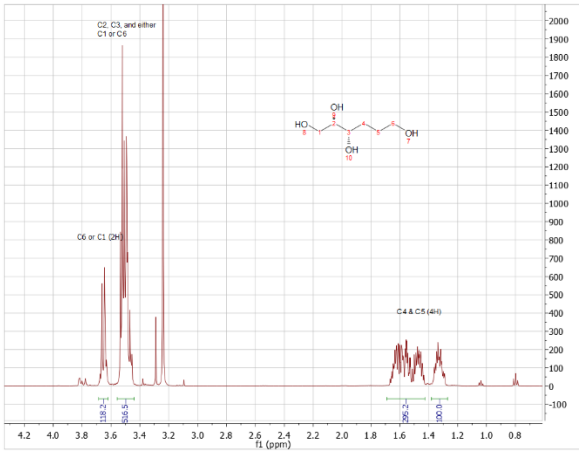

Figure 8.12. *^{1}H NMR of 2R, 3S-1236-tetrol (water suppression)*

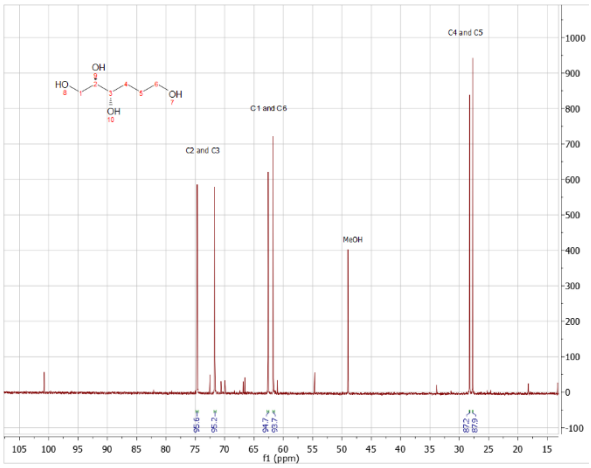

Figure 8.13. *^{13}C NMR of 2R, 3S-1236-tetrol*

- ^{13}C multiplicities confirmed with DEPT-NMR

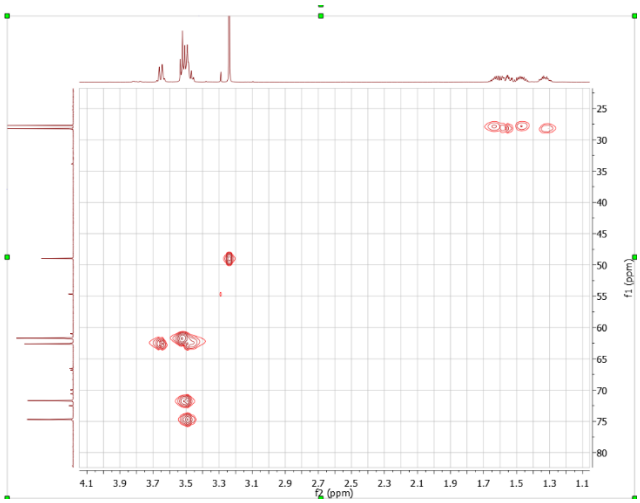

Figure 8.14. *^{1}H-^{13}C HSQC NMR of 2R, 3S-1236-tetrol*

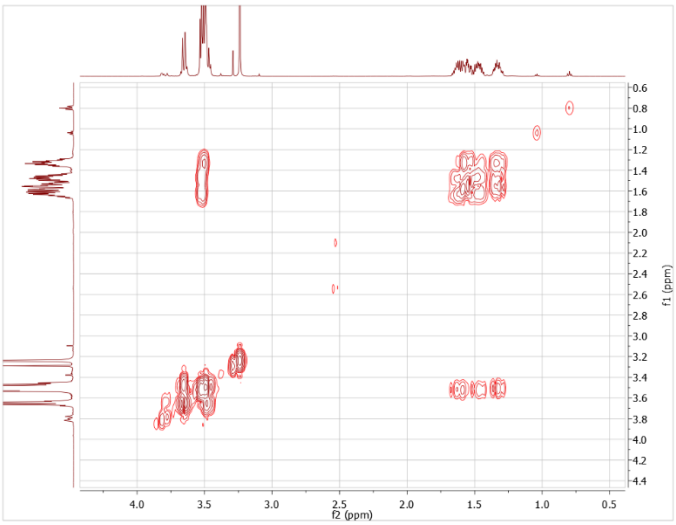

Figure 8.15. *^{1}H-^{1}H COSY NMR of 2R, 3S-1236-tetrol (water suppression)*

ii) HPLC:

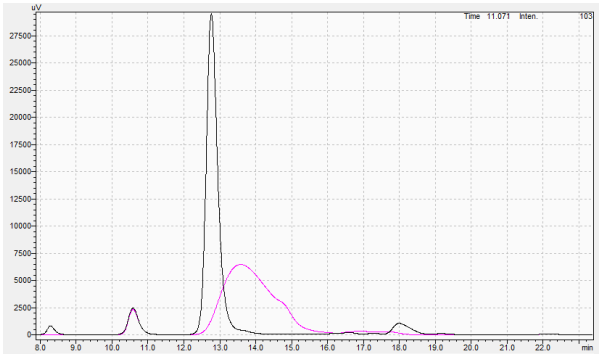

Figure 8.16. *HPLC of 2R, 3S-1236-tetrol. Pink – feed. Black – product.*

iii) Optical rotation: α^{25}_{D} = -6.5 (c = 1.2 , MeOH); lit -7.1 (water).[11]

B) 4R, 5S -145-HT

i) NMR

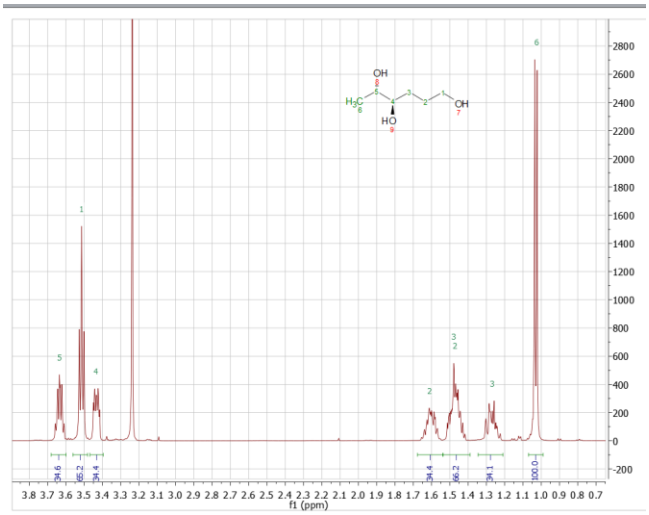

Figure 8.17. *^{1}H NMR of 4R, 5S-145-HT (water suppression)*

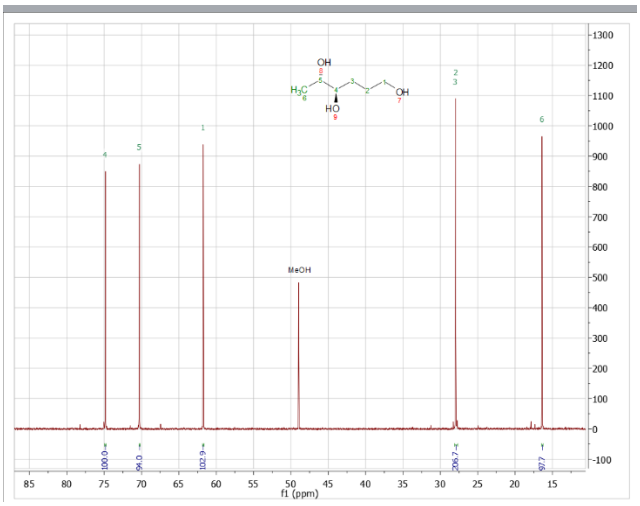

Figure 8.18. *^{13}C NMR of 4R, 5S-145-HT*

- ^{13}C multiplicities confirmed with DEPT-NMR

-^{13}C NMR agrees with lit reference: [12]

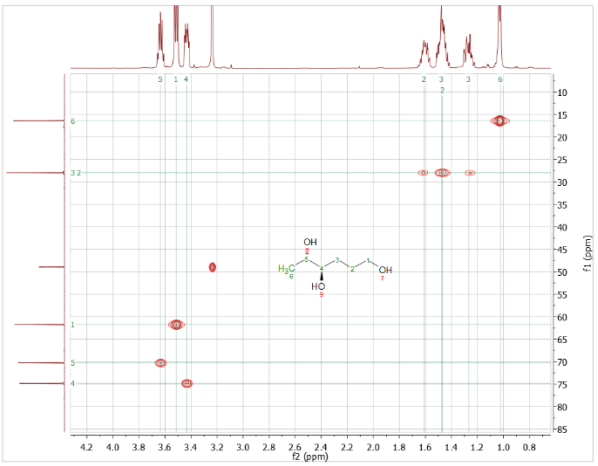

Figure 8.19. *^{1}H-^{13}C HSQC NMR of 4R, 5S-145-HT*

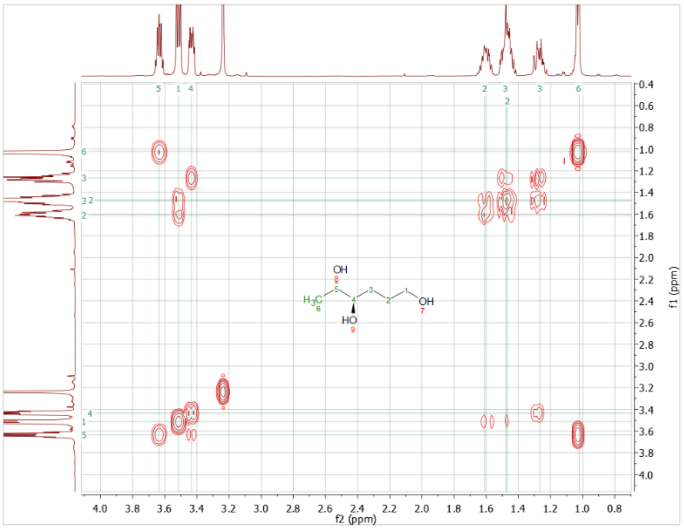

Figure 8.20. *^{1}H-^{1}H COSY NMR of 4R, 5S-145-HT (water suppression)*

ii) HPLC:

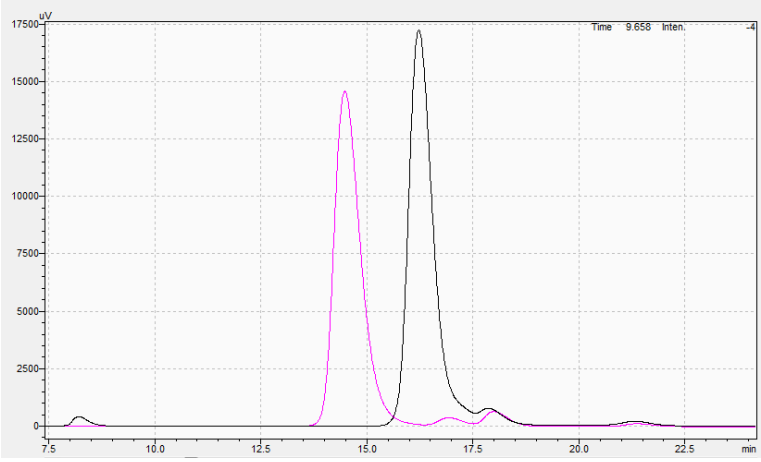

Figure 8.21. *HPLC of 4R, 5S-145-HT. Pink – feed. Black- product.*

iii) Optical rotation: α^{25}_{D} = +23.5 (c = 1.1, MeOH); lit –18.2 (c = 1.4, MeOH) for its enantiomer (4S, 5R)-1,4,5-hexanetriol.[13] Enantiomers have equal and opposite specific rotations.

C) 2R, 5S (meso)- 1256-HT (Pt/SiAl)

i) NMR:

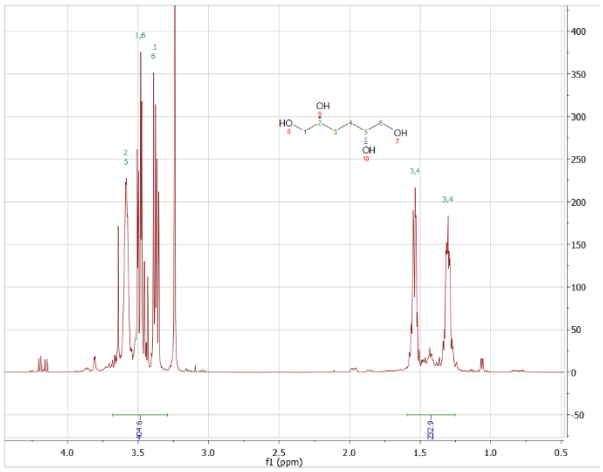

Figure 8.22. *^{1}H NMR of 2R, 5S-1256-HT (water suppression)*

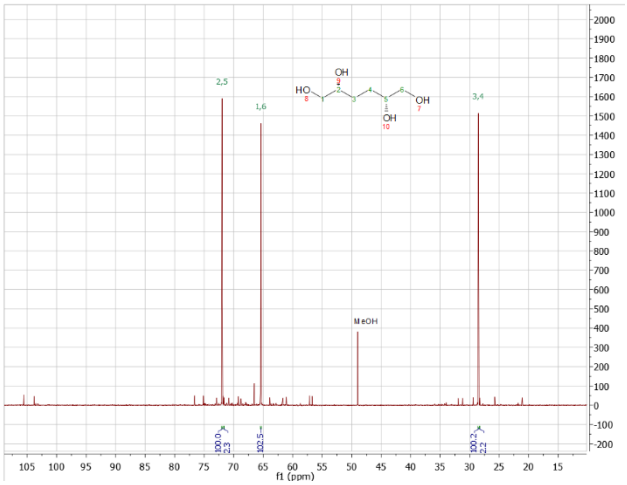

Figure 8.23A. *Full ^{13}C NMR spectrum*

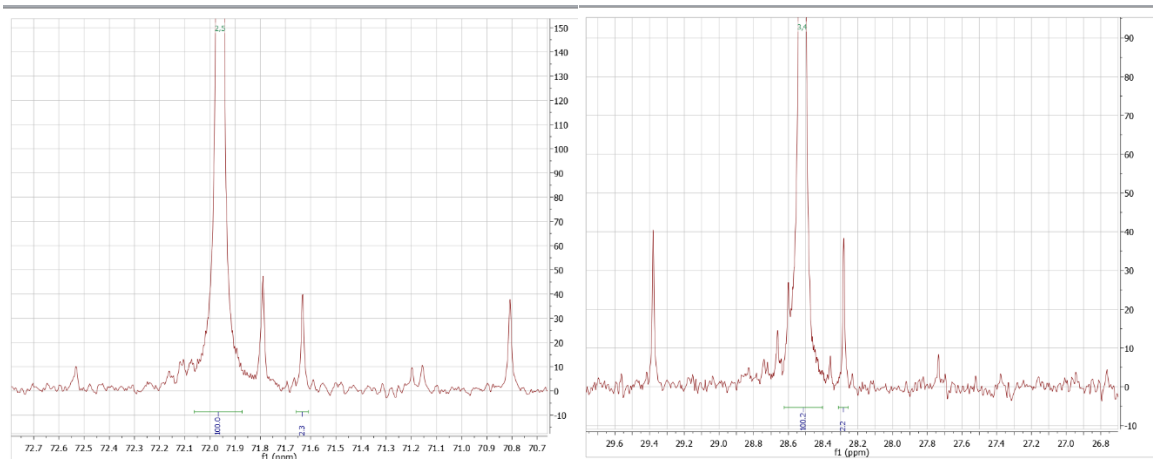

Figure 8.23B. *Stereoselectivity measurement*

Figure 8.23. *^{13}C NMR of 2R, 5S-1256-HT*

^{13}C NMR agrees with lit reference:[14]

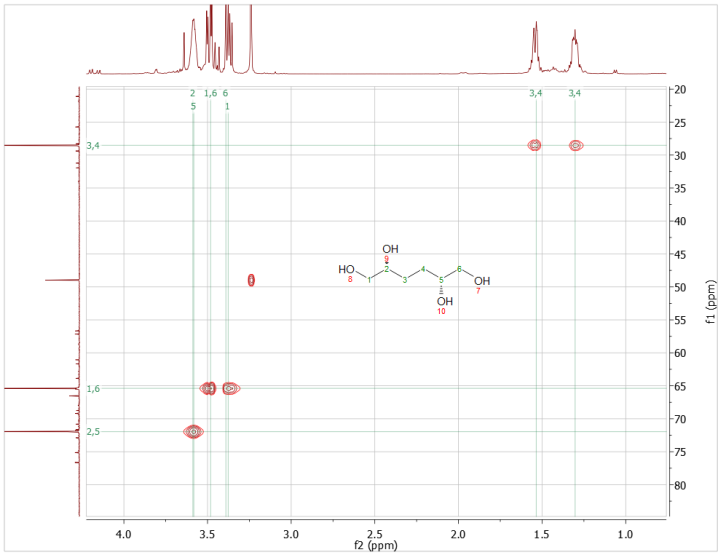

Figure 8.24. *^{1}H-^{13}C HSQC NMR of 2R, 5S-1256-HT*

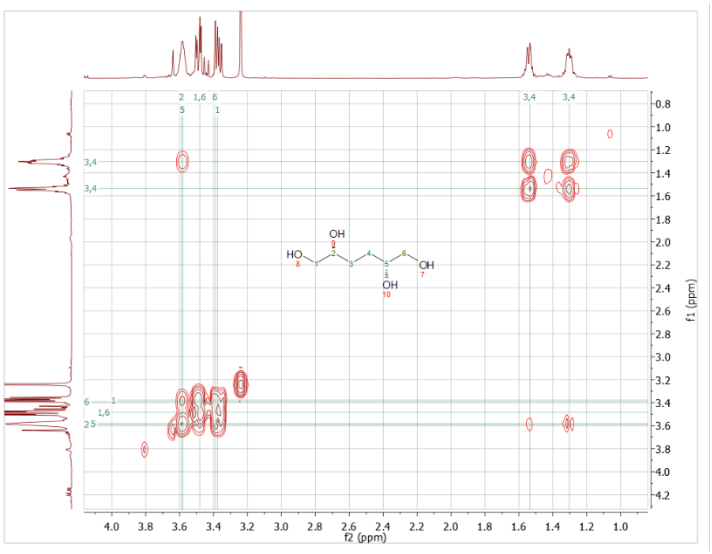

Figure 8.25. *^{1}H-^{1}H COSY NMR of 2R, 5S-1256-HT (water suppression)*

ii) HPLC

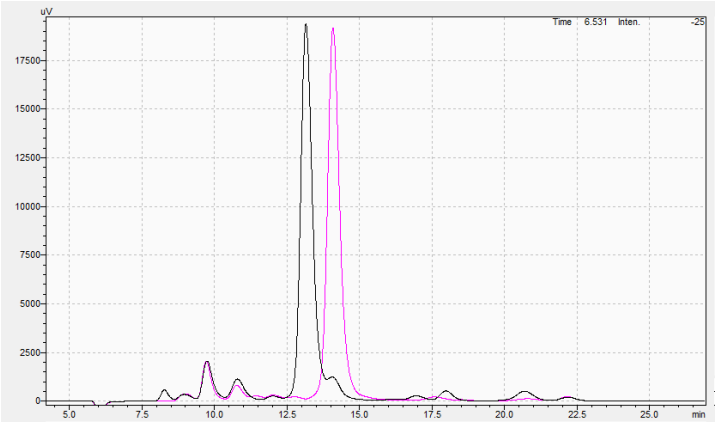

Figure 8.26. *HPLC of 2R, 5S-1256-HT. Pink – feed. Black – product.*

vi) Optical rotation:

Zero optical rotation is expected because the product is a *meso* compound. A specific rotation of -8.2 (c = 0.92, MeOH) was measured. However, the reaction product mixture contains 2% of the diastereomer 2S, 5S-1,2,5,6-hexanetetrol (specific rotation of -24.0 reported in the literature, c =

1.69, MeOH)[15] , and 6% of residual beta-D-methyl-galactopyranoside (specific rotation measured -76.1, c = 0.87, MeOH). Accounting for these impurities, the specific rotation of the major product is α^{25}_{D} = -3.4 (c = 0.92, MeOH). The deviation of this value from zero is likely due to the presence of small side-products with non-zero optical rotations.

D) 2S, 5S- 125-HT (Pt/SiAl)

i) NMR

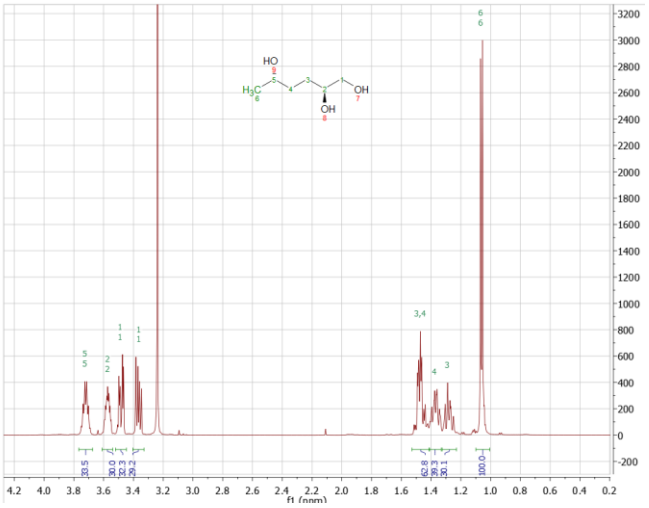

Figure 8.27. *^{1}H NMR of 2S, 5S-125-HT (water suppression)*

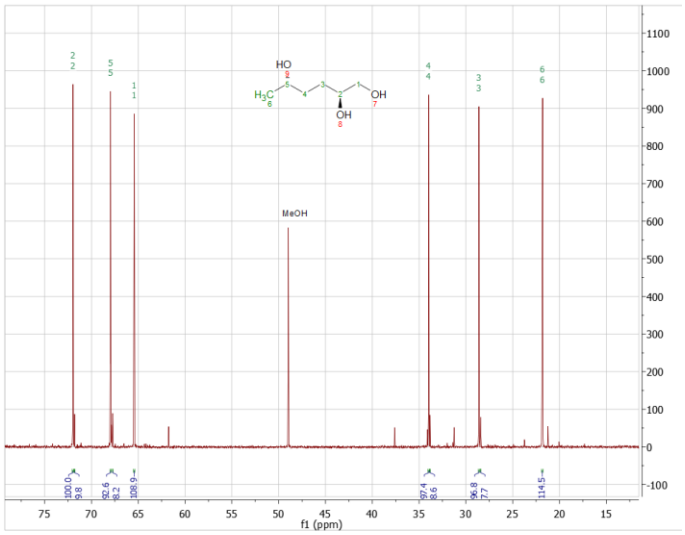

Figure 8.28A. *Full ^{13}C NMR spectrum*

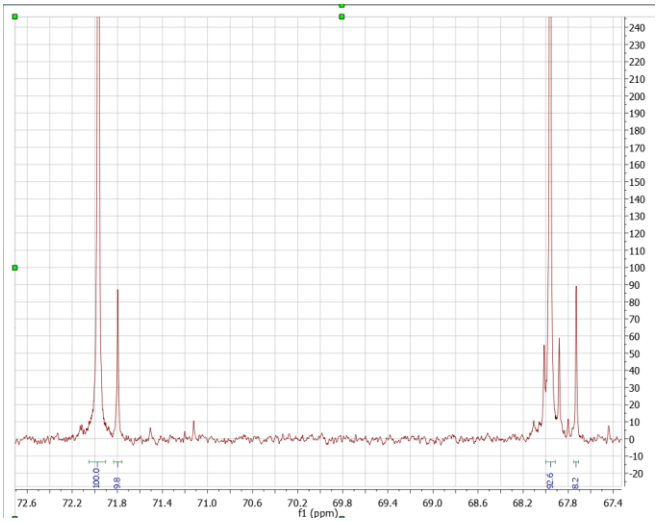

Figure 8.28B. *Stereoselectivity measurement*

Figure 8.28. *^{13}C NMR of 2S, 5S-125-HT*

- ^{13}C multiplicities confirmed with DEPT-NMR

-^{13}C NMR agrees with lit reference: [16]

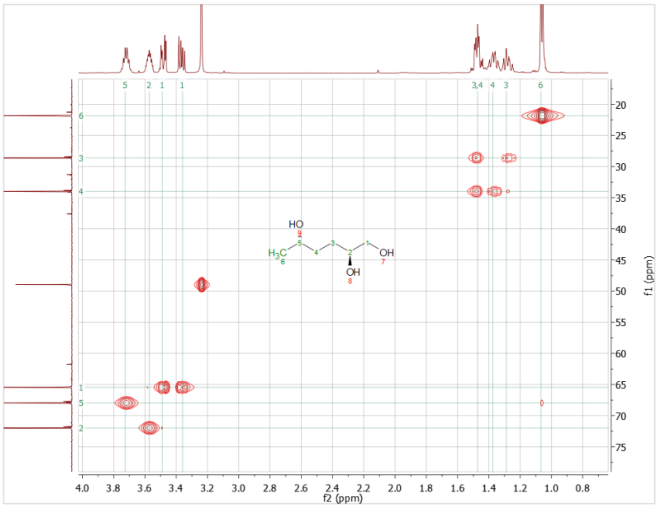

Figure 8.29. *^{1}H-^{13}C HSQC NMR of 2S, 5S-125-HT*

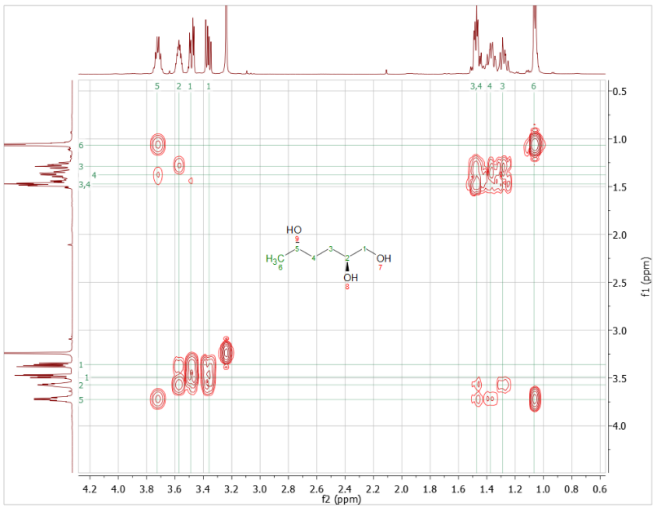

Figure 8.30. *^{1}H-^{1}H COSY NMR of 2S, 5S-125-HT (water suppression)*

ii) HPLC:

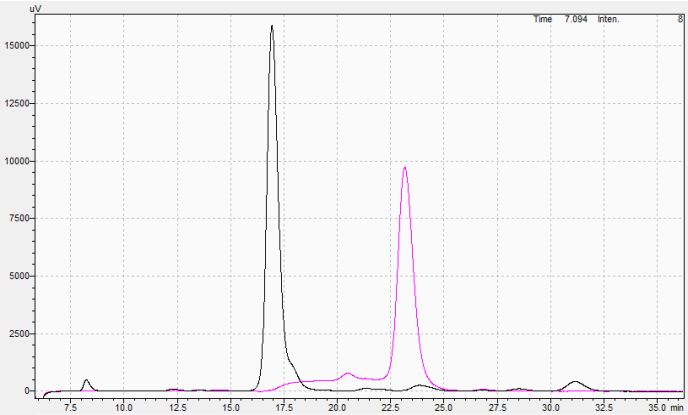

Figure 8.31. *HPLC of 2S, 5S-125-HT. Pink – feed. Black – product.*

vi) Optical rotation: α^{25}_{D} = -1.9 (c = 0.89, MeOH). No literature sources could be found for optical rotation of (2S, 5S)-1,2,5-hexanetriol. The specific rotation of its diastereomer (2S, 5R)-1,2,5-hexanetriol has been reported: -51.3 (c = 0.15, MeOH).[17] This comparison provides evidence that our reaction product does not have (2S, 5R) or (2R, 5S) stereochemistry.

8.5.2. NMR and ESI-MS identification of reaction intermediates

A) 3,4-dideoxy-mannose (23-Dman)

Quantitative-^{13}C NMR + DEPT analysis shows that there are six C_6 species, each with one C-H peak in the anomeric region (102-90 ppm), two CH peaks and one CH2 peak in the C-O bond (60-85 ppm) region, and two CH2 peaks in the upfield region (20-35 ppm). Letters “A-F” indicate the assignment of the six different species. There are six ^{13}C signals for each species A-F. “C” and “D” have similar peak areas so they cannot be distinguished; similar with “E” and “F”. Note that the peak at 21.9 ppm is overlapped with an impurity present in the feed, causing its area to be greater than the other “EF” peaks. No aldehyde peak is observed by NMR. ESI-MS shows m/z =

171 (pyranose/furanose + Na) as major peak, 153 (anhydro- species + Na) as minor peak. The ESI-MS results rule out a hydrated geminal diol or a C_{12} dimers. m/z = 118 and 245 peaks are impurities which were present in a blank sample containing no feedstock. These results strongly suggest the presence of "pyranose", "furanose", both of which can exist in alpha and beta forms, as well as and "anhydro-pyranose" and "anhydro-furanose" species.

	Range (ppm)	Area	DEPT	Species #
1	101.60 .. 101.56	92.82	CH	CD
2	99.69 .. 99.66	69.01	CH	EF
3	98.32 .. 98.27	80.71	CH	CD
4	97.99 .. 97.94	68.74	CH	EF
5	95.53 .. 95.45	192.08	CH	A
6	90.35 .. 90.27	137.97	CH	B
7	80.06 .. 80.01	66.01	CH	EF
8	79.78 .. 79.69	192.89	CH	A
9	78.78 .. 78.74	58.02	CH	EF
10	78.50 .. 78.45	90.58	CH	CD
11	76.88 .. 76.84	90.62	CH	CD
12	74.16 .. 74.10	67.35	CH	EF
13	73.40 .. 73.31	139.69	CH	B
14	72.85 .. 72.78	84.12	CH	CD
15	67.26 .. 67.21	66.26	CH	EF
16	66.14 .. 66.10	90.65	CH	CD
17	65.94 .. 65.89	93.89	CH2	CD
18	65.40 .. 65.35	140.02	CH	B
19	65.24 .. 65.19	183.43	CH	A
20	63.52 .. 63.46	71.42	CH2	EF
21	63.10 .. 63.06	63.66	CH2	EF
22	62.85 .. 62.79	91.94	CH2	CD
23	61.38 .. 61.31	196.81	CH2	A
24	61.05 .. 61.00	140.97	CH2	B
25	32.98 .. 32.92	72.55	CH2	EF
26	32.46 .. 32.40	85.94	CH2	CD
27	31.10 .. 31.02	186.52	CH2	A
28	29.85 .. 29.80	176.89	CH2	A
29	28.87 .. 28.82	132.17	CH2	B
30	27.72 .. 27.68	70.92	CH2	EF
31	26.68 .. 26.64	90.69	CH2	CD
32	25.64 .. 25.57	137.47	CH2	B
33	24.81 .. 24.75	77.39	CH2	CD
34	24.05 .. 24.01	59.53	CH2	EF
35	23.71 .. 23.65	79.64	CH2	CD
36	21.92 .. 21.85	125.51	CH2	EF

Table 8.10. *13C NMR chemical shifts and multiplicities of 23-Dman*

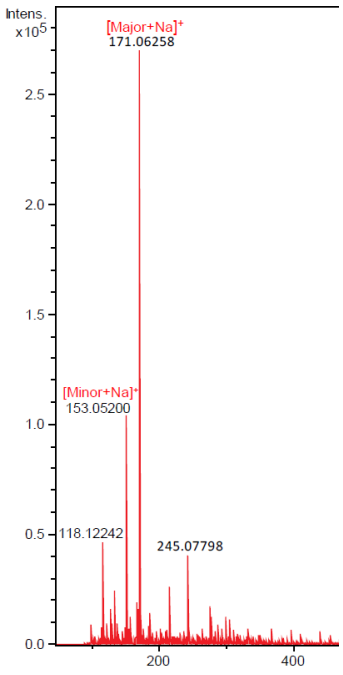

Figure 8.32. *ESI-MS of 23-Dman*

B) 2,3-dideoxy-rhamnose (23-Drha)

Quantitative-^{13}C NMR + DEPT analysis shows that there are four C_6 species, each with one C-H peak in the anomeric region (102-90 ppm), two CH peaks in the C-O bond (60-85 ppm) region, two CH2 peaks in the upfield region (20-35 ppm), and one CH3 peak in the methyl region (10-20 ppm). Letters "A-D" indicate the assignment of the four different species. ESI-MS shows a single major peak at m/z = 155 (pyranose/furanose + Na). These results strongly suggest the presence of "pyranose", and "furanose" species, both of which can exist in alpha and beta forms. 23-Drha cannot form an anhydro- species.

	Range (PPM)	Area	DEPT	Assignment
1	98.41 .. 98.35	86.98	CH	C
2	97.83 .. 97.78	63.95	CH	D
3	95.49 .. 95.33	222.9	CH	A
4	90.33 .. 90.23	140.69	CH	B
5	84.23 .. 84.17	64.64	CH	D
6	82.16 .. 82.09	96.3	CH	C
7	75.76 .. 75.66	223.76	CH	A
8	71.16 .. 71.09	125.84	CH	B
9	70.79 .. 70.66	233.88	CH	A
10	69.51 .. 69.45	128.07	CH	B
11	69.24 .. 69.17	57.94	CH	D
12	68.36 .. 68.30	92.77	CH	C
13	49.11 .. 48.86	676.09		MEOH
14	33.13 .. 33.06	50.26	CH2	D
15	32.56 .. 32.49	83.65	CH2	C
16	31.40 .. 31.32	200.73	CH2	A
17	29.79 .. 29.67	210.82	CH2	A
18	29.25 .. 29.14	128.07	CH2	B
19	25.61 .. 25.49	135.05	CH2	B
20	23.81 .. 23.75	60.88	CH2	D
21	22.80 .. 22.75	81.71	CH2	C
22	18.11 .. 18.03	62.37	CH3	D
23	17.75 .. 17.69	78.56	CH3	C
24	17.31 .. 17.23	215.4	CH3	A
25	17.12 .. 17.03	128.63	CH3	B

Table 8.11. *13C NMR chemical shifts and multiplicities of 23-Drha*

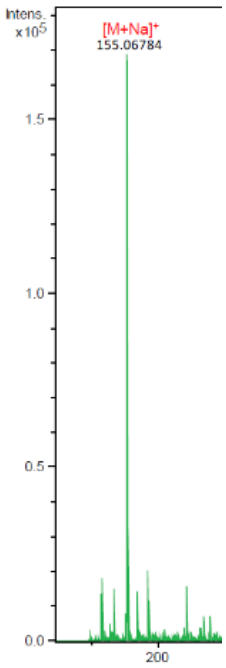

Figure 8.33. *ESI-MS of 23-Drha*

C) 3,4-dideoxygalactose (34-Dglu)

Quantitative-^{13}C NMR shows that the products are comprised of “34-Dglu-pyranose_1”, “34-Dglu-pyranose_2”, (alpha and beta tautomers of 34-Dglu-pyranose) and “erythro-Lgol”, by comparison to our previous work .[14b] ESI-MS shows a major peak at m/z = 171 (34-Dglu-pyranose + Na) and a minor peak at m/z = 153 (erythro-Lgol+ Na). 34-Dglu cannot form a furanose species.

	Range (ppm)	Normalized	Assignment
1	101.29 .. 101.22	32.9	anhydro-DG
2	98.22 .. 98.05	100	DG-pyranose_1
3	91.89 .. 91.83	29.44	DG_pyranose_2
4	76.71 .. 76.59	100.28	DG-pyranose_1
5	73.65 .. 73.56	28.78	anhydro-DG
6	70.42 .. 70.31	97.05	DG-pyranose_1
7	68.73 .. 68.68	29.13	DG_pyranose_2
8	67.84 .. 67.78	26.76	DG_pyranose_2
9	66.43 .. 66.37	25.94	anhydro-DG
10	65.83 .. 65.77	24.43	anhydro-DG
11	63.99 .. 63.94	25.73	DG_pyranose_2
12	63.91 .. 63.82	96.36	DG-pyranose_1
13	29.46 .. 29.37	89.06	DG-pyranose_1
14	25.84 .. 25.71	97.56	DG-pyranose_1
15	25.48 .. 25.39	31.38	DG_pyranose_2
16	24.38 .. 24.32	25.43	DG_pyranose_2
17	23.91 .. 23.83	22.02	anhydro-DG
18	22.04 .. 21.98	22.7	anhydro-DG

Table 8.12. *13C NMR chemical shifts and multiplicities of 34-Dglu*

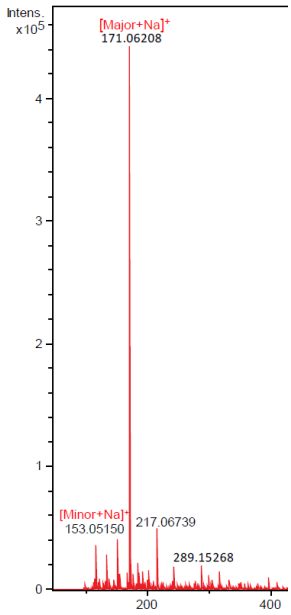

Figure 8.34. *ESI-MS of 34-Dglu*

D) 3,4-dideoxyfucose (34-Dfuc)

Quantitative-^{13}C NMR + DEPT analysis shows that there are two C_6 species, each with one C-H peak in the anomeric region (102-90 ppm), two CH peaks in the C-O bond (60-85 ppm) region, two CH2 peaks in the upfield region (20-35 ppm), and one CH3 peak in the methyl (10-20 ppm) region). Letters A & B indicate the two tautomers. ESI-MS shows m/z = 155 (pyranose + Na) as major peak. m/z = 118 and 245 peaks are impurities which were present in a blank sample containing no feedstock. These results strongly suggest the presence of alpha and beta pyranose. 34-Dfuc cannot form furanose or anhydro- species.

	Range (ppm)	Area	DEPT	Assignment
1	98.16 .. 97.97	100	CH	A
2	91.97 .. 91.90	24.63	CH	B
3	72.98 .. 72.80	99.77	CH	A
4	70.47 .. 70.25	101.94	CH	A
5	67.90 .. 67.82	23.81	CH	B
6	65.13 .. 64.99	22.31	CH	B
7	31.60 .. 31.50	94.52	CH2	A
8	31.28 .. 31.21	24.57	CH2	B
9	29.87 .. 29.77	91.14	CH2	A
10	24.84 .. 24.77	23.04	CH2	B
11	20.09 .. 20.02	90	CH3	A
12	19.99 .. 19.94	24.19	CH3	B

Table 8.13. *13C NMR chemical shifts and multiplicities of 34-Dfuc*

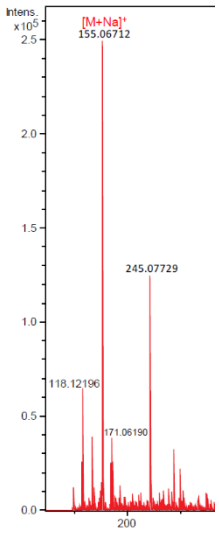

Figure 8.35. *ESI-MS of 34-Dfuc*

8.6. References

1. Miftakhov, M. S.; Gaisina, I. N.; Valeev, F. A.; Shitikova, O. V., Synthesis of 1,6-anhydro-3-bromo-3,4-dideoxy-β-d-threo-hex-3-enopyranose. *Russ Chem Bull* **1995,** *44* (12), 2350-2352.
2. Connolly, T. J.; Considine, J. L.; Ding, Z.; Forsatz, B.; Jennings, M. N.; MacEwan, M. F.; McCoy, K. M.; Place, D. W.; Sharma, A.; Sutherland, K., Efficient Synthesis of 8-Oxa-3-aza-bicyclo[3.2.1]octane Hydrochloride. *Organic Process Research & Development* **2010,** *14* (2), 459-465.
3. Tagirov, A.; Biktagirov, I.; Galimova, Y.; Faizullina, L.; Salikhov, S.; Valeev, F., Opening of the 1,6-anhydro bridge with selective reduction of the acetal moiety in levoglucosenone and its derivatives. *Russian Journal of Organic Chemistry* **2015,** *51* (4), 569-575.
4. Finch, J. N.; Clark, A., Effect of water content of silica-alumina catalyst on 1-butene isomerization and polymerization. *The Journal of Physical Chemistry* **1969,** *73* (7), 2234-2238.

5. van Bokhoven, J. A.; van der Eerden, A. M. J.; Koningsberger, D. C., Flexible aluminium coordination of zeolites as function of temperature and water content, an in-situ method to determine aluminium coordinations. In *Studies in Surface Science and Catalysis*, Aiello, R.; Giordano, G.; Testa, F., Eds. Elsevier: 2002; Vol. 142, pp 1885-1890.
6. Curtiss, L. A.; Redfern, P. C.; Raghavachari, K., Gaussian-4 theory using reduced order perturbation theory. *The Journal of Chemical Physics* **2007,** *127* (12), 124105.
7. (a) Maldonado, G. M. G.; Assary, R. S.; Dumesic, J. A.; Curtiss, L. A., Acid-catalyzed conversion of furfuryl alcohol to ethyl levulinate in liquid ethanol. *Energ Environ Sci* **2012,** *5* (10), 8990-8997; (b) Maldonado, G. M. G.; Assary, R. S.; Dumesic, J.; Curtiss, L. A., Experimental and theoretical studies of the acid-catalyzed conversion of furfuryl alcohol to levulinic acid in aqueous solution. *Energ Environ Sci* **2012,** *5* (5), 6981-6989; (c) Assary, R. S.; Kim, T.; Low, J. J.; Greeley, J.; Curtiss, L. A., Glucose and fructose to platform chemicals: understanding the thermodynamic landscapes of acid-catalysed reactions using high-level ab initio methods. *Physical Chemistry Chemical Physics* **2012,** *14* (48), 16603-16611.
8. Marenich, A. V.; Cramer, C. J.; Truhlar, D. G., Universal Solvation Model Based on Solute Electron Density and on a Continuum Model of the Solvent Defined by the Bulk Dielectric Constant and Atomic Surface Tensions. *The Journal of Physical Chemistry B* **2009,** *113* (18), 6378-6396.
9. Schlegel, H. B.; Iyengar, S. S.; Li, X.; Millam, J. M.; Voth, G. A.; Scuseria, G. E.; Frisch, M. J., Ab initio molecular dynamics: Propagating the density matrix with Gaussian orbitals. III. Comparison with Born–Oppenheimer dynamics. *The Journal of Chemical Physics* **2002,** *117* (19), 8694-8704.
10. Frisch, M. J.; Trucks, G. W.; Schlegel, H. B.; Scuseria, G. E.; Robb, M. A.; Cheeseman, J. R.; Scalmani, G.; Barone, V.; Mennucci, B.; Petersson, G. A.; Nakatsuji, H.; Caricato, M.; Li, X.; Hratchian, H. P.; Izmaylov, A. F.; Bloino, J.; Zheng, G.; Sonnenberg, J. L.; Hada, M.; Ehara, M.; Toyota, K.; Fukuda, R.; Hasegawa, J.; Ishida, M.; Nakajima, T.; Honda, Y.; Kitao, O.; Nakai, H.; Vreven, T.; Montgomery Jr., J. A.; Peralta, J. E.; Ogliaro, F.; Bearpark, M. J.; Heyd, J.; Brothers, E. N.; Kudin, K. N.; Staroverov, V. N.; Kobayashi, R.; Normand, J.; Raghavachari, K.; Rendell, A. P.; Burant, J. C.; Iyengar, S. S.; Tomasi, J.; Cossi, M.; Rega, N.; Millam, N. J.; Klene, M.; Knox, J. E.; Cross, J. B.; Bakken, V.; Adamo, C.; Jaramillo, J.; Gomperts, R.; Stratmann, R. E.; Yazyev, O.; Austin, A. J.; Cammi, R.; Pomelli, C.; Ochterski, J. W.; Martin, R. L.; Morokuma, K.; Zakrzewski, V. G.; Voth, G. A.; Salvador, P.; Dannenberg, J. J.; Dapprich, S.; Daniels, A. D.; Farkas, Ö.; Foresman, J. B.; Ortiz, J. V.; Cioslowski, J.; Fox, D. J. *Gaussian 09*, Gaussian, Inc.: Wallingford, CT, USA, 2009.
11. Regeling, H.; Chittenden, G. J. F., Synthesis of some monodeoxy- and dideoxy-hexitols, and derivatives thereof, from d-glucono-1,5-lactone. *Carbohydrate Research* **1990,** *205*, 261-268.
12. Henkel, T.; Breiding-Mack, S.; Zeeck, A.; Grabley, S.; Hammann, P. E.; Hütter, K.; Till, G.; Thiericke, R.; Wink, J., Secondary metabolites by chemical screening, 18. Narbosines, new carbohydrate metabolites from Streptomyces. *Liebigs Annalen der Chemie* **1991,** *1991* (6), 575-580.
13. Marco, J. L., Synthesis of (4S, 5R)-1,4,5-Hexanetriol and D-Amicetose. *Synthetic Communications* **1989,** *19* (3-4), 485-490.
14. (a) Maier, M. E.; Reuter, S., Double Asymmetric Dihydroxylation of 1,5-Hexadiene. *Liebigs Annalen* **1997,** *1997* (10), 2043-2046; (b) Krishna, S. H.; De bruyn, M.; Schmidt, Z. R.; Weckhuysen, B. M.; Dumesic, J. A.; Huber, G. W., Catalytic production of hexane-1,2,5,6-tetrol from bio-renewable levoglucosanol in water: effect of metal and acid sites on (stereo)-selectivity. *Green Chemistry* **2018,** *20* (19), 4557-4565.
15. Machinaga, N.; Kibayashi, C., General entry to the 3,5-disubstituted indolizidine class of dendrobatid alkaloids. Total syntheses of both enantiomers of indolizidines 195B, 223AB, 239AB, and 239CD from a common chiral synthon. *The Journal of Organic Chemistry* **1992,** *57* (19), 5178-5189.
16. Schiavo, V.; Descotes, G.; Mentech, J., *Hydrogenation of 5-Hydroxymethylfurfural*. 1991; Vol. 128, p 704-711.
17. Sharma, G. V. M.; Srikanth, G.; Reddy, P. P., Stereoselective total synthesis of dinemasone A by double intramolecular hetero-Michael addition (DIHMA). *Organic & Biomolecular Chemistry* **2012,** *10* (40), 8119-8124.